Aus der Klinik für Augenheilkunde
der Medizinischen Fakultät Charité – Universitätsmedizin Berlin

DISSERTATION

Characterization of transient receptor potential vanilloid 4 (TRPV4) channels in human corneal keratocytes

zur Erlangung des akademischen Grades
Doctor medicinae (Dr. med.)

vorgelegt der Medizinischen Fakultät
Charité – Universitätsmedizin Berlin

von

Vivien Schmädicke

aus Berlin

Datum der Promotion: 03.03.2023

Table of Contents

List of Figures

List of Tables

Abbreviations

ADDE	Aqueous deficient dry eye
$[Ca^{2+}]_i$	Intracellular calcium concentration
C_M	Membrane capacitance
COVID-19	Coronavirus disease 2019
DED/DES	Dry Eye Disease/Dry Eye Syndrome
DMSO	Dimethyl sulfoxide
DMEM	Dulbecco's Modified Eagle's Medium
EC_{50}	Half maximal effective concentration
ECM	Extracellular matrix
EDE	Evaporative dry eye
FCS	Fetal calf serum
Fura-2/AM	Fura-2-acetoxymethyl ester
GSK1016790A	GlaxoSmithKline 1016790A: TRPV4 agonist
GSK2193874	GlaxoSmithKline 2193874: TRPV4 antagonist
HCK	Human corneal keratocytes
HE	Hematoxylin and eosin
HEPES	4-(2-hydroxyethyl)-1-piperazineethanesulfonic acid
IC_{50}	Half maximal inhibitory concentration
IL-1α	Interleukin 1α (a proinflammatory cytokine)
IL-6	Interleukin 6 (a proinflammatory cytokine)
IP_3	Inositol-1,4,5-triphosphate
LASIK	Laser-assisted in situ keratomileusis
MMPs	Matrix metalloproteinases
N.	Nervus
NaGlu	Sodium gluconate
NaCl	Sodium chloride
PBS	Phosphate buffered saline
PGE_2	Prostaglandin E_2
PIP_2	Phosphatidylinositol-4,5-bisphosphate

PMCA	Plasma membrane Ca^{2+} ATPase
RCF	Relative centrifugal force
RPE	Retinal pigment epithelium
R_S	Access resistance
RT-qPCR	Reverse transcriptase quantitative polymerase chain reaction
RuR	Ruthenium Red
RyR	Ryanodine receptor
RVD	Regulatory volume decrease
SARS-CoV-2	Severe acute respiratory syndrome coronavirus type 2
SEM	Standard error of the mean
SERCA	Sarcoplasmic/ endoplasmic reticulum calcium ATPase
SOCs	Store-operated channels
TGF-β	Transforming growth factor beta
TRPs	Transient receptor potential channels
TRPV4	Transient receptor potential vanilloid 4
VO(C)Cs	Voltage-operated (calcium) channels
V1	N. ophthalmicus, first main branch of N. trigeminus
4αPDD	4α-phorbol-12,13-didecanoate
5,6-EET	5,6-epoxyeicosatrienoic acid

Abstract

The transient receptor potential vanilloid 4 (TRPV4) ion channel is a nonselective cation channel and osmosensor, which is permeable to calcium in response to various stimuli like moderate heat, hypotonicity, shear stress and pharmacological agonists like GSK1016790A. The functional expression of TRPV4 has already been validated in two out of three cellular layers of the cornea of the human eye, namely the corneal epithelium and endothelium. However, TRPV4 has not yet been investigated in the dominating cells of the corneal stroma, including the human corneal keratocytes (HCK). These cells contribute to the functionality of the cornea and play an important role in corneal wound healing. This Ca^{2+}-dependent process has to take place in an orderly manner, which is not least important for haze-free regeneration after ophthalmological surgical procedures or after keratitis. TRPV4 may have a great influence on Ca^{2+} regulation in HCK, and it therefore may also be involved in the complex process of stromal wound healing. Therefore, the aim of this thesis was to characterize the functional expression of TRPV4 channels in HCK using different activation mechanisms.

For this purpose, a SV40-induced immortalized permanent cell line of HCK was used as an *in vitro* cell model for stromal keratocytes. Fluorescence calcium imaging was used to measure intracellular calcium during the experiments. In addition, the classical and planar patch-clamp techniques were used to measure whole-cell currents.

Extracellular application of the specific TRPV4 agonist GSK1016790A (5 µmol/l) led to an increase of the fluorescence ratio f_{340}/f_{380}, which is proportional to the intracellular calcium concentration ($[Ca^{2+}]_i$). In addition, in- and outward whole-cell currents were also increased in the presence of GSK1016790A (10 µmol/l). Furthermore, two other TRPV4 activation mechanisms, namely hypotonic challenge as well as moderate heat (28°C – 34°C), led to similar effects in comparison with the pharmacological approach. The specific TRPV4 antagonist GSK2193874 (10 µmol/l) was able to suppress the GSK1016790A and hypotonicity induced calcium increase in HCK. Moreover, classical patch-clamp recordings revealed a chloride conductivity of HCK, since the negative reversal potential became more positive when sodium chloride was replaced by sodium gluconate in the extracellular measuring solution.

In conclusion, the results of this study demonstrate the functional expression of TRPV4 in HCK for the first time.

Zusammenfassung

Der Transient Receptor Potential Vanilloid 4 (TRPV4) Ionenkanal ist ein nichtselektiver Kationenkanal und Osmosensor, der als Reaktion auf verschiedene Stimuli wie moderate Hitze, Hypotonie, Scherstress und pharmakologischen Agonisten wie GSK1016790A für Kalzium permeabel ist. Die funktionelle Expression von TRPV4 konnte bereits in zwei von drei Zellschichten der Hornhaut des menschlichen Auges nachgewiesen werden, und zwar im Hornhautepithel und -endothel, jedoch noch nicht in den dominierenden Zellen des Hornhautstromas einschließlich der humanen Hornhautkeratozyten (HCK). Diese tragen zur Funktionalität der Hornhaut bei und spielen in der kornealen Wundheilung eine wichtige Rolle. Dass dieser calciumabhängige Prozess in geordneter Art und Weise abläuft, ist nicht zuletzt wichtig für eine trübungsfreie Regeneration nach ophthalmologischen operativen Eingriffen oder nach Keratitiden. Die TRPV4-Kanäle haben vermutlich einen großen Einfluss auf die Calciumregulierung in HCK und sind daher möglicherweise auch im komplexen Prozess der stromalen Wundheilung involviert. Das Ziel dieser Arbeit war daher die funktionelle Expression von TRPV4-Kanälen über verschiedene Aktivierungsmechanismen in HCK näher zu charakterisieren.

Zu diesem Zweck wurde eine SV40-induziert immortalisierte permanente HCK-Zelllinie als in vitro Zellmodell für stromale Keratozyten verwendet. Über das Fluoreszenz-Kalzium-Imaging wurde die intrazelluläre Kalziumkonzentration während der Versuche gemessen. Zusätzlich wurde die klassische und die planare Patch-Clamp Technik zur Messung von Ganzzellströmen verwendet.

Die extrazelluläre Zugabe des spezifischen TRPV4-Agonisten GSK1016790A (5 µmol/l) führte zu einem Anstieg des Fluoreszenzverhältnisses f_{340}/f_{380}, welches proportional zur intrazellulären Kalziumkonzentration ($[Ca^{2+}]_i$) ist. Die ein- und auswärtsgerichteten Ganzzellströme erhöhten sich ebenfalls in Gegenwart von GSK1016790A (10 µmol/l). Zwei weitere TRPV4 Aktivierungsmechanismen, wie hypotoner Stress und moderate Hitze (28°C – 34°C) führten zu ähnlichen Effekten wie im pharmakologischen Ansatz. Der spezifische TRPV4-Antagonist GSK2193874 (10 µmol/l) war in der Lage, den durch GSK1016790A und Hypotonie induzierten Calciumanstieg in HCK zu unterdrücken. Darüber hinaus zeigten klassische Patch-Clamp Messungen eine Chloridleitfähigkeit von HCK, da das negative Umkehrpotential nach Ersetzen von Natriumchlorid durch Natriumgluconat in der extrazellulären Messlösung positiver wurde.

Zusammenfassend lässt sich sagen, dass die Ergebnisse dieser Studie erstmals eine funktionelle Expression von TRPV4 in HCK demonstrieren.

1. Introduction

1.1 The human cornea

The human cornea belongs to the outermost layer (tunica fibrosis bulbi) of the eye and merges into the sclera, the second part of the outermost layer, at the so-called limbus **(Figure 1)**. In contrast to the conjunctiva, it is avascular and receives its nutrients only through diffusion from the tear fluid and from the aqueous humour in the anterior chamber of the eye. Small blood vessels at the outer edge of the cornea also support the nutrition exchange (1). In contrast to the lack of blood vessels, the cornea is a densely innervated tissue and is for example responsible for the corneal reflex caused by touch. The corresponding nerve for the cornea is the nervus (N.) ophthalmicus, the first main branch of the N. trigeminus (V1).

In its main function as a light breaker, the cornea, together with the tear film, constitutes two-thirds of the eye's total refractive power (1), corresponding to approximately 40 diopters (2). The shape of the cornea resembles an aspheric lens, and the cornea is more curved than the rest of the eye to provide this strong refractive power. The adult cornea measures an average horizontal diameter (white-to-white) of 11.71 ± 0.42 millimeters (mm) (3) and a vertical diameter of about 1 mm smaller, leading to a slight elliptical shape (2). The center of the cornea with 0.52 mm represents the thinnest point, whereas the limbus can measure 0.67 mm (2).

The cornea is divided into 5 parts: 3 cellular layers, namely the epithelium, the stroma and the endothelium, and 2 interfaces namely the Bowman's layer and Descemet's membrane (reviewed in (1); **Figure 2**). An additional Pre-Descemet's layer (Dua's layer) was discovered in 2013 (4).

The most special feature of the cornea is its transparency, which allows it to be like a transparent front window of the eye.

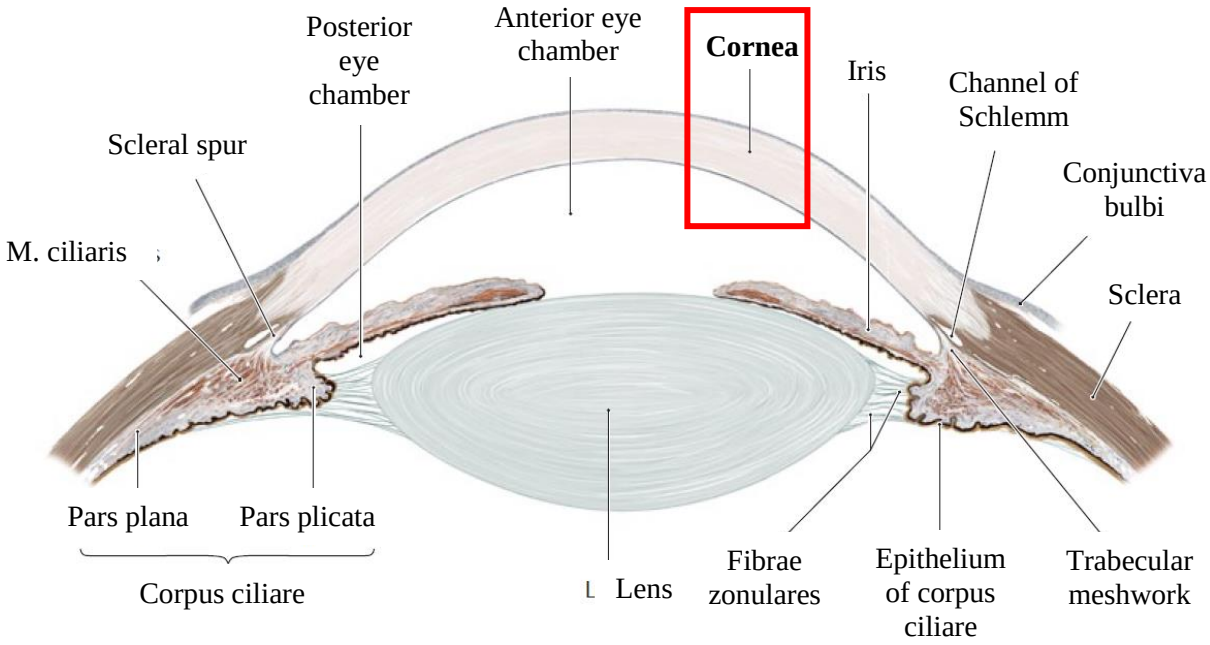

Figure 1: Scheme of a cross section of a cornea, lens and its holding apparatus, giving an overview of the location of the most important layer of the eye for this thesis: the cornea (framed in red). Picture adapted from Schuenke et al., 2018 (5, 6).

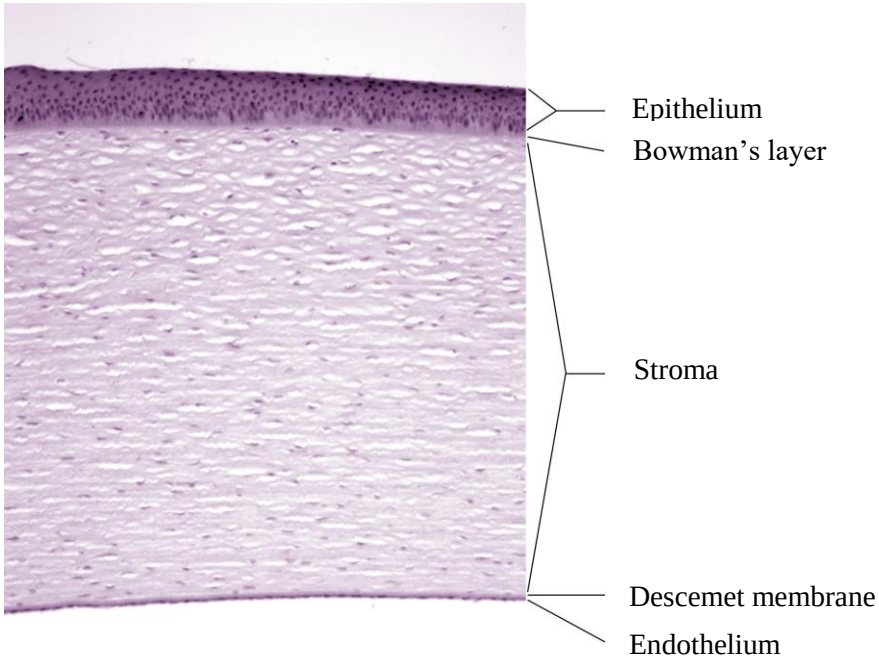

Figure 2: Light microscopic image of a cross section of the human cornea. The histological layers are shown in hematoxylin and eosin (HE) staining at 100x magnification. The corneal epithelium forms the outermost layer of the cornea, followed by a thin interface called Bowman's layer (reviewed in (1)). The corneal stroma is the thickest part of the cornea and is bounded to the anterior chamber of the eye by the

Descemet membrane and the thin endothelium, which is only one layer of cells. Adapted from Mergler et al., 2014 (7) and reprinted with permission.

The corneal epithelium

As the outermost layer of the eye, the corneal epithelium acts as a barrier to the outside environment (reviewed in (1)). It is classified as a non-keratinized stratified squamous epithelium and consists of 4 – 6 layers with a total thickness of 40 – 50 µm (1, 8). The corneal epithelium has the ability to renew itself through mitosis-capable basal cells in the lowest layer of the epithelium (9). Notably, the epithelial cells live about a week (10), and after apoptosis they are shed into the tear film but are constantly renewed by the basal cells (11). The basal cells are also responsible for the production of type IV collagen and laminin, the main contents of the epithelial basement membrane underneath the basal cells (1). The precursors of the basal cells are the stem cells located in the basal limbal epithelium, which migrate centripetally from there (12).

The corneal endothelium

The innermost layer of the cornea is the endothelium, with its hexagonal shaped cells. They form a low cuboidal or simple squamous monolayer with a thickness of approximately 4 µm in adulthood (1). Their main task is to maintain a proper fluid balance in the cornea and to keep the turgor in the stroma relatively low (pump and barrier function) (13). In contrast to the corneal epithelium, human corneal endothelial cells are not able to regenerate, which causes a decrease in the number of cells over lifetime (14, 15). In order to compensate for cell gaps and to ensure adherence, endothelial cells enlarge their cell bodies (1). If the cell density becomes too low, it impairs their maintaining of a balanced fluid content in the cornea, leading to stromal swelling and a decrease of transparency (1).

The corneal stroma

The Bowman layer is the acellular and condensed first part of the stroma, with a thickness of 15 µm and no regeneration ability (1). The corneal stroma is sandwiched between this layer and the Descemet membrane and makes up 90% of the entire corneal thickness ((16); **Figure 2**). It contains regularly arranged collagen fibers and superimposed keratocytes – the cells which were used in this study **(Figure 3)**. The majority of these sparsely distributed keratocytes are detectable in the anterior part of the stroma (17). The cells are connected to each other all over the stroma by cell extensions (dendrites) (18). The cell density in the human central stroma is about 20,500 cells/mm³ and decreases with age (17). Keratocytes are able to produce the important parts of the extracellular

matrix, like glycosaminoglycans, matrix metalloproteinases (MMPs) and collagen molecules, which is important for stromal homeostasis (1). These are mainly type I collagen in combination with type V collagen, forming strictly arranged collagen fibers in a parallel manner (19). Some parallel fibers form units together called fibrils, whereby these fibrils are arranged sequentially in parallel lamellae or layers (1). There are 200 to 250 lamellae in the corneal stroma of the human eye. Each lamellae forms a right angle to the fibers lying in adjacent lamellae (20). This type of precise arrangement of collagen fibers in combination with the extracellular matrix is amongst others responsible for the cornea's transparency, due to reduced light scattering (20-22).

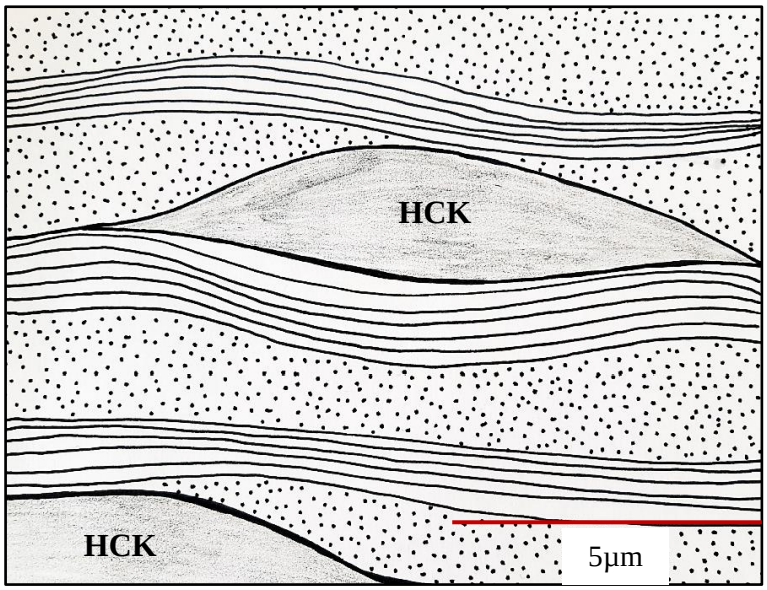

Figure 3: Illustration of the structure of the corneal stroma. The human corneal keratocytes (HCK) are located between the regularly arranged collagen fibers. The dots symbolize the collagen fibers in cross section and the lines the ones in longitudinal section. Drawing by Vivien Schmädicke after Cheng et al., 2015 (scale bar ≈ 5 µm) (23).

1.2 Corneal wound healing

There are several reasons for corneal injuries, including traumatic damage and above all ophthalmic surgeries. Furthermore, there are infectious diseases of the cornea such as bacterial or viral keratitis and trachoma caused by chlamydia. Recently, Kuo et al. published a case report of a female patient infected with the new SARS-CoV-2 presenting a unilateral keratouveitis. After her infection, the virus was detected in the corneal epithelium and limbus via RT-qPCR (24). Scarring in the cornea plays a major role in disease and healing processes. In particular, if the scar affects the visual axis, severe visual impairment and even blindness may occur (25). The ophthalmic surgeries that lead to cornea injuries include often performed interventions such as keratoplasty and refractive surgery (e.g. Laser-assisted in situ Keratomileusis (LASIK)), whose frequency is constantly increasing (26). After surgery, there is also the possibility of abnormal wound healing affecting the transparency of the cornea (26). Overall, corneal wound healing is a process – and often a problem – that occurs ubiquitously in ophthalmology. Nonetheless, the current commonly used treatment methods for corneal injuries are largely based on infection control and pain reduction (27). The therapy usually does not focus on wound healing and may even delay it (27). It is therefore important to understand how this biological mechanism works in detail to provide for an orderly wound healing with pharmacological or surgical aids. This would help to reduce the incidence of abnormal wound healing and scarring which is accompanied by corneal opacity (26).

The process of corneal wound healing is complex and can be attributed to the corneal cells (26). The mechanisms are different depending on the affected corneal layer but also interact with one another (26). In the corneal epithelium, the wound healing process is based on cell migration and differentiation of limbal stem cells (26). Therefore, the epithelium is able to renew itself through mitosis-capable cells in the basal cell layer, as mentioned before (9). Accordingly, no transformation into other cell types is necessary for the healing process in the epithelium (26). This is a special feature of stromal wound healing, wherein the keratocytes are able to transform into fibroblasts and myofibroblasts (28). After a stromal injury, the keratocytes located directly in the wound undergo cell death, but other ones nearby change their morphology (29). Keratocytes are normally quiescent. However, in the case of stromal damage, these cells become activated into fibroblasts by enlarging and becoming richer in cell organelles (28, 30). They migrate to the wound, proliferate by performing many mitoses (31) and produce matrix metalloproteinases (MMPs) as well as enzymes that have the ability to dismantle of the damaged extracellular matrix (ECM) (30). In these processes, some biological messenger substances like the proinflammatory cytokine interleukin-1α (IL-1α) play an important role. The cytokines reach the stroma through

the defective epithelial basement membrane, which no longer acts as a barrier (32). IL-1α is responsible for the triggering of the cell death of some underlying keratocytes, as well as and for the activation and transformation into activated keratocytes (**Figure 4**, (30, 32)). Other biological messengers from the epithelium are growth factors like transforming growth factor beta (TGF-β), which is responsible for the transformation of a little subpopulation from keratocytes into myofibroblasts (33). Myofibroblasts are able to produce a huge amount of new unstructured ECM (**Figure 4**, (33)). Under normal and good conditions, a proper healing process goes on with the repair of the epithelial basement membrane, which is promoted by keratocytes and fibroblasts (19). Finally, TGF-β can no longer pass the membrane and the myofibroblasts undergo cell death (30). The production of IL-1α is taken over by the activated keratocytes. Thus, they are able to preserve themselves and order the newly formed ECM with the help of produced MMPs (30). The regression of myofibroblasts is important for haze-free healing due to their opacity. Myofibroblasts are only capable of forming corneal crystallins to a limited extend, which makes them opaque because of light scattering (34). Therefore, the transformation from fibroblasts to myofibroblasts can be critical especially if excessive conversion occurs, e.g. in the context of abnormal wound healing. On the one hand, myofibroblasts are helpful due to their contractility and the prevention of the progressive widening of the wound gap in the context of wound repair (35). On the other hand, they are associated with corneal opacity (35-37). The produced fibrotic and disorganized extracellular matrix leads to maze and visual restrictions (35). Due to this disordered production, the repair of the epithelial basal membrane is hindered. In addition, the growth factors can still pass the membrane unimpededly, so that the myofibroblast production persists (37). In conclusion, disturbances in the healing process of the epithelial basement membrane are correlated to a prolonged turbidity of the cornea (38). Therefore, the transformation process of corneal keratocytes during the wound healing process is able to regenerate the tissue. Unfortunately, this process may also lead to fibrosis and scarring affecting the corneal transparency forever, or at least for a long time (19).

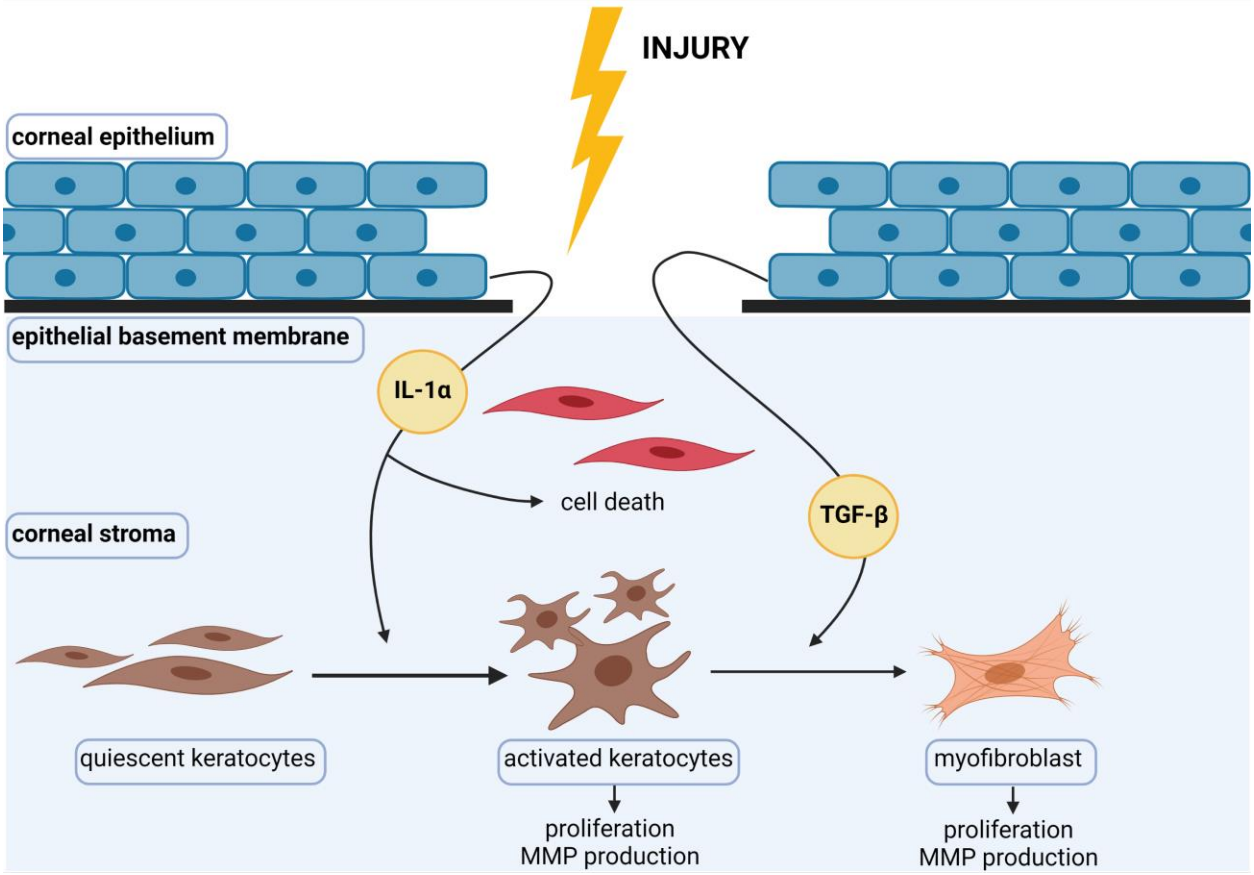

Figure 4: Scheme summarizing corneal wound repair at cellular level. The corneal epithelium produces messenger substances that reach the stromal keratocytes via the defective epithelial basement membrane (32). IL-1α, which is one of these substances, ensures that some keratocytes in the close environment of the damage undergo cell death. Furthermore, the activation of quiescent keratocytes nearby is supported (30, 32). After being activated to fibroblasts, these cells proliferate and produce matrix metalloproteinases (MMPs). MMPs are enzymes that are able to degrade the damaged extracellular matrix (ECM) (30). The growth factor TGF-β can also pass through the gap in the basement membrane, and it stimulates some activated keratocytes to transform to myofibroblasts. They are able to produce a huge amount of new ECM (33). Created with BioRender.com by Vivien Schmädicke. Modified by West-Mays et al., 2006 (30).

1.3 Corneal wound healing and calcium

As described in detail in the previous chapter, corneal wound healing is a complex procedure (26). It involves basic cellular processes such as cell proliferation, migration and differentiation as well as cell death (11, 39). All of these processes are mediated by a physiologically very important cation: calcium. The properties of human corneal keratocytes, which were used in this thesis, are also formed by calcium-dependent regulatory mechanisms, like other cells.

For example, cells are able to migrate during the wound healing process due to integrin-mediated adhesion which is dependent on calcium (40). Directly after an injury, calcium waves can be detected as an important signal for the beginning of wound healing and communication with unharmed cells nearby (41). Tran et al. revealed an intracellular calcium increase in the cells located directly at the wound bed (42). They influenced this rise in concentration by blocking the calcium influx into the cell (42). This led to a reduced cell motility, the functionality of which is actually essential for wound closure (42). In contrast, artificially increasing calcium intake resulted in improved cell motility (42).

These facts provide convincing evidence that calcium plays an important role in the process of corneal wound healing and that it is worth having a closer look at calcium regulation as well as the cell structures involved in it.

1.4 Ion channels and their role in calcium regulation

As mentioned before, the exchange of calcium ions is crucial since the calcium homeostasis is essential for major cell functions like signaling and apoptosis (43, 44). There is a huge Ca^{2+} concentration difference across the Ca^{2+}-impermeable cell membrane with, on one hand, 0.1 µmol/l inside the cytosol and, on other hand, a free Ca^{2+} concentration of 1200 µmol/l outside the cell (**Figure 5**, (45)). Therefore, even very small Ca^{2+} concentration changes manage cellular calcium signaling (45).

Proteins are essential for this ion exchange transport. They are located in the cell membrane, but also in the membrane of cell organelles, such as the endoplasmic reticulum. Amongst others, these proteins include ion pumps and channels, the latter being passive. Ion channels are transmembrane proteins forming a pore to enable the passage of electrically charged particles across membranes along the existing electrochemical gradient. They have a passage rate of over ten million ions per second (46). There are some classification possibilities for these channels, e.g. regarding the gating options. Thus, ion channels can be opened by voltage changes of the membrane potential, by mechanical stimuli, by light, by temperature but also by specific ligands (47). They can be selective for specific ions like potassium, or unspecific like most of the transient receptor potential channel superfamily, the TRPs (48).

An increase of intracellular calcium concentration can be caused by a calcium influx from extracellular space through ion channels to the intracellular space of the cell. The channels responsible for this influx are, for example, transient receptor potential channels (TRPs), voltage-operated calcium channels (VOCs) and store-operated channels (SOCs). In contrast, the plasma

membrane Ca^{2+} ATPase (PMCA) is an ion pump contributing to an active calcium efflux from inside the cell to extracellular space (**Figure 5**). The Na^{+}/Ca^{2+} exchanger NCX is also able to cause an efflux unless it can also work in a reverse mode after depolarization in excitable cells (49). In addition to the TRPs, VOCs and SOCs, an intracellular calcium increase can be triggered by a calcium release from intracellular calcium stores such as the from endoplasmic reticulum (ER) (50). In the intracellular space of a cell, there are Ca^{2+} releasing channels like ryanodine- or inositol-1,4,5-trisphosphate (IP_3) receptors leading to this intracellular calcium increase. This process in turn activates the SOCs in the cell membrane for a further increase in $[Ca^{2+}]_i$. The effect of the release of calcium from intracellular stores can be subsequently compensated by internal calcium pumps like sarcoplasmic/endoplasmic reticulum calcium ATPase (SERCA) (51).
Overall, a large group of Ca^{2+} permeable channels, such as the transient receptor potential channels (TRPs), predominantly contribute to the regulation of $[Ca^{2+}]_i$.

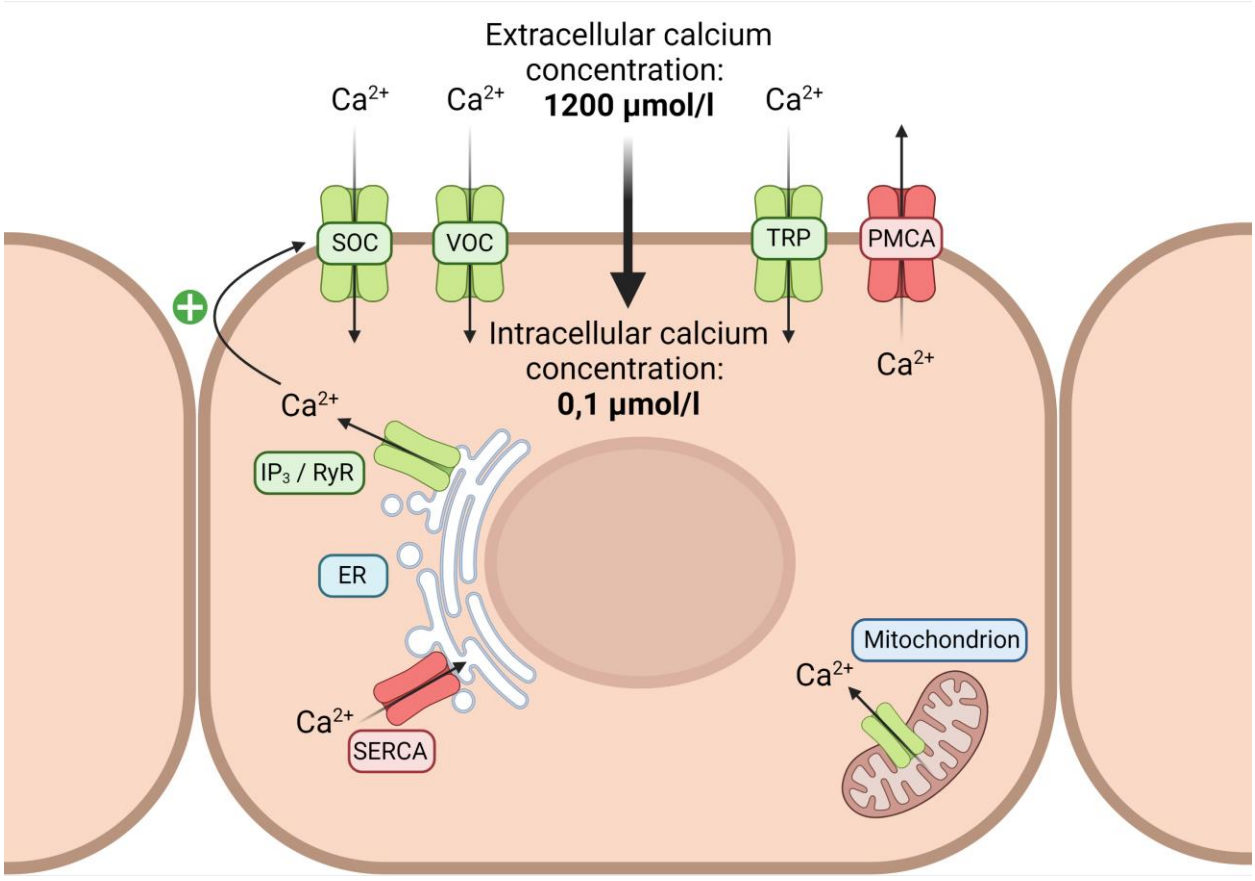

Figure 5: Schemata of the Ca^{2+} transporters and concentration difference in a sample cell. The extracellular calcium concentration is 1200 µmol/l, whereas the intracellular calcium concentration is much lower with 0.1 µmol/l (45). The green channel icons stand for the possibilities for calcium influx into the cytoplasm (SOCs, VOCs, TRPs at the outstanding plasma membrane of the cell, and IP_3 or ryanodine receptors (RyR) in membranes of cell organelles like the ER). The red channel icons represent the ion pumps, with the help

of which a calcium efflux is possible from the cytosol to the extracellular space (PMCA) or to intracellular stores (SERCA). A calcium release into the cytoplasm from intracellular stores of mitochondria is also possible. Created with BioRender.com by Vivien Schmädicke.

1.5 The transient receptor potential channel superfamily

The transient receptor potential (TRP) multigene superfamily consists of 28 different subunit genes (46, 52, 53). All of them encode for integral membrane proteins, functioning as non-selective cation channels with various activation modalities (54). Based on their amino acid sequence, the TRPs are subdivided into 7 subfamilies **(Figure 6)**: TRPA (ankyrin), TRPC (canonical/classical), TRPM (melastatin), TRPML (mucolipin), TRPP (polycystin), TRPV (vanilloid) and TRPN (Drosophila NOMP protein; NOMP = No-mechano-potential C), which is the only one not found in mammals (46, 53).

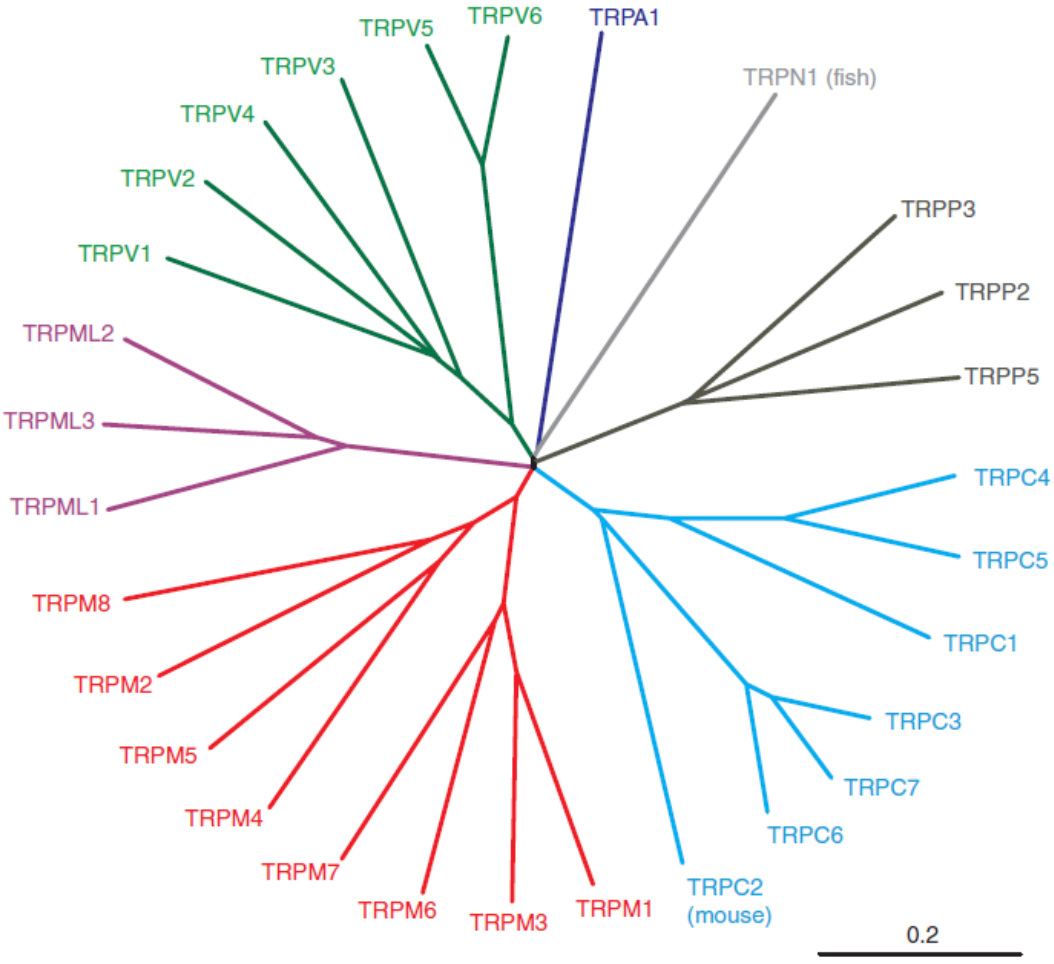

Figure 6: Overview of the 7 subfamilies of TRP channels, arranged according to their phylogenesis. Picture reprinted with permission from Nilius et al., 2011 (54).

TRPs were first detected in the sensory system of the fruit fly Drosophila melanogaster (55, 56). In 1969, Cosens and Manning made the observation of a Drosophila mutant called “trp” behaving as blind in response to steady light and also showing also a different electroretinogram: instead of developing a persistent membrane current as the wild type did, the “trp” mutant flies showed a transient current which led to their name (55). The photopigment characteristics and the light-sensitive channels of the flies appeared normal. Therefore, it was suggested that the “trp” defect leads to a lack of a protein responsible for an intermediate step (57). Over 20 years were needed until Montell and Rubin identified the “trp” gene as a transmembrane protein in 1989 (58).

A TRP channel amino acid consists of 6 transmembrane domains (S1 – S6), wherein a pore loop is located between the fifth and sixth segment (48, 59). The amino (NH_2) and the carboxyl (COOH) ending are both located intracellularly and are variable in composition and length (**Figure 7**, (48)). At the N-terminal end, the TRPC, TRPV, TRPA and TRPN channels show ankyrin repeats in different extents and are part of the group 1 TRPs (59). The TRPP and TRPML subfamilies contain a long loop between S1 and S2 and are, due to their differences, counted together as group 2 TRPs (**Figure 8**, (59)). Closely related TRPs are able to form heteromultimers with each other since this capability is a possibility for the channels to vary their functions and features (59). They can also build complexes with accessory or signaling proteins (54).

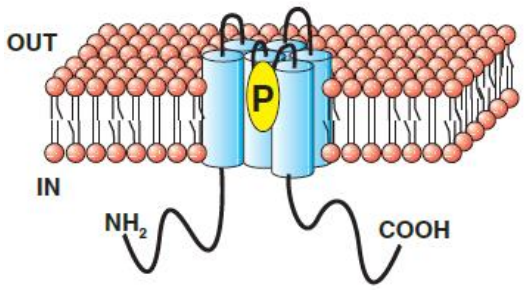

Figure 7: Molecular structure of TRPs. Picture reprinted with permission from Nilius et al., 2011 (54).

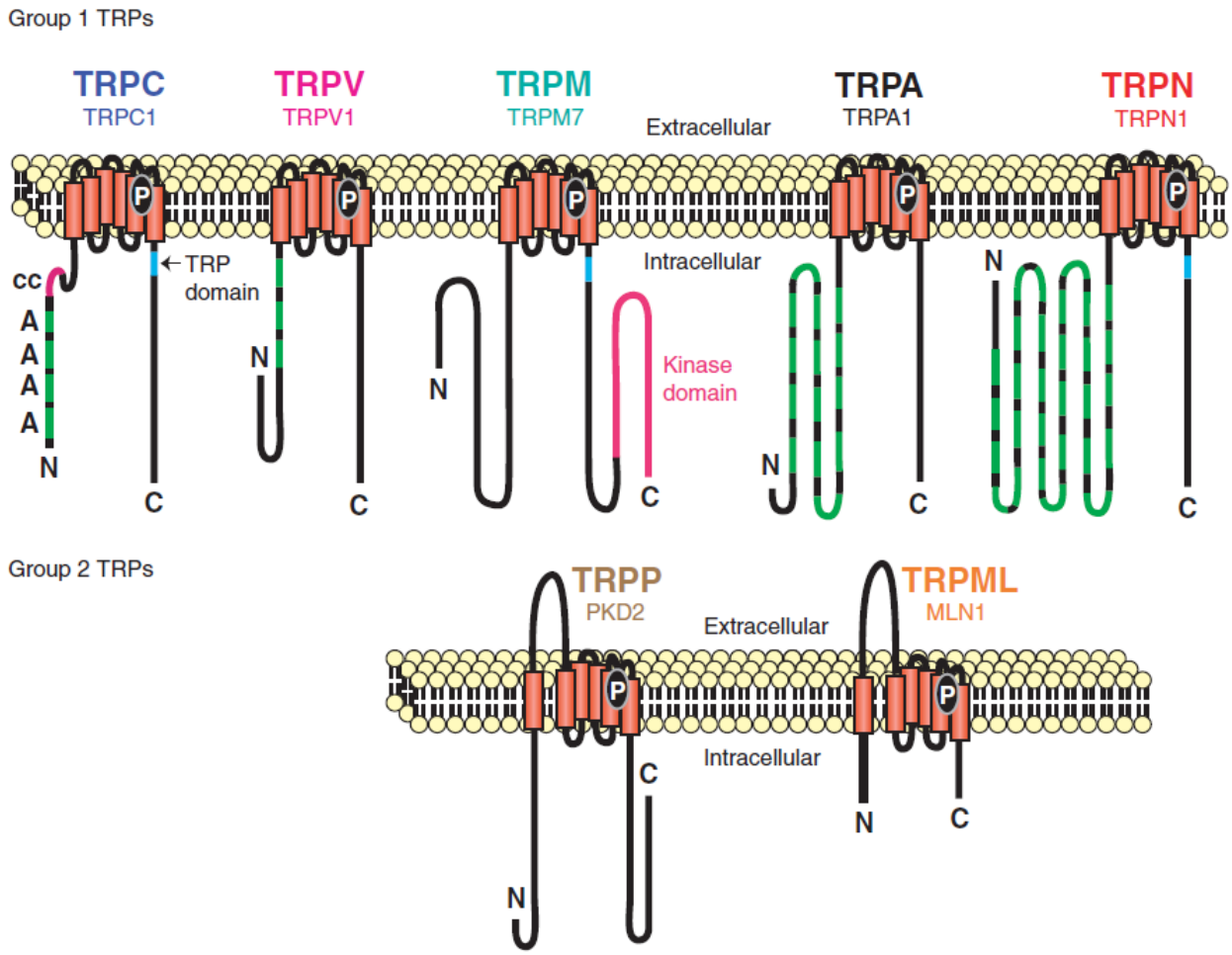

Figure 8: Differences in molecular structure between the two TRP groups. The letter "A" stands for the ankyrin repeats, the letter "N" for the amino ending and "C" for the carboxy ending of the amino acid. Picture adapted from Montell, 2005 (53).

TRPs can be found in almost every tissue and are located in nearly all membranes – especially in plasma membranes, where they control the ion exchange and therefore things like osmoregulation and muscle contractions (reviewed by Nilius et al., 2011 (54)). This also applies to ocular structures. Notably, there should be a differentiation between TRPs in excitable cells (neurons in corneal nerve bundles within the corneal epithelium and stroma) and non-excitable cells in the surrounding cell tissues. More precisely, some subtypes of TRPs have been detected in non-excitable ocular cells like the retinal pigment epithelium (RPE (60, 61)) and on excitable dendrites of ON-bipolar neuronal cells of the human retina (62). Additionally, human uvea (61) and lenses (63) containing non-excitable cells express numerous TRP channel types. To focus on TRPs in the human cornea, one can resume a wide distribution of channels across all layers of the cornea (see **Table 1**).

TRP channel	Tissue localization	References
TRPC4	epithelium	(64)
TRPV1	nerve, epithelium, keratocytes, fibroblasts, endothelium, conjunctiva	(65), (66), (67), (68), (69), (70)
TRPV2	epithelium, endothelium	(68), (71)
TRPV3	epithelium, endothelium	(68), (71)
TRPV4	epithelium, endothelium	(72), (73)
TRPM2	endothelium	(74)
TRPM8	nerve, epithelium, keratocytes, endothelium	(75), (67), (76), (77)
TRPA1	nerve, endothelium	(78), (79)

Table 1: Overview of TRPs in the cornea. Adapted and modified from Mergler et al., 2019 and 2020 (80, 81) and from Reinach et al., 2015 (82, 83).

All TRPs are permeable to calcium cations, with the exception of TRPM4 and TRPM5 (59, 84-88). This leads to the conclusion that TRPs are involved in many calcium mediated signaling cascades, resulting in an influence on basic cellular functions, which also includes apoptosis.
In excitable cells, TRPs are crucial for sensory functions like vision, olfaction, hearing, taste, touch, pheromone signaling, nociception and thermal sensation as well as acting as cellular sensors (reviewed in Damann et al., 2008 (89) and in Nilius et al., 2011 (54)). Moreover, they are capable of sensing mechanical stress in membranes and changes in pH, and can be activated and regulated by a wide range of options (**Figure 9**, (54)). Among these options is voltage dependent activation (90, 91). Furthermore, there is modulation by membrane phospholipids (e.g., phosphatidylinositol 4,5-bisphosphate (PIP_2, (92)) and kinase-dependent phosphorylation as well as regulation by endogenous or exogenous ligands (54). For example, temperature-sensing channels like TRPV1 (the "heat receptor") is activated by capsaicin (93), a spicy natural alkaloid, and TRPM8 (the "cold receptor") is enabled by menthol, an extract from the mint plant (94, 95). In conclusion, environmental stimuli can be converted into Ca^{2+} transients by TRP channels (80). These ion influxes via TRPs depolarize the cell membrane and in turn trigger activation potentials from a certain threshold potential. In contrast, TRPs are also expressed in non-excitable cells. In human corneal epithelial cells, it was demonstrated that TRPV1 activation by capsaicin led to a release of pro-inflammatory cytokines through mitogen-activated protein kinase (MAPK) signaling (66).

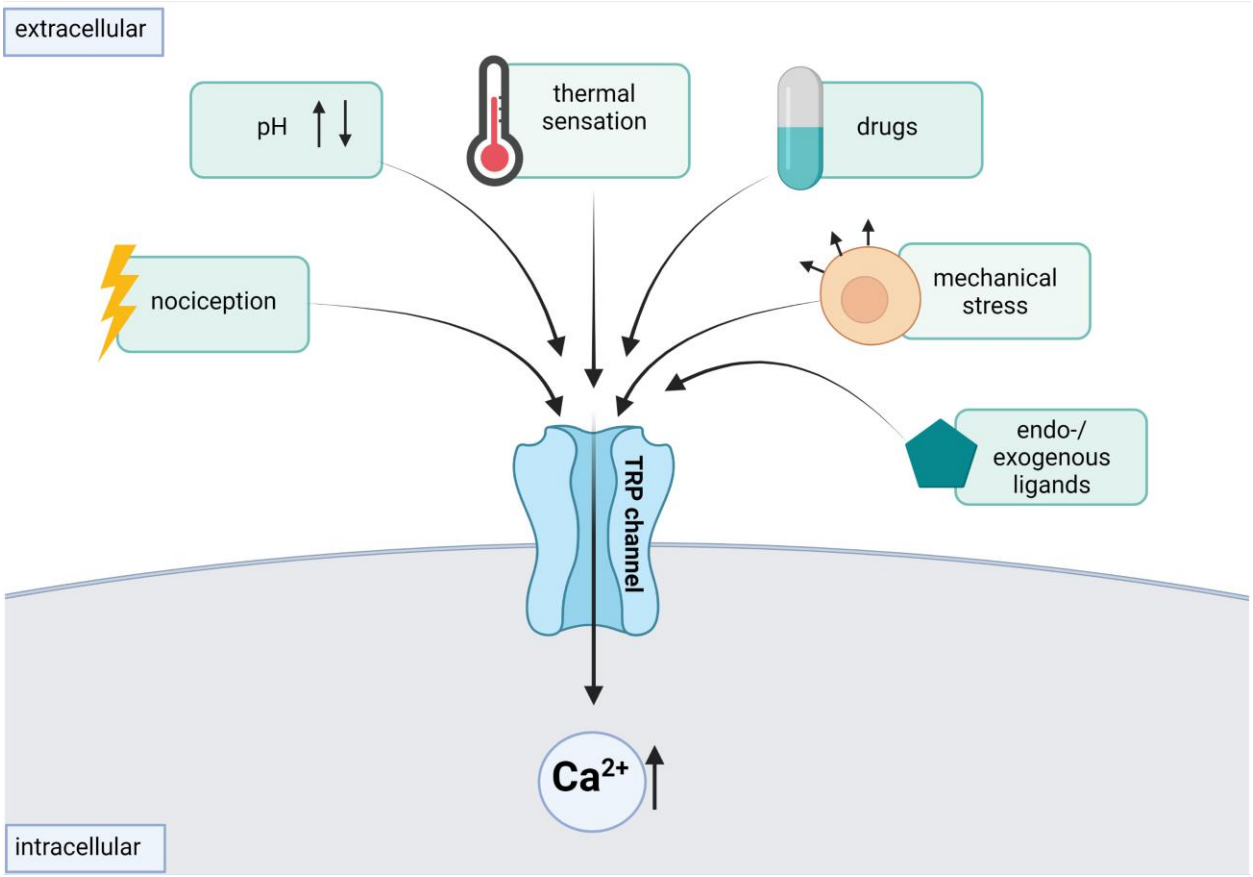

Figure 9: Schematic overview of the most common activation possibilities of TRP channels. Created with BioRender.com by Vivien Schmädicke.

Broadening the horizon of research into physiological processes, the TRP channel investigation also revealed some pathophysiological explanations for diseases (reviewed by Nilius et al. (88, 96)). The defects of several TRP genes lead to so-called “channelopathies”, which are hereditary diseases caused by altered ion flows due to amended channel functions (54). To give an example, one of over 50 mutations in the TRPV4 gene is responsible for skeletal dysplasia pathogenesis, more precisely the autosomal dominant brachyolmia (97). It has also been suggested that some channelopathies are involved in the development of cancer. Notably, in 2001 Tsavaler et al. revealed the relation of altered TRPM8 expression with prostate, breast, colon and lung cancer as well as dysplasias of skin origin (98).

It is thus self-explanatory that the TRPs have gained great pharmacological research interest and become important pharmacological targets (54).

1.5.1 The transient receptor potential vanilloid 4 (TRPV4) channel

This doctoral thesis is mainly focused on the transient receptor potential vanilloid member 4 (TRPV4) channel. This channel was first described as a nonselective and calcium-permeable cation channel and osmosensor by Liedtke and Strotman in the year 2000 (99, 100). At that time, this channel was initially listed under various names: "vanilloid-receptor related osmotically activated channel" (VR-OAC), "vanilloid receptor-like channel 2" (VRL-2), "OSM9-like transient receptor potential channel, member 4" (OTRPC4) and "transient receptor potential 12" (99-102).
The human TRPV4 protein is composed of 871 amino acids (100), which show a symmetric tetrameric architecture according to other TRPV channels (103). The TRPV4 channels are used to build homotetramers (104), but heterotetramers are also possible, e.g., with TRPC1 (105) or TRPP2 (106).
TRPV4 can be detected ubiquitously in multiple tissues (107), and thus also in the human eye (see Chapter 1.5.2).
Interestingly, TRPV4 is only weakly calcium selective, and more permeable to divalent cations like barium (Ba^{2+}), strontium (Sr^{2+}) and magnesium (Mg^{2+}) than to monovalent cations like potassium (K^{+}), sodium (Na^{+}) and cesium (Cs^{+}) (108, 109). TRPV4 exhibits both inward and outward rectification and an Eisenman IV permeability sequence (108).
TRPV4 can be activated by a wide range of stimuli, which has led to the appropriate description of a "promiscuous opening behavior" by Nilius et al. (110, 111). The first described activation mechanism was cell swelling due to hypotonic challenges. Therefore, the TRPV4 channel was designated as "osmosensor" (99, 100). In contrast, an increase in osmolarity (hypertonicity) inhibited the channel activity, which was initially triggered by hypotonicity (112). Consequently, Becker et al. assumed in 2005 that TRPV4 is of importance for regulatory volume decrease (RVD, (113)). This describes the ability of a cell to recover from swelling in a hypotonic surrounding (113). Conversely, hypertonic cell stress led to shrinking cells (114). Moderate heat in a range from ≈ 27 - 35°C was exposed as another stimuli for TRPV4 activation (115-117). This phenomenon led to the assumption that the channel is active at body temperature (118). Although the human cornea is exposed to environmental influences (e.g. temperature), the average human corneal temperature is approximately between 32°C and 34°C (119). However, the role of TRPV4 in regulating the behavior according to temperature has not yet been sufficiently clarified (120). Further activation stimuli are shear stress (121) and a range of chemical substances, as further described below (109, 122). Interestingly, the channel possesses the ability to be spontaneously activated without any agonist stimulation (120). This observation underlines its great importance in basic physiological functions like calcium homeostasis and osmoregulation (120). The TRPV4

channel is also involved in processes like vascular tonicity (123), bone homeostasis (124) and nociception (125).

Pharmacologically, the TRPV4 channel can endogenously be activated by 5,6-epoxyeicosatrienoic acid (5,6-EET), an oxidative metabolite of arachidonic acid **(Figure 10 A)**, (122)). Furthermore, TRPV4 can be activated by phorbol ester compounds like 4α-phorbol-12,13-didecanoate (4αPDD; **Figure 10 B**) (109). Notably, GSK1016790A is the most reliable TRPV4 tool for functional TRPV4 channel detection. It is a very sensitive and potent TRPV4 agonist for the electrophysiological characterization of the TRPV4 channel (**Figure 10 C**) (126, 127).

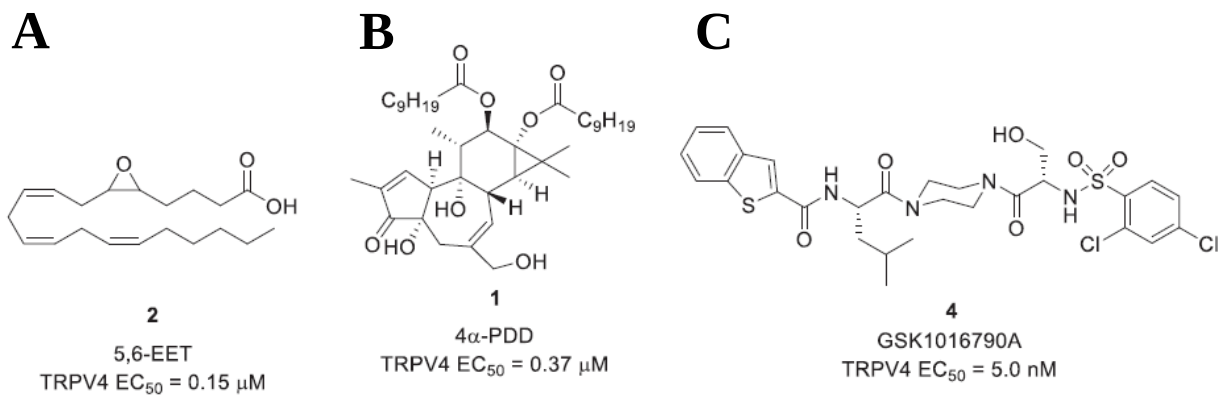

Figure 10: The chemical structure of important TRPV4 agonists. (**A)**: 5,6- epoxyeicosatrienoic acid (5,6-EET); (**B)**: 4α-phorbol 12,13-didecanoate (4αPDD); (**C)**: GSK1016790A. This agonist was used in this study. EC_{50} stands for the *half maximal effective concentration* – a measure of the potency of a drug. Pictures reprinted with permission from Lawhorn et al., 2020 (107).

To inhibit the TRPV4 channel, there are some non-selective blockers like Ruthenium Red (RuR, (109)) and citral, a bioactive component of lemongrass (121). In addition, more selective and specific blockers are RN-1734 (127), HC-067047 (128) and GSK2193874 **(Figure 11**) (129, 130). Specifically, GSK2193874 was shown to have a preventive and resolutive effect on lung edema as part of heart failure (130). Interestingly, another GSK TRPV4 blocker, GSK2798745, represents a promising and feasible approach for the treatment of lung edema in COVID-19 (131, 132).

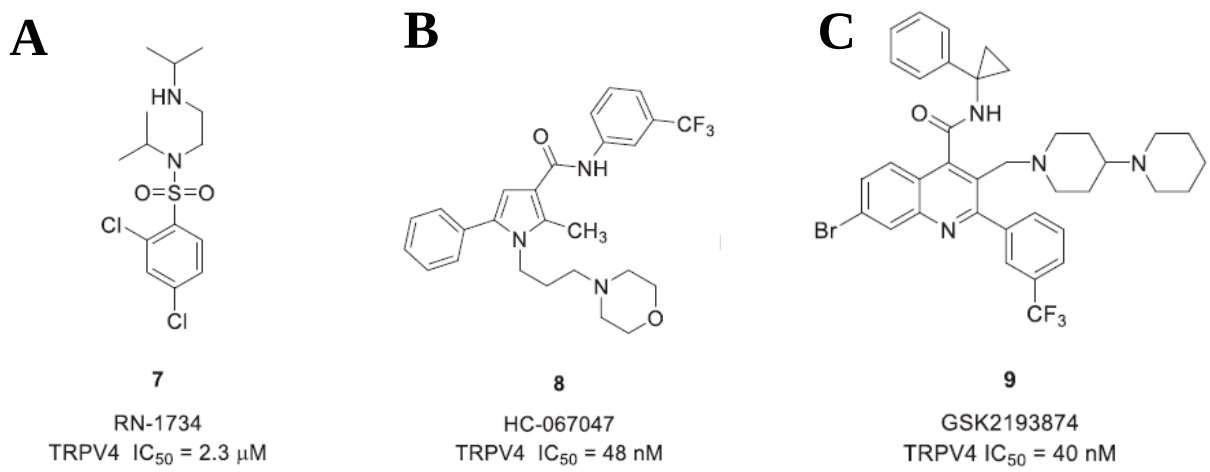

Figure 11: The chemical structure of important selective TRPV4 inhibitors. (**A):** RN-1734; (**B):** HC-067047; (**C):** GSK2193874. This antagonist was used in this study. IC_{50} means the *half maximal inhibitory concentration* – a measure of the potency of a drug to inhibit a process. Pictures reprinted with permission from Lawhorn et al., 2020 (107).

Besides its expression in the epithelium and endothelium of the cornea (see **Table 1**) (72, 73), TRPV4 channels can be found in the conjunctiva (69), in RPE cells (60) and in porcine lens epithelium (133).

The existence of the TRPs in ocular structures is relevant for many physiological processes taking place in healthy eyes. It is therefore obvious that altering TRP expression may play a role in the pathogenesis and treatment of ocular diseases. Accordingly, the corneal transparency will decrease if the TRP channel functions in the corneal endothelium fail (73, 134). More specifically, Pan et al. revealed that TRPV4 activation in the human corneal epithelium is essential for initiating RVD behavior (72), which is an essential process for maintaining vital cells. Notably, the TRPV4 channel itself is involved in the regulation of the intraocular pressure and, therefore, a potential pharmacological target for the treatment of ocular hypertension (135). Osmosensitive TRPs like TRPV4 (and also TRPV1) are important in the formation of inflammatory mediators and alteration of tear composition (69). This makes them possible therapeutics for the dry eye disease (DED, Keratoconjunctivis sicca), which many people worldwide suffer from (69).

1.5.2 TRPs and wound healing

TRPs also have an influence on the complex process of corneal wound healing, as mentioned in Chapter 1.2. As already stated, the transformation from keratocytes into myofibroblasts is regulated by the transforming growth factor TGF-β. This causes opacity that often lasts for a long time – up to years after the injury – or irreversible scarification (33, 35-37). The regeneration of the cornea can only lead back to complete transparency if the extracellular matrix is formed into an ordered structure again and the myofibroblasts become apoptotic (37, 136). The latter happens as soon as TGF-β can no longer reach the cells (37). Okada et al. found out in 2011, in an alkali burn model of mice cornea, that the lack of one member of the TRPs, the TRPV1 channel, leads to a reduction of TGF-β gene expression (137). Accordingly, the myofibroblast differentiation was blocked as well, making this channel an interesting target for therapies concerning improved wound healing (137). Turan et al. recently took advantage of this information for their own study and revealed that L-carnitine, an osmoprotective agent, is able to suppress TRPV1 activity in HCK cells leading to an improved wound healing (138). Therefore, it is suggested that the TRPV4 channel may have an impact on corneal wound healing. Notably, it was found that TRPV4 is responsible for fibrosis and inflammation since the loss of this channel in knock-out mice lead to a notable improvement in the wound healing of alkali-burning mouse corneas (139). Inflammatory processes such as the release of interleukin-6 (IL-6) from macrophages and the expression of genes relevant for fibrosis were downregulated in the absence of TRPV4 (139). Interestingly, the changed TRPV4 expression had no impact on TGF-β (139). These findings are in line with the previously postulated fact that TRPV4 activation is responsible for idiopathic pulmonary fibrosis in mice (140). Specifically, Okada et al. revealed in their study that TRPV4 is associated with a TGF-β modulating effect and myofibroblast transdifferentiation (139). In contrast to the previously mentioned negative influences of TRPV4 activation on haze-free corneal healing, Okada et al. also revealed in 2019 that the TRPV4 channel situated in impaired trigeminal nerves provides for corneal epithelial repair in a sensory denervated cornea (141). This occurs via TRPV4-associated stimulation of limbal stem cells and upregulation of nerve growth factor (NGF, see **Figure 12**, (141)).

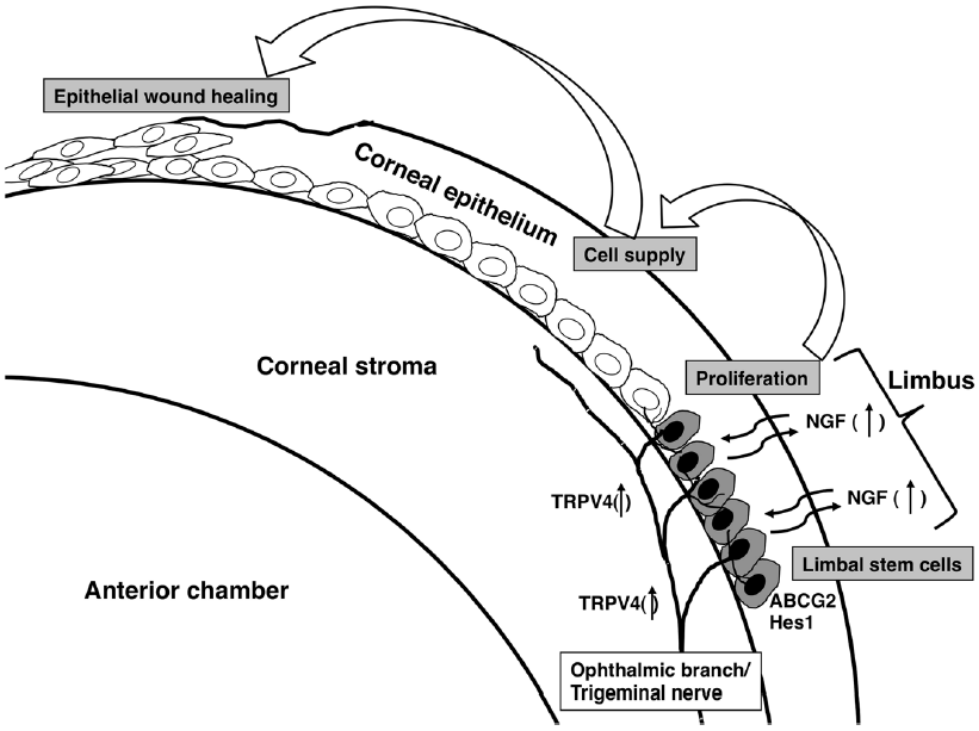

Figure 12: Sketch of the research findings of Okada et al., 2019. In sensory denervated cornea, the TRPV4 channel situated in trigeminal nerves provides for an activation of limbal stem cells and the release of nerve growth factor (NGF) (141). Thus, the epithelial wound healing is promoted. Picture reprinted with permission from Okada et al., 2019 (141).

Based on these studies, the role of TRPV4 in the maintenance of a vital cornea and in wound repair is complex and elusive. It is therefore worth pursuing these approaches further and advancing research in this area to find new therapeutic options that prevent abnormal corneal wound healing.

1.6 Aims of study

Since the TRPV4 channel has already been examined in the corneal epithelium and endothelium (69, 72, 73), it has been suggested to ascertain whether this channel is also functionally expressed in HCK. Therefore, this study was undertaken to investigate putative functional TRPV4 expression in HCK using different activation mechanisms and different experimental methods. To achieve this, the study was subdivided into different parts according to the main functions of TRPV4 **(Figure 13)**:

1) Pharmacological approach

   To identify TRPV4 channels in HCK, the specific agonist GSK1016790A and the specific antagonist GSK2193874 were used (126, 129). Two functional assays were used for the pharmacological approach: the calcium imaging method and the planar patch-clamp technique.

2) Examination of the TRPV4 properties as an osmosensor

   HCK were exposed to hypotonic stress using a hypotonic solution with an osmolarity below physiological values (~233 mOsmol). The calcium imaging method was used to analyze the calcium response pattern.

3) TRPV4 activation by moderate heat

   HCK cells were exposed to moderate heat (28°C – 34°C) to measure any change occurring in $[Ca^{2+}]_i$ that is attributed to a TRPV4 activation. The calcium response patterns were analyzed using the calcium imaging method.

4) Role of anion channels: examination of a putative chloride conductivity of HCK cells

   Classical whole-cell patch-clamp recordings of HCK were used to evaluate whole-cell current patterns, with a focus on chloride as charge carrier. Specifically, the chloride conductivity in a high chloride- and in a low chloride-containing solution was measured.

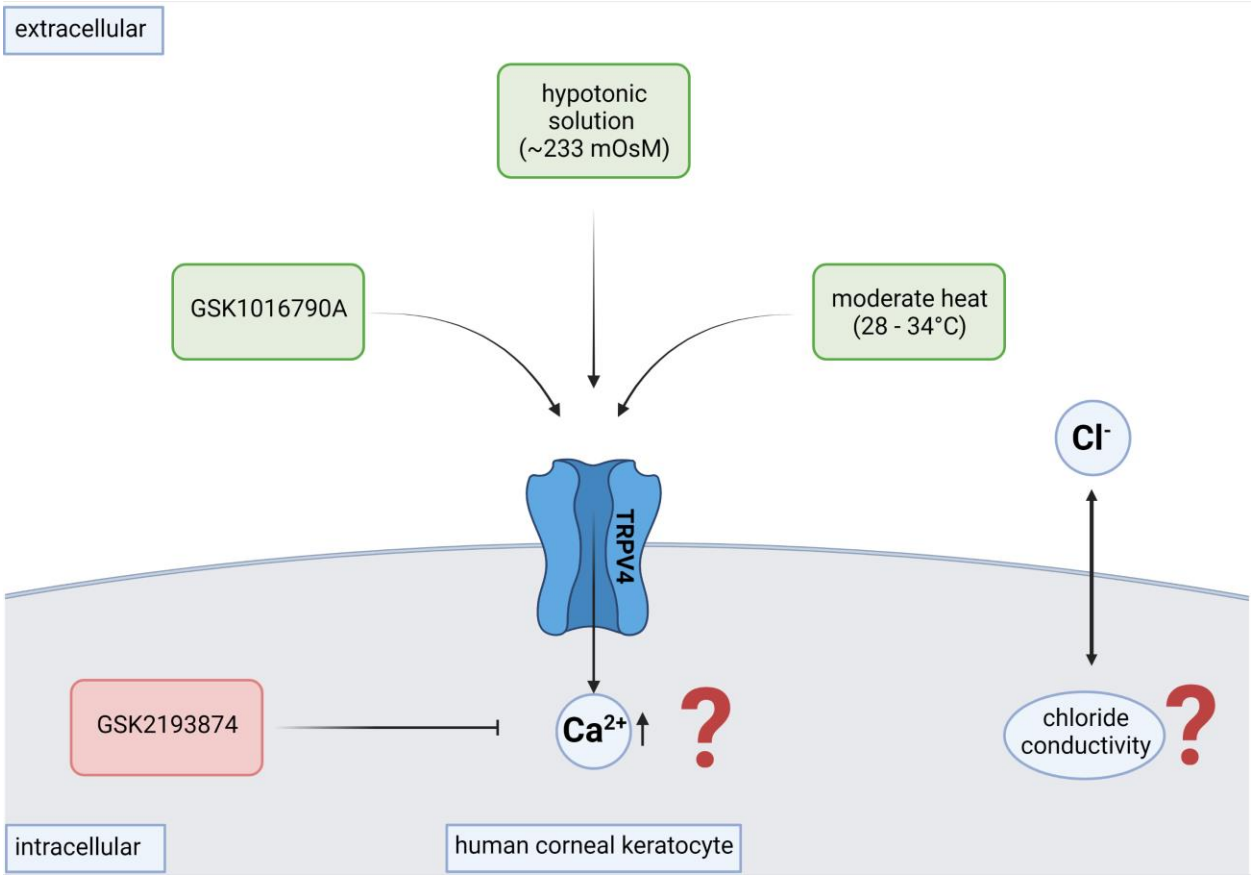

Figure 13: Schematic overview of the research objectives of this thesis. Created with BioRender.com by Vivien Schmädicke.

As mentioned before, changes in TRP channel expression and activation can lead to diseases and impaired wound healing. This suggests that these channels may be potential targets for a possible pharmacological treatment of corneal diseases or corneal damage. Therefore, it is worth gaining more knowledge about TRPs, such as TRPV4 channels in HCK.

2. Materials and methods

2.1 Chemicals and solutions

Solutions and chemicals for cell culture

The supplements for the cell culture and the medium were purchased from Biochrom AG (Berlin, Germany), Life Technologies Invitrogen (Karlsruhe, Germany) or Sigma-Aldrich (Munich, Germany).

Solution and chemicals for calcium imaging

The Ringer-like solution was used as control solution for calcium imaging experiments containing (mmol/l): 150 NaCl, 6 CsCl, 1.5 $CaCl_2$, 1 $MgCl_2$, 10 HEPES and 10 glucose at pH 7.4 and an osmolarity of 317 mOsmol (142).

The isotonic and hypotonic solution for the cell swelling recordings in the calcium imaging setup consisted of (mmol/l): 105 NaCl, 6 CsCl, 1,5 $CaCl_2$, 1 $MgCl_2$, 10 HEPES-acid and 10 glucose with an additional 80 D-Mannitol in the isotonic solution. Both solutions were at pH 7.4, with an osmolarity of 313 mOsmol in the isotonic solution and 233 mOsmol in the hypotonic solution (142).

Solution and chemicals for classical patch-clamp recordings

The solutions were prepared according to Spahn et al., 2014 (143).

The internal solution for classical patch-clamp recordings contained (mmol/l): 15 NaCl, 5 KCl, 10 HEPES, 120 NaGlu, 5 EGTA, and10 Mannitol with an osmolarity of 305 mOsmol.

At the beginning of the experiment, the external or "bath" solution consisted of (mmol/l): 135 NaCl, 5 KCl, 10 HEPES, 2 $MgCl_2$, 2 $CaCl_2$ and 10 glucose at pH 7.4. Since the osmolarity of this solution is calculated to be 312 mOsmol, it was adjusted to the internal solution prior to the start of the experiment.

The bath solution in the second part of the experiment with sodium gluconate contained (mmol/l): 7 NaCl, 5 KCl, 10 HEPES, 2 $MgCl_2$, 2 $CaCl_2 \cdot 2 H_2O$, 10 glucose, 128 NaGlu at pH 7.4 and an osmolarity of 312 mOsmol that was adjusted.

Solution and chemicals for planar patch-clamp recordings (Port-a-Patch®)

Both the internal and the external solution for the planar patch-clamp recordings were standardized and provided by Nanion, Munich, Germany.

The internal solution contained (mmol/l): 50 CsCl, 10 NaCl, 60 CsF, 20 EGTA, and 10 HEPES at pH ≈ 7.2 and ≈ 288 mOsmol.

The external solution consisted of (mmol/l): 140 NaCl, 4 KCl, 1 $MgCl_2$, 2 $CaCl_2$, 5 D-glucose monohydrate and 10 HEPES at pH ≈ 7.4 and ≈ 298 mOsmol.
A specific solution to improve the seal (seal enhancing solution) contained (mmol/l): 80 NaCl, 3 KCl, 10 $MgCl_2$, 35 $CaCl_2$, 10 HEPES (Na^+ salt), at pH 7.4 adjusted with HCl and an osmolarity of 298 mOsmol.

Drugs

Fura-2/AM and Ruthenium Red (RuR) were purchased from TOCRIS Bioscience (Bristol, United Kingdom), and GSK1016790A and GSK2193874 from GlaxoSmithKline (Munich, Germany).
For obtaining a stock solution, the drugs were dissolved in dimethyl sulfoxide (DMSO), but the working concentration of DMSO did not exceed 0.1%.

2.2 Cell cultivation of human corneal keratocytes

The human corneal keratocytes (HCK) used in this study belong to a SV40-induced immortalized permanent cell line, which was kindly provided by Michaela Zorn-Kruppa et al. (Eppendorf-Hospital in Hamburg, Germany). She and her colleagues transinfected the primary cells with a recombinant SV40 adenovirus vector (144), and in this way created an appropriate cell model that responds in toxicology tests in most cases like the primary cells (145). The HCK show a flattened phenotype with cell extensions **(Figure 14)**.

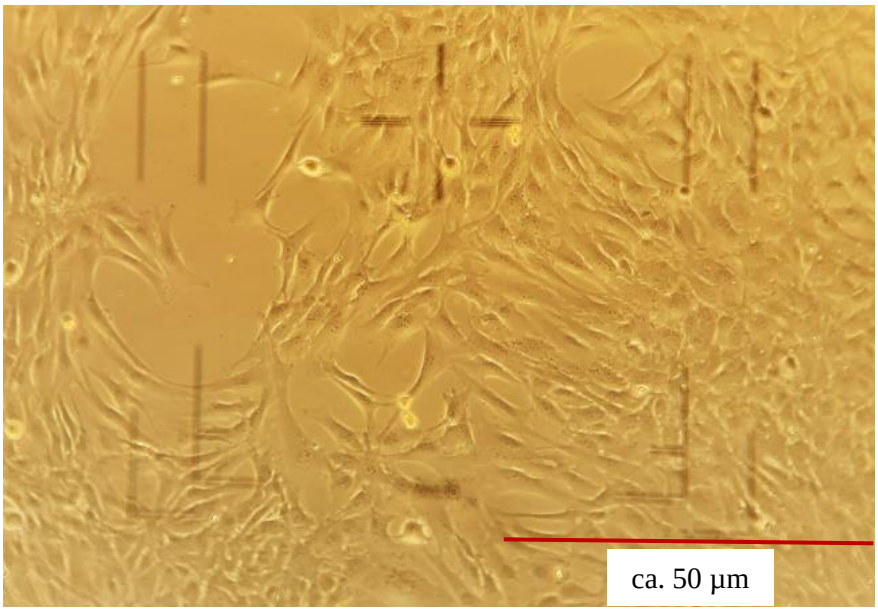

Figure 14: Microscopic image of human corneal keratocytes seeded on a cover slip for a calcium imaging experiment. The cells have long branched continuations and are longish shaped. They form groups of cell clusters. Picture taken by Vivien Schmädicke.

The cells were cultivated as previously published (138). In brief, Dulbecco's Modified Eagle's Medium (DMEM) with added 10 % fetal calf serum (FCS) was used for cell cultivation. The medium was changed every second to third day. Zorn-Kruppa et al. observed a doubling time of the HCK permanent cell line of 34 hours (144). The cells were maintained in an humified 5 % CO_2 incubator at 37°C.

According to their cell density, the cells were passaged 2 – 3 times per week by using the enzyme accutase (PAA Laboratories, Pasching, Australia). Serum-supplemented DMEM was used to stop the enzymatic reaction and the cells were washed in phosphate buffered saline (PBS).

2.3 Intracellular calcium imaging

Fluorescence calcium imaging is a highly sensitive fluorescence optical method for measurements of very small changes of the intracellular calcium concentration ($[Ca^{2+}]_i$). Grynkiewicz and Tsien et al. first introduced this assay in 1985 by using several fluorescent dyes, such as Fura-2 and Indo-1 (146). In this thesis, Fura-2-acetoxymethyl ester (Fura-2/AM) was used, which diffuses into the cells during the loading process. After being de-esterified by cellular esterases, Fura-2 free acid is formed (147), which is now trapped in the cell due to its changed structure. Fura-2 is a fluorescent dye that changes its photometric characteristics according to its contact to calcium. More specifically, it has an emission peak at 510 nm and two excitation wavelengths – one at 340 nm and the other one at 380 nm (146). The fluorescence ratio (f_{340}/f_{380}) is proportional to $[Ca^{2+}]_i$ (146). At a wavelength of 340 nm, the fluorescence signal is also proportional to $[Ca^{2+}]_i$, but at significantly lower levels (146). In many cases, changes of the fluorescence signal at 340 nm are barely noticeable. In contrast, the fluorescence signal is disproportional to $[Ca^{2+}]_i$ at 380 nm, but also at low levels (146). As a result, however, the calculated ratio of the fluorescence response signals (f_{340}/f_{380}) makes very small changes of $[Ca^{2+}]_i$ better visible (146). This demonstrates the advantage of Fura-2 in comparison to other fluorescent dyes such as fluoro-4, which only has one excitation wavelength (148). The isosbestic point is precisely the point where $[Ca^{2+}]_i$ is independent of the fluorescence intensity - this is at 360 nm (149). Fura-2/AM (1 mmol/l stock solution) was stored at -20°C in a dry container where it would be stable for months (147). It was used at a room temperature of ≈ 21°C during the experiments.

Before the fluorescence measurements, the cells were cultivated on 15 mm glass cover slips placed in a 12-cell culture well plate. Glass cover slips were used instead of plastic dishes because of the recurrent photometric property of plastic, expressing autofluorescence at ultraviolet excitation wavelengths (147). The cells were not used until they had reached a semi-confluent state of 60 –

80 % density, so as to keep a monolayer formation. This state was reached after approximately one to three days. Prior to the experiment, Fura-2/AM was added into the culture medium of the well for preincubation in a dark incubator at 37°C and 5 % CO_2 (**Figure 15**, steps 1 and 2). The staining time was on average ≈ 31 minutes. It never exceeded a dye concentration of 1 µmol/l, since concentrations above 6 µmol/l or 10 µmol/l affect the calcium metabolism of the cell and can induce a bleaching effect (150, 151). After preincubation, the cover slip was transferred into a Petri dish containing Ringer-like solution for 5 minutes to provide an adaption to the room temperature (≈ 21°C, **Figure 15**, step 3). By rinsing, possible cell debris were washed off and the Fura-2 staining process was stopped. Then, the cover slip was placed into a chamber on the stage of an inverted microscope (Olympus BW50WI, Olympus Europa Holding GmbH, Hamburg, Germany, **Figure 15**, step 4).

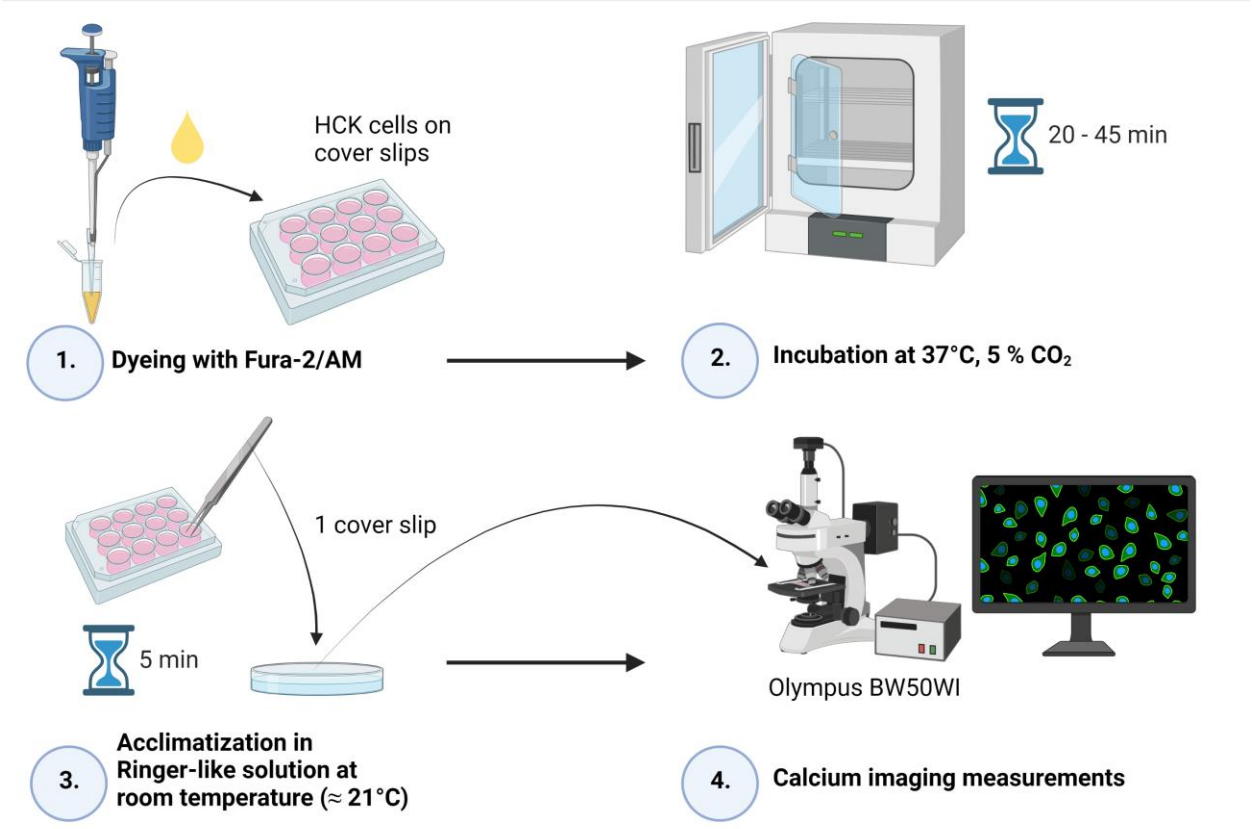

Figure 15: Procedure for the preparation of a calcium imaging experiment. Created with BioRender.com by Vivien Schmädicke.

Depending on the experiment performed, the chamber was filled with Ringer-like solution or an isotone solution at room temperature. For the temperature measurements, a temperature sensor

was installed in the chamber so that this sensor could be immersed in the liquid. With the help of specific filters and a LED light source (LED-Hub by Omikron, Rodgau-Dudenhoven, Germany) the wavelengths of 340 nm and 380 nm could be excited in an alternating manner. The fluorescence response signals were transmitted and measured with a digital camera (Olympus XM-10). The Life Science imaging software "cellSens" was used for the recordings and evaluations (**Figure 16**, Olympus, Hamburg, Germany).

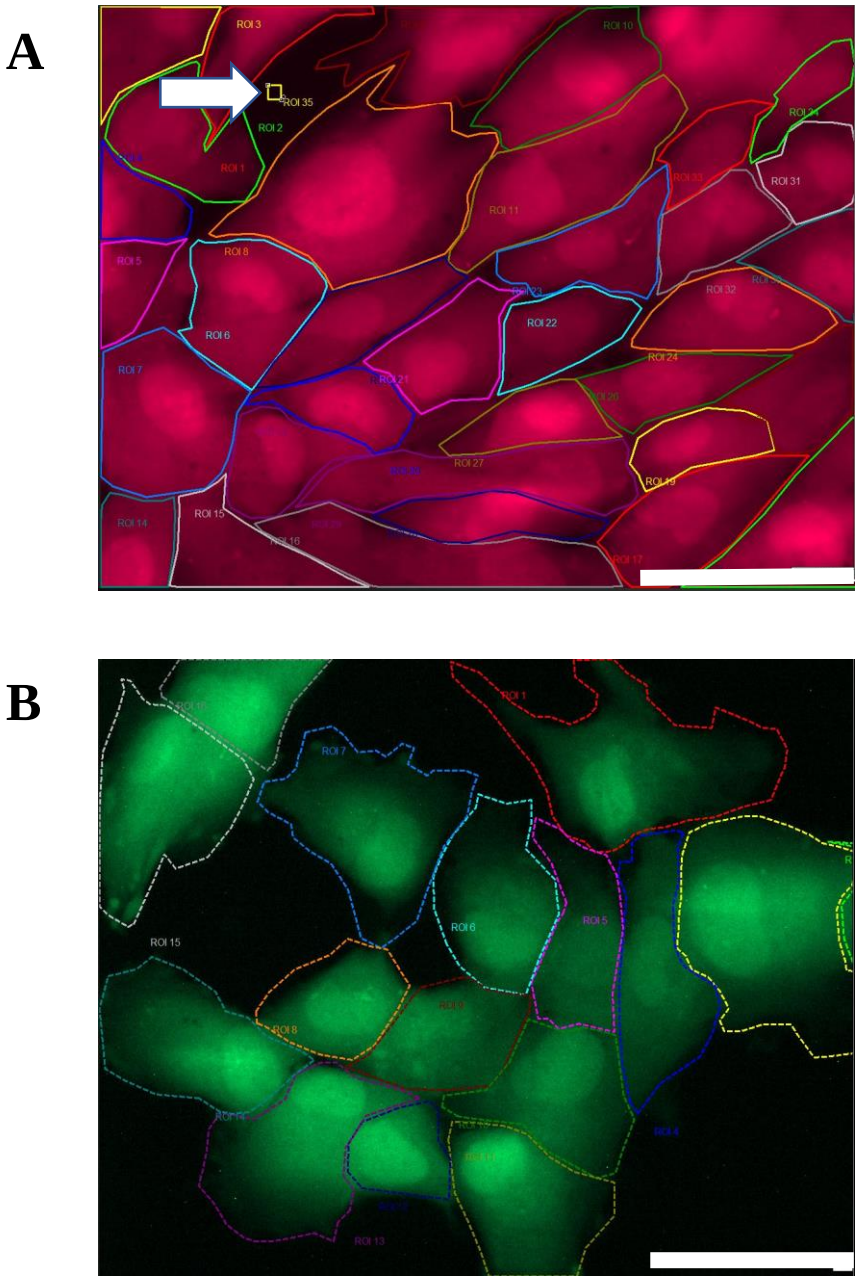

Figure 16: Fluorescence image of HCK cells in the "cellSens" software, which was used for the calcium imaging experiments in this thesis. The white scale bar is 50 µm. Picture **(A)** shows a dense cell cluster of HCK on a cover slip in a wavelength of 380 nm (software colored in magenta). The cells were manually

marked before starting the measurement to define the regions of interest (ROI). One dark region is assigned as background (marked with a white arrow). Picture **(B)** illustrates low cell density of HCK, with the marked ROI at a wavelength of 340 nm (software colored in green). The ROI for the background here lies outside the picture section. Pictures taken by Vivien Schmädicke.

5 to 35 cells (on average 17 cells) were marked per cover glass and monitored simultaneously during one single recording. The baseline measurements ("control") with Ringer-like solution or isotonic solution were repeated using at least two coverslips each since low data scattering could be generally observed. In contrast, up to 29 independent coverslips were used in all other experiments because of a bit more data scattering in some measurements. Each measurement lasted 5 or 10 minutes respectively whereby the first 2 or 4 minutes were baseline measurements. According to the experimental design, the drug, the hypotonic or the warm solution was then carefully added to the bath chamber with a pipette (see next paragraph for more details). A perfusion pump helped to keep the liquid level in the chamber constant. The cellSens software calculated the ratio of the performed experiment, and it was exported as an Excel data file for further analysis as described below.

The experimental procedures for "control vs. GSK1016790A" calcium imaging measurements (with and without blocker) were as follows:

After starting the recording (Step 4 in **Figure 15**), a baseline measurement was carried out without adding any agonist. Then, after two minutes, 2 ml of the solution with 5 µmol/l GSK1016790A was added carefully to the bath chamber with a pipette until a complete solution change was achieved. The total recording time was 5 minutes. After that, the experimental data were saved and the cover slip with the cells discarded.

To investigate the effect of the TRPV4 antagonist GSK2193874, the previous experiment was repeated in the presence of this antagonist in all solutions. More specifically, 10 µmol/l GSK2193874 was added to the culture medium of the well for preincubation in the incubator together with the fluorescent dye fura-2/AM. In addition, it was also added to the Ringer-like solution in a petri-dish for adapting to room temperature. Finally, it was also added to the control solution as well as to the Ringer-like solution containing the TRPV4 agonist GSK1016790A.

The experimental procedures for "isotonic control vs. hypotonic solution" calcium imaging measurements (with and without blocker) were as follows:

Similar to the experiments described above in the experimental procedure of the "hypotonic challenge" trials, a calcium baseline measurement was firstly performed after the start of the recording. In this case, however, an isotonic solution (see above for composition) was used instead of the control solution. In addition, the recording time of the experiment was 10 instead of 5 minutes. Accordingly, the solution change with hypotonic solution was performed after 4 minutes. After 8 minutes, a washout with isotonic solution was performed (see **Figure 17** for an illustration of the experimental procedure).

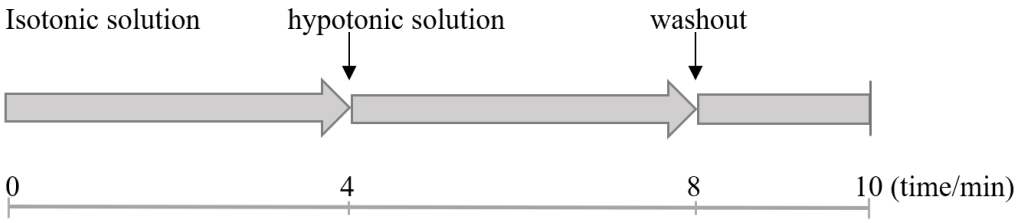

Figure 17: Time line to illustrate the experimental procedure for "isotonic control vs. hypotonic solution" calcium imaging measurements. Created with Microsoft Office Word 2019 by Vivien Schmädicke.

To block the TRPV4 activation effect, 10 µmol/l GSK2193874 was added to each measuring solution as in the previous experiments with GSK1016790A. In the subsequent experiments, the same procedure was followed as without antagonist: adding of hypotonic solution (in the presence of 10 µmol/l GSK2193874) after 4 minutes and washing out with isotonic solution (also in the presence of GSK2193874) after 8 minutes.

The experimental procedures for "control vs. moderate heating" calcium imaging measurements were as follows:

As mentioned before, the temperature sensor of a digital thermometer was installed in the chamber. As preparation, some control solution was moderately heated in a water bath. After running the experiment for 2 minutes with control solution at room temperature (~ 22 °C), the heated control (28 – 34°C) solution was added. The recording time of the experiment was 5 minutes. To try to block this effect, the previous experiment was repeated in the presence of the non-selective TRP blocker Ruthenium Red (RuR). Accordingly, this antagonist was also added to each measuring solution including the medium during preincubation.

2.4 Classical patch-clamp recordings

The patch-clamp technique is another experimental method to assess ion conductance. In particular, it opens up the possibility of measuring very small ion channel currents in a single cell. It was developed by E. Neher and B. Sakmann in 1976, and made them Nobel prize winners in 1991 (152, 153). The broad approach of this technique is to put a thin glass pipette filled with an electrolyte solution in connection with a micro-electrode on the cell membrane of a single cell on a coverslip. Since these measurements are very vibration sensitive, not only an anti-vibration table is needed, but also a skilled experimenter (154). Firstly, the contact between the opening of the glass pipette and the cell membrane should be established. After suck in and sealing, an "on-cell" or "cell-attached" configuration is established (154). At this point, it is possible to quantify the ion currents flowing through the channels situated on the part of the cell membrane (patch) that is enclosed by the pipette tip (154). With the help of a little suction, the membrane can rip open to break into the "whole-cell" configuration **(**(154); **Figure 19)**. This connection is important in order to be able to measure whole-cell currents of the whole cell membrane after voltage stimulation. During the experiment, it is possible to change the external solution to observe how ionic currents across the cell membrane change.

The classical patch-clamp technique in this thesis was performed at the Institute of Veterinary Physiology at Freie Universität Berlin according to their protocols (155-157). The experiments took place on a vibration damped table and in a Faraday cage for electrical shielding. A glass pipette filled with the internal solution was used (for composition, see previous chapter), with a very small tip (opening about 1 µm). For preparing the patch pipettes, glass tubes made of borosilicate were pulled on a DMZ Universal Puller (Zeitz Instruments, Munich, Germany) to a resistance of 3 – 5 MΩ. The tips were heat polished to smooth the edges, and to allow an electrically sealed connection between the pipette and the cell membrane. The pipettes served as a measuring electrode because a silver wire coated with silver chloride was dipped into the electrolyte solution. The glass pipette could be positioned by using an x, y, z micromanipulator and an inverted microscope (from Zeiss Axiovert; **Figure 18**). Another silver wire electrode lay in the bath solution. All classical patch-clamp recordings were performed at ≈ 23°C. The bath chamber was continuously perfused by external solution and was replaced during the experiment with the low chloride solution containing sodium gluconate instead of sodium chloride (for composition of both solutions, see previous chapter).

For the ion channel recordings, an EPC 9 patch-clamp amplifier in connection with PatchMaster software version 2.6 (HEKA Electronic, Lambrecht, Germany) was used.

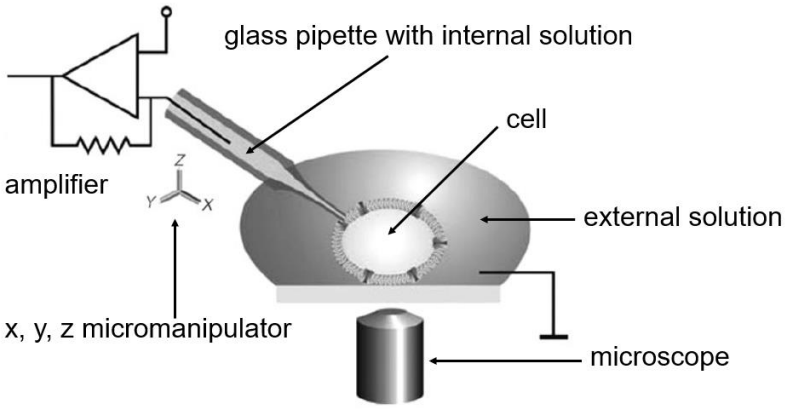

Figure 18: Schematic of the classical patch-clamp technique. Adapted figure from Bruggemann et al., 2006 (158). Reprinted with permission.

2.5 Planar patch-clamp recordings

An extended method used in this thesis was the planar patch-clamp technique (Port-a-Patch ®, Nanion, Munich, Germany). With this high throughput method, it was also possible to measure whole-cell currents, as explained in the previous chapter. The measuring principle is the same, but a microchip was used instead of a patch-pipette as an interface between the cell and the electrical system. Compared to the classical patch-clamp method, several points were improved to especially increase the usability and throughput for pharmaceutical drug testing (154, 158, 159). Thus, a vibration damped table, microscope or micro-manipulator were not needed (154). Additionally, cell suspensions were necessary, which were put on a microchip consisting of borosilicate with a small opening of ≈ 1 – 2 µm ((154); **Figure 19 B, 20 and 21 C**) and a resistance of 2 – 3.5 MΩ. The suction of a software-controlled pump helped to get a cell sealed on the aperture of the chip ("cell-attached mode"; (154)). After increasing the suction, a "whole-cell configuration" was achieved (**Figure 19 B)**. In most cases, however, the fragile HCK cells automatically broke into whole-cell configuration during sealing, but the measurements could be continued since the connection nonetheless improved. The recordings were started after a few minutes using an EPC10 patch-clamp amplifier and PatchMaster software (Version 2.6, HEKA, Lamprecht, Germany).

Using a cell culture protocol provided by Nanion, a HCK single cell suspension was prepared for the measurements as previously described (154, 159). More specifically, semi confluent cells in a 25 ml culture flask were washed with 10 ml of calcium and magnesium-free phosphate-buffered saline (PBS), and incubated with 2 ml accutase for 3 minutes at 37°C and 5 % CO_2. To stop the enzymatic reaction, medium with supplemented fetal calf serum (FCS) was added. By pipetting the cell suspension gently up and down, the detachment of the cells was supported until there were

80 – 90 % single cells. Afterwards, the cells were centrifuged at 800 relative centrifugal force (RCF) (≈ 1 g) for 5 minutes and the supernatant was discarded. The cell pellet was resuspended in Nanion external solution (for content, see above) to obtain a cell density of 1x 10^6 – 5x 10^7/ml, which was roughly visually estimated using a light microscope with a 100 µm grid.

According to the protocol of Nanion for the patch-clamp measurements, 5 µl of the internal solution (for content, see above) was firstly added to the inner surface **(Figure 21 C)**, and 5 µl of the external solution was added afterwards to the top of the microchip. The Cesium (Cs^{2+}) in the internal solution ensures the blockade of outward potassium channel currents, whereas the fluoride hydrate-covering can inhibit possible anion chloride channels (160). Finally, 5 µl of the cell suspension was added to the top of the chip. The suck in process was conducted by a software-controlled pump. Specifically, a single cell was sucked into the aperture of the chip as described above. Since there was no microscope, this cell connection could therefore only be detected by a small reduction of a current after a simple voltage stimulation (sweep). After further suction, the "whole-cell configuration" was reached. If the seal resistance exceeded 10 MΩ, seal enhancing solution was added to reach a seal above 500 MΩ. Sometimes, there were small leak currents around 50 – 100 pA. The seal enhancing solution was washed out afterwards to avoid toxic effects due to its high calcium content. In most cases, the seal remained stable.

The access resistance (R_s) and the membrane capacitance (C_M) were estimated with PatchMaster software. Slow and fast capacity transients and series-resistance errors were compensated for by the software in connection with the patch-clamp amplifier. If leak currents exceeded 100 pA, the cells were discarded from evaluation. The holding potential (HP) was set to 0 mV to eliminate any possible involvements of voltage-dependent calcium or sodium channel currents. The liquid junction potential correction factor was calculated to 4 mV and the liquid junction potentials were considered during data acquisition (161). A voltage-step and a ramp protocol were used for stimulation, with a voltage range from -60 until +130 mV. The whole-cell currents were recorded each time for 400 ms in increments of 10 mV, and formed sweeps as a response to the voltage pulses. The resulting currents were normalized to cell membrane capacitance since the cells differed in their membrane capacity and size. Therefore, the current amplitude (pA) was divided by cell membrane capacitance (pF) to obtain current density (pA/pF).

The recordings took place in a room with air-conditioning at a constant temperature of ≈ 22°C for a maximum of 4 hours according to the vitality of the cells. After breaking into whole-cell configuration, test recordings were performed until the whole-cell currents stabilized. If applicable, another leak current subtraction and cell membrane capacitance compensation was carried out. After 20 sweeps (= 100 s, one sweep = 5 seconds), 10 µmol/l GSK1016790A was

extracellularly added. After at least another 100 s (20 sweeps), 10 µmol/l GSK1016790A was added in the presence of 10 µmol/l GSK2193874. If the seal remained stable, the substances were washed out in reverse order. More specifically, the antagonist was firstly washed out to check whether the blocking effect could be suppressed. Afterwards, the agonist was washed out by replacing it with control solution (see **Figure 22** for a progress chart for a better overview). If the seal was still stable, the experimental procedure could be again repeated.

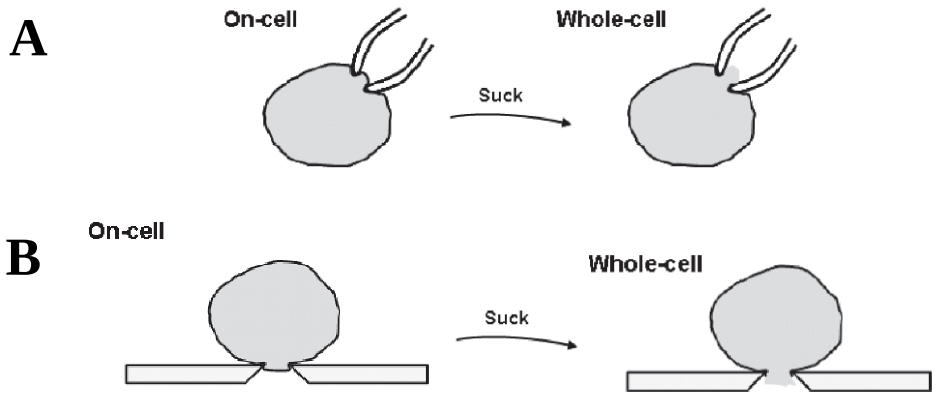

Figure 19: Schematic drawing of two different patch clamp configurations: the "on-cell" and the "whole-cell" configuration. Illustrative comparison of them between **(A)** the classical patch-clamp technique and **(B)** the planar patch-clamp method. Pictures reprinted with permission from Bruggemann et al., 2008 (154).

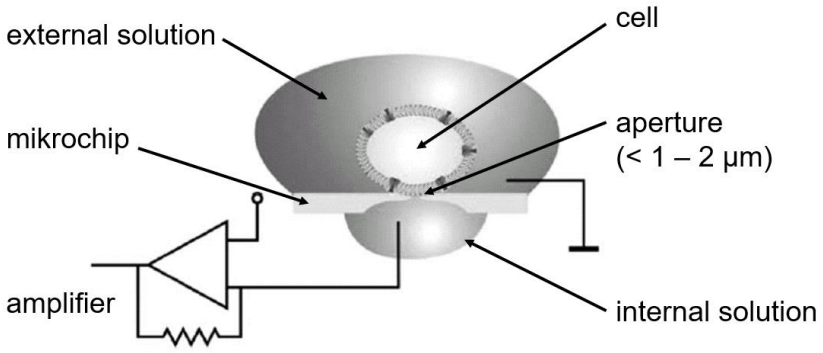

Figure 20: Schema of the planar patch-clamp technique with microchip. Adapted figure from Bruggemann et al., 2006 (158). Reprinted with permission.

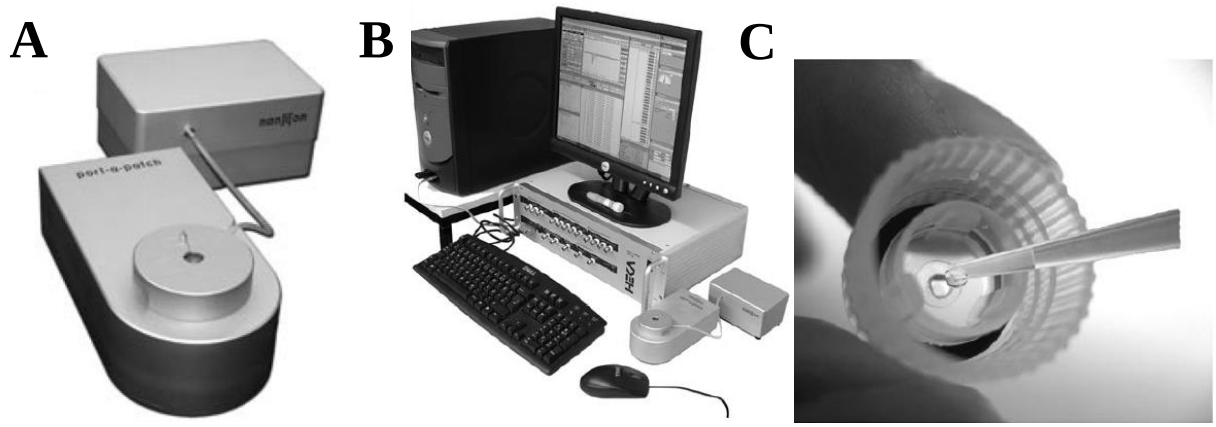

Figure 21: Important tools for planar patch-clamping. (**A):** Port-a-Patch workstation and pump; **(B):** Port-a-Patch setup with amplifier and PC; **(C):** Pipetting the internal solution into the microchip. Pictures reprinted with permission from Bruggemann et al., 2006 (158).

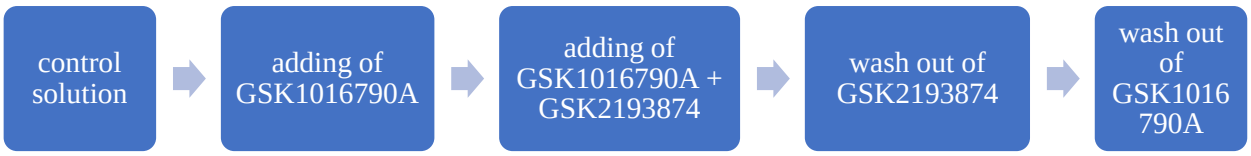

Figure 22: Progress chart visualizing the sequence of the application of the drugs in the planar patch-clamp experiments performed for this thesis. Created with Microsoft Office Word 2019 by Vivien Schmädicke.

2.6 Good scientific practice

The statutes of good scientific practice from Charité Universitätsmedizin Berlin were acknowledged and observed for the whole time while working on this thesis („Neufassung der Satzung der Charité-Universitätsmedizin Berlin zur Sicherung Guter Wissenschaftlicher Praxis" (162), dated 29.03.2018 (AMB Charité Nr. 092, S.658)).

Since only an established cell line was used, no ethical review committee votes were necessary, and no animal protection guidelines had to be respected.

Safe data storage on the servers and PCs of the Charité Universitätsmedizin Berlin is arranged and ensured for 10 years.

2.7 Data analyses and statistics

The raw data from the planar patch-clamp and calcium imaging experiments were collected and saved as Excel data files (Microsoft Excel 2010, Redmond, USA). The TIDA analysis software (HEKA Elektronik GmbH, Lambrecht/Pfalz, Germany) was used to assemble the raw data of each calcium imaging test series. With this software, it was possible to normalize and make a drift correction of the traces if there was a bleaching. Traces which had too many pipetting errors or artifacts were discarded from evaluation.

The statistical analysis as well as the plots and bars were created with SigmaPlot software version 14.0 for Windows (Systat Software, San Jose, California, U.S.A) and GraphPad Prism version 9.00 (La Jolla, California, USA), also for Windows.

First, the data were normality tested to check whether a Gaussian distribution existed or not. At this point, three different normality tests were carried out using the GraphPad Prism software such as the D'Agostino and Pearson normality test and Shapiro-Wilk normality test as well as the Kolmogorow-Smirnow normality test. If the paired data were normally distributed, the parametric Student's t-test was used. Otherwise, the non-parametric Wilcoxon matched-pairs signed ranks test was used. For unpaired data, the unpaired t-test was used. If the normality test failed, the non-parametric Mann-Whitney-U test was used. The data from the classical patch-clamp experiments were analyzed after the Student-Newman-Keuls method (163). All values are given as mean ± SEM (standard error of the mean) and the number of repeats (n) can be found in brackets. Error bars are drawn in both directions. P-values (p) < 0.05 were considered to be significant. The level of significance is related to the number of asterisks (*) used in the charts: * means p-values < 0.05; ** means p-values < 0.01; *** means p-values < 0.001 and **** stands for p-values < 0.0001. The same legend applies to hashtags (#), where correlations of unpaired data are described.

3. Results

3.1 Identification of TRPV4 in HCK

Established synthetic compounds such as GSK1016790A (TRPV4 agonist) and GSK2193874 (TRPV4 antagonist) were used in this thesis as highly sensitive and potent TRPV4 modulators (129, 164, 165).

During the calcium imaging experiment, 5 µmol/l GSK1016790A was added 2 minutes after the beginning of the recording. This led to an increase of the fluorescence ratio f_{340}/f_{380} from 0.1007 ± 0.0001323 at 100 s (control) to 0.1124 ± 0.002330 at 160 seconds (filled circles in **Figure 23 A**; n = 292; p = <0.0001), which is proportional to a rise of intracellular Ca^{2+} (146). In contrast, a control measurement showed a constant Ca^{2+} baseline (open circles in **Figure 23 A**).

The GSK1016790A-induced Ca^{2+} increase could be clearly suppressed by using 10 µmol/l TRPV4 blocker GSK2193874 (e.g., at 160 seconds 0.09945 ± 0.0003498; n = 51; p = < 0.0001 if compared to f_{340}/f_{380} without antagonist at the same time; **Figure 23 B, 23 C**). Prior the experiment, the cells were pre-incubated in 10 µmol/l GSK2193874 for 44 minutes on average.

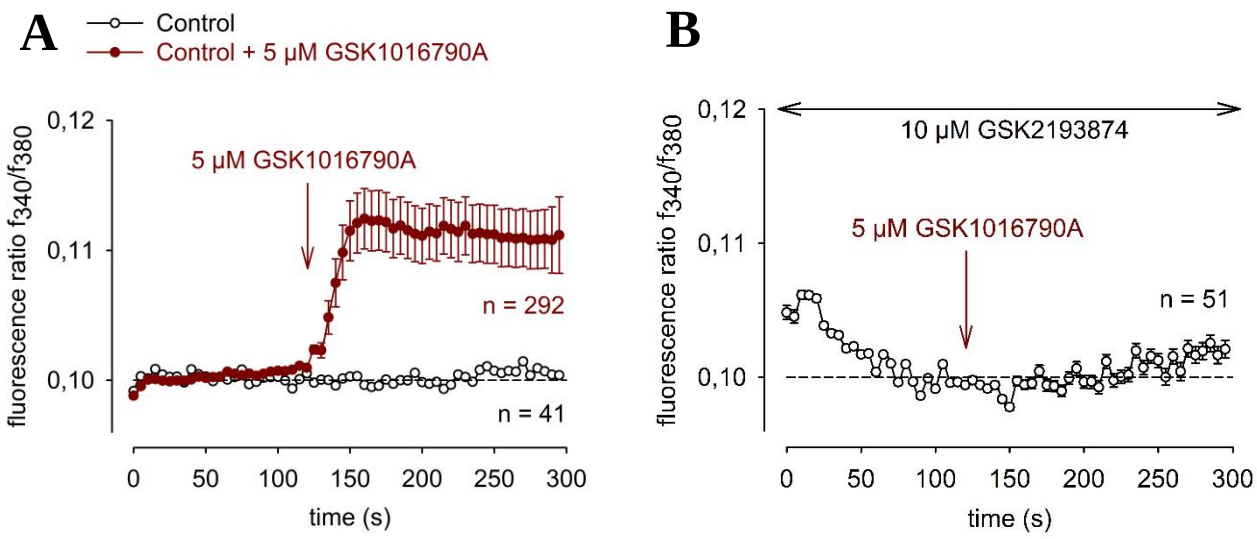

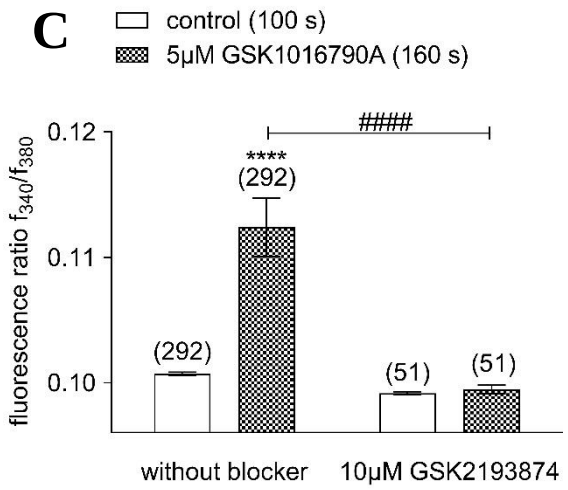

Figure 23: Pharmacological identification of TRPV4 in HCK. The effect of GSK1016790A and GSK2193874 on intracellular calcium concentration was investigated. **(A)** The time on the x-axis is plotted against the fluorescence ratio f_{340}/f_{380} on the y-axis, so each trace shows mean fluorescence ratios, which are proportional to the $[Ca^{2+}]_i$. The agonist was added at the time indicated by an arrow. The addition of GSK1016790A (5 µmol/l) increased $[Ca^{2+}]_i$ (n = 292; filled circles) in comparison to the control (n = 41; open circles). **(B)** The same experiment as shown in (A), but in the presence of the TRPV4 antagonist GSK2193874 (10 µmol/l). The GSK1016790A-induced Ca^{2+} increase was clearly suppressed (n = 51). **(C)** Bar chart summarizing the effects of GSK1016790A and GSK2193874 on HCK. The fluorescence ratio f_{340}/f_{380} is again plotted on the y-axis. The asterisks (****) denote significant increases in $[Ca^{2+}]_i$ after addition of GSK1016790A in comparison to the control respectively Ca^{2+} base level at 100 s (n = 292 without antagonist; $p < 0.0001$ at the minimum; tested with Wilcoxon matched-pairs signed rank test). The hashtags (####) designate statistically significant differences in fluorescence ratios without and in the presence of GSK2193874 at 160 s (n = 51 – 292; $p < 0.0001$ at the minimum; tested with Mann-Whitney-U test). Error bars (SEM) are given in black in both directions. The numbers of experiments (n) are given in brackets. The baseline measurements were repeated using 2 independent coverslips containing 41 cells. For the control vs. GSK1016790A experiments 29 coverslips containing 292 cells were used. The measurements with the antagonist GSK2193874 were repeated with 7 different cover slips containing 51 cells. The traces were superimposed to increase the numbers for the statistical evaluation. µM ≙ µmol/l.

The underlying whole-cell currents were determined by using the planar patch-clamp technique. Specifically, the time-dependent changes of the currents could be shown. Also, it was possible to evaluate the corresponding current-voltage relationships at the indicated time points A, B and C (**Fig. 24 A, 24 B**). At positive voltages (130 mV), 10 µmol/l GSK1016790A increased the outward currents. Interestingly, the control currents were at high levels indicating other ion channel currents, such as anion (chloride) channel currents. Also, the inward currents clearly increased at

negative voltages (-60 mV) (**Fig. 24 A, 24 B**). In the measurement showed in **Figure 24 A**, there was a short interruption due to leak compensation.

Specifically, the mean inward current density at -60 mV increased from -21.34 ± 10.11 pA/pF to -31.46 ± 11.22 pA/pF (n = 5; p < 0.05), whereas the increase of the outward current density at +130 mV did not reach statistical significance (n = 5; **Figure 24 C**).

After the addition of GSK1016790A together with GSK2193874, the mean inward current density at -60 mV slightly decreased to -24.34 ± 7.957, which did not achieve statistical significance (n = 5; p > 0.05). Interestingly, the currents at +130 mV even fell below the control currents to 130.7 ± 65.94 pA/pF (n = 5; p > 0.05; **Figure 24 C**).

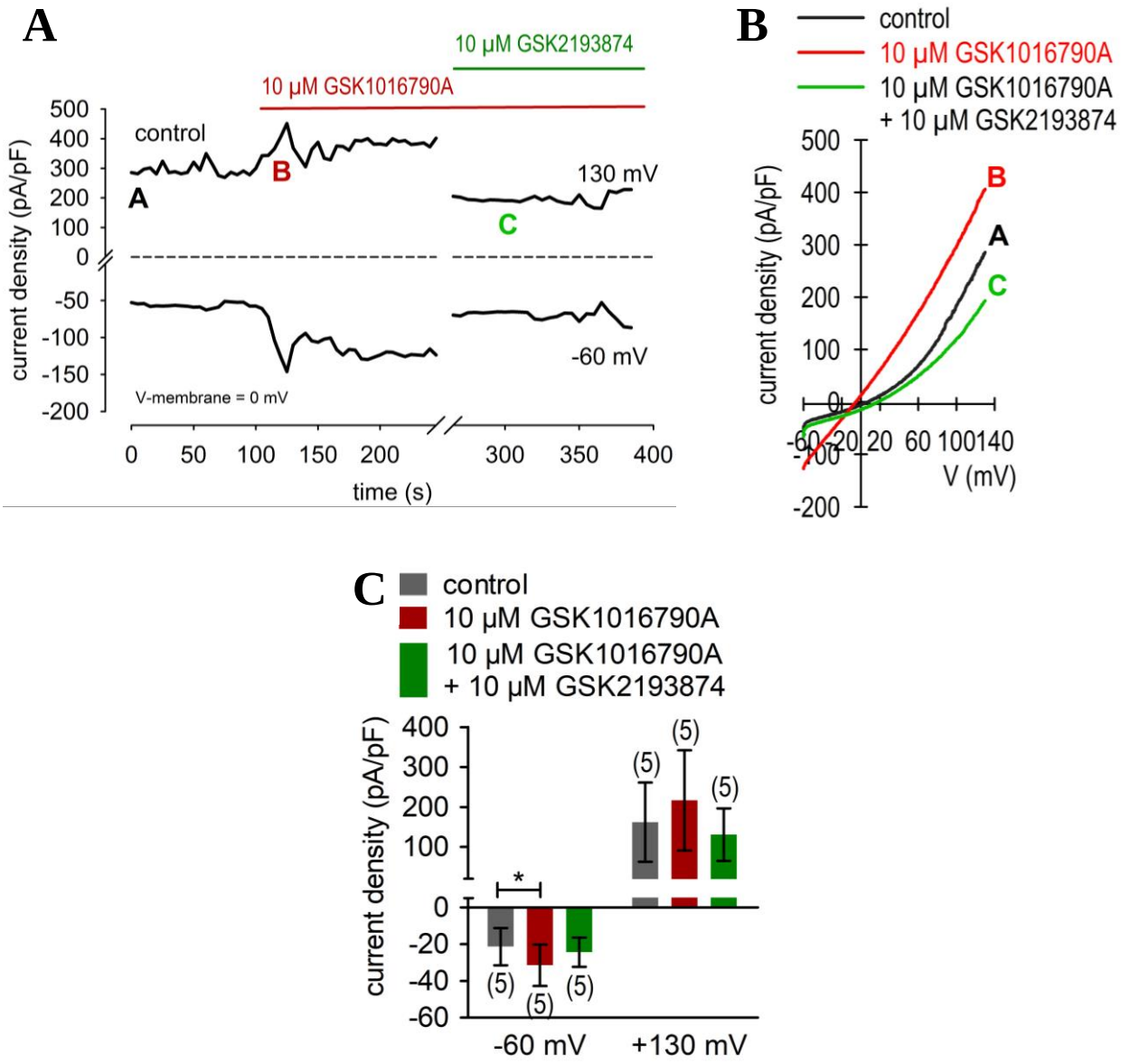

Figure 24: Pharmacological TRPV4 identification in HCK. The effect of GSK1016790A and GSK2193874 on whole-cell currents in HCK was analyzed. **(A)** Time course of one of the patch-clamp experiments. The

time on the x-axis (in seconds) is plotted against the current density, given in pA/pF, on the y-axis. The arrows indicate the solution changes. The letters “A”, “B” and “C” label different parts of the experiment: under control solution (“A”), in the presence of 10 µM GSK1016790A (“B”) and after the addition of 10 µM GSK1016790A and 10 µM GSK2193874 (“C”). The inward currents clearly increased at -60 mV in “B”, as did the outward currents at +130 mV. The two lines on the x-axis denote an interruption due to leak compensation. **(B)** Display of the points of time “A”, “B” and “C” in a diagram of voltage, given in mV on the x-axis, plotted against the current density, given in pA/pF on the y-axis. **(C)** Bar chart summarizing all patch-clamp experiments with GSK1016790A and GSK2193874. The three bars on the left show the current density in pA/pF at -60 mV, and the three bars on the right show it at +130 mV. The asterisk (*) denote a significant increase when comparing the values at -60 mV of the control solution against the ones in the presence of 10 µM GSK1016790A (n = 5; p = < 0.05, normally distributed data (according to Shapiro-Wilk and Kolmogorow-Smirnow normality test) tested with paired t-test). Error bars (SEM) are given in black in both directions. µM ≙ µmol/l.

3.2 Activation of TRPV4 by hypotonic challenge

Since the TRPV4 channel is also an osmosensor, this channel can be also activated by hypotonicity (99, 100, 166). In this thesis, the activation mechanism was demonstrated in HCK by using a hypotonic solution with an osmolarity of about 233 mOsmol in a series of calcium imaging experiments. This is 75 % of the osmolarity of the isotonic control solution, which was around 313 mOsmol. The use of the hypotonic solution led to cell swelling and associated stretching of the plasma membrane and subsequent recovery (regulatory volume disease) (166). The hypotonic challenge was applied from 4 minutes after the beginning of the recording and replaced the isotonic solution until it had been washed out after 8 minutes. In HCK, a hypotonic challenge led to an irreversible increase of intracellular Ca^{2+} from 0.1002 ± 3.855e-005 at 180 s (control) to 0.1041 ± 0.0002 at 450 seconds (n = 151; p = < 0.0001, filled circles in **Figure 25 A**). After washout, the fluorescence ratio f_{340}/f_{380} still reached 0.1062 ± 0.0003 at 595 seconds (n = 151; p = < 0.0001). In contrast, a control measurement showed a constant Ca^{2+} baseline (n = 38; open circles in **Figure 25 A**).

This increase was clearly suppressed in the presence of 10 µM GSK2193874 (e.g., at 450 seconds: 0.0992 ± 0.001 (n = 253; p > 0.05; **Figure 25 B**)).

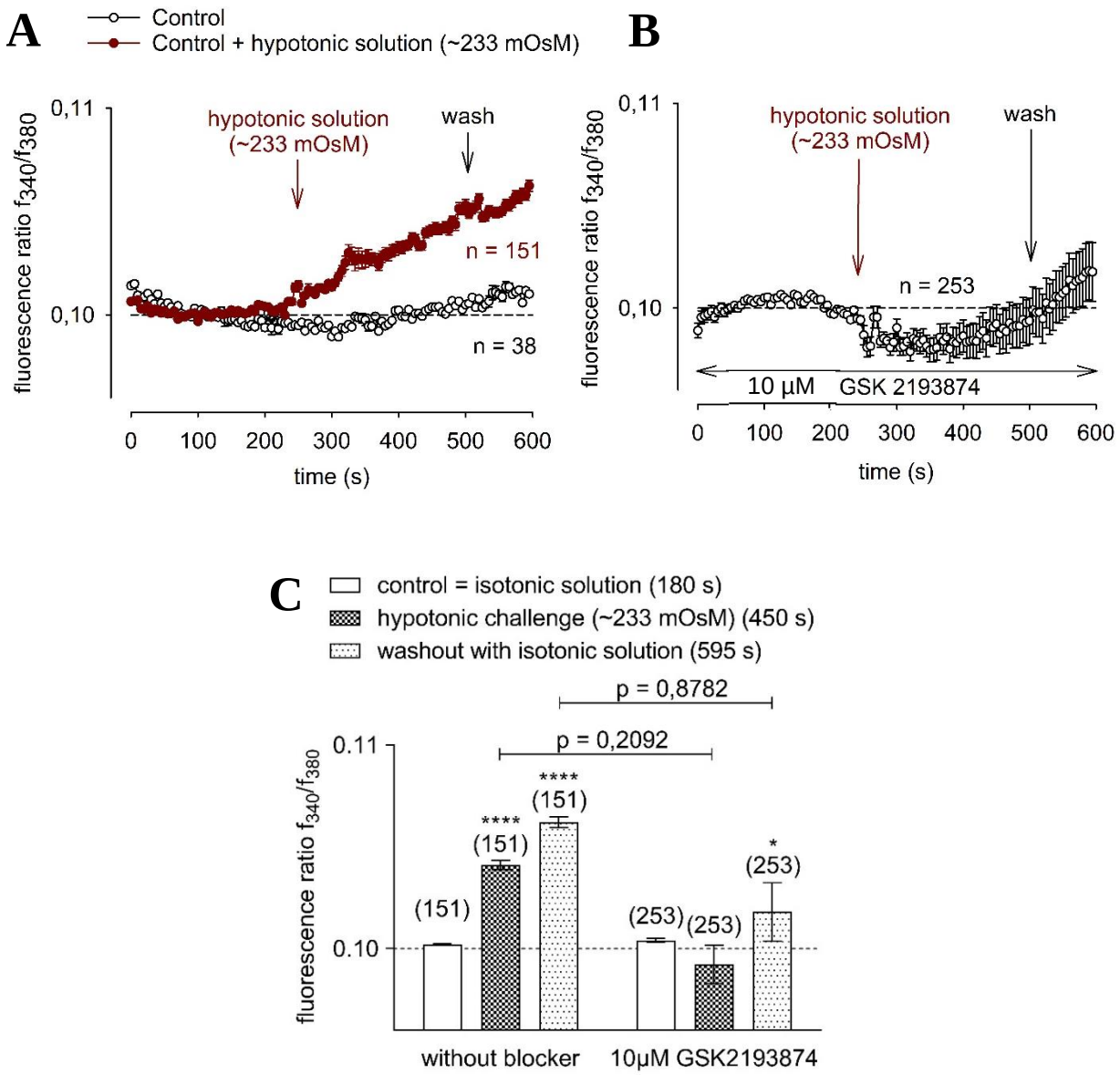

Figure 25: TRPV4 osmosensitivity. The effect of hypotonic stress on intracellular Ca^{2+} concentration in HCK was investigated. **(A)** The time on the x-axis is plotted against the fluorescence ratio f_{340}/f_{380} on the y-axis. The arrows indicate the points of time of solution changes, namely the addition of the hypotonic solution (233 mOsmol) at 240 seconds and the washout with isotonic control solution (313 mOsmol) at 480 seconds. The hypotonic challenge increased $[Ca^{2+}]_i$ (*n* = 151; filled circles) in comparison to the control (*n* = 38; open circles). **(B)** The same experiment as shown in (A) but in the presence of 10 µM GSK2193874. The hypotonicity-induced Ca^{2+} increase was suppressed (*n* = 253). **(C)** Bar chart summarizing the effect of hypotonic stress on HCK. The fluorescence ratio f_{340}/f_{380} is again plotted on the y-axis. The three bars on the left represent the experiment without antagonist, and the three bars on the right represent the one in the presence of 10 µM GSK2193874. The asterisks (****) show significant increases in fluorescence ratio f_{340}/f_{380} when values are compared to their respective control measurement (e.g., without blocker at 450 seconds: *n* = 151; $p < 0.0001$; without blocker after washout (595 seconds): *n* = 151; $p < 0.0001$, tested

with Wilcoxon matched-pairs signed rank test). The two other p-values given in the chart were determined by running the Mann-Whitney-U test. Error bars (SEM) are given in black in both directions. The numbers of experiments (*n*) are given in brackets. The measurements with isotonic control solution were repeated using 2 independent coverslips containing 38 cells. For the isotonic control vs. hypotonic solution experiments 15 different coverslips containing 151 cells were used. The measurements with the antagonist GSK2193874 were repeated with 10 different cover slips containing 253 cells. µM ≙ µmol/l.

3.3 Activation of TRPV4 channels by moderate heat

Another possibility for activating TRPV4 is to physically heat the measuring solution above 28°C. Accordingly, the effect of moderate heat was tested in the following set of calcium imaging experiments. Since also other TRPs such as TRPV1 – 3 can be activated by temperature increases (117), the Ringer-like solution used in this set of experiments was warmed up to 28 – 34°C, which is the temperature threshold where TRPV4 can be activated (167). The mean warm temperature was 30.11 ± 0.6°C. In this way, it was tried to minimize the effects on calcium influx caused by other thermosensitive TRPs. The warm Ringer-like solution was added from 2 minutes after the beginning of the recording. As a result, an increase of the fluorescence ratio f_{340}/f_{380} was detectable. Specifically, f_{340}/f_{380} increased from 0.1005 ± 0.0001299 at 100 s (control) to 0.1064 ± 0.001524 at 150 seconds (n = 79; p < 0.0001, filled circles in **Figure 26 A**). In contrast, a control measurement with Ringer-like solution at room temperature showed a constant Ca^{2+} baseline (n = 41; open circles in **Figure 26 A**).

This heat-induced increase could not be suppressed by the unselective TRP blocker Ruthenium Red (n = 192; p 0.0788; **Figure 26 B**).

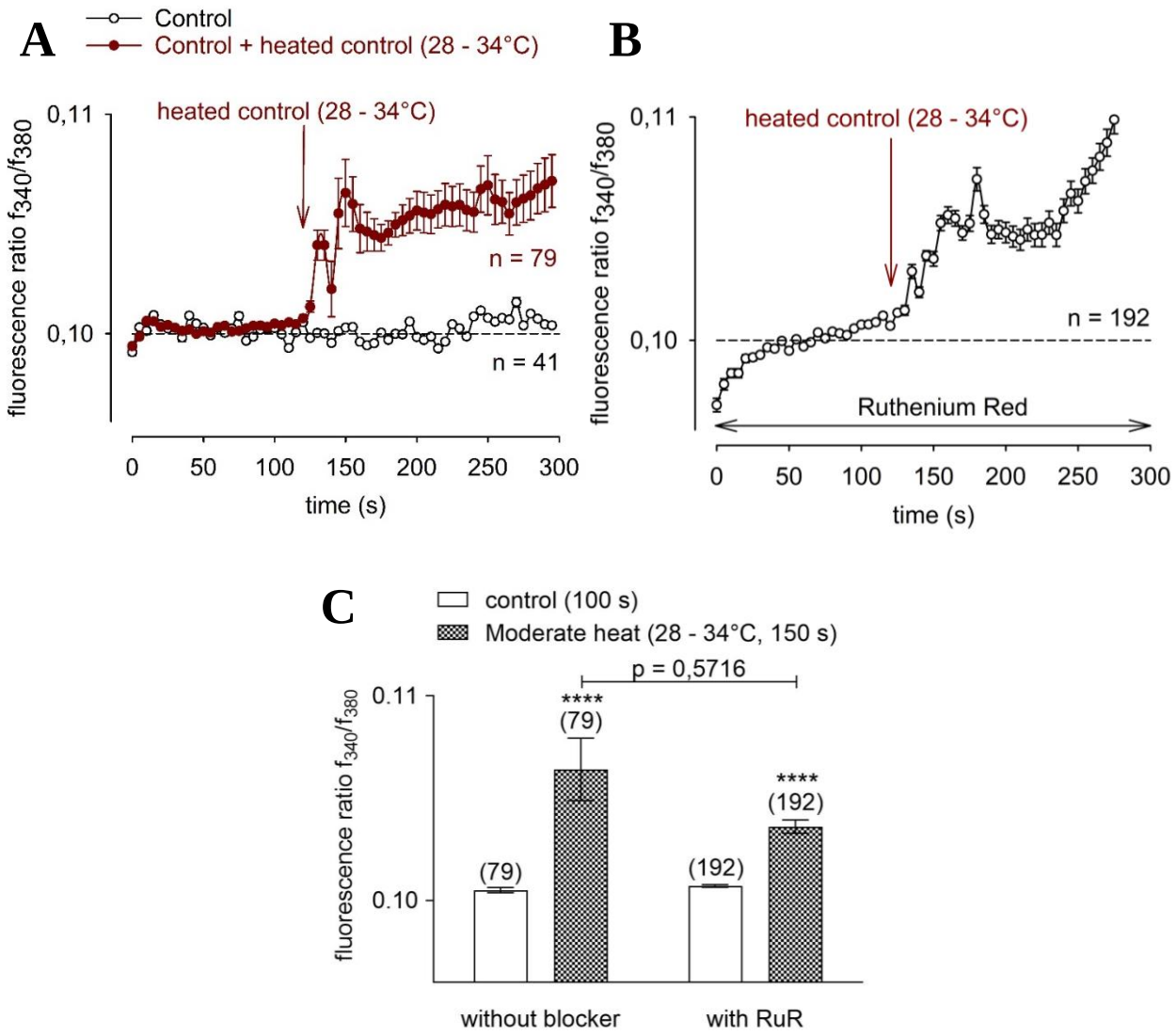

Figure 26: TRPV4 temperature sensitivity. The effect of moderate heating on intracellular Ca^{2+} was investigated in HCK. **(A)** The time on the x-axis is plotted against the fluorescence ratio f_{340}/f_{380} on the y-axis. The arrow marks the point of time when the heated Ringer-like solution was added. The moderate heat increased $[Ca^{2+}]_i$ (*n* = 79; filled circles) in comparison to the control (*n* = 41; open circles). **(B)** The same experiment as shown in (A) but in the presence of Ruthenium Red (≈ 10 µmol/l). The heat-induced effect could not be suppressed (see chapter 4.5 "limitations"). **(C)** Bar chart illustrating the effect of the unselective TRPV4 channel blocker RuR on moderate heat-induced $[Ca^{2+}]_i$-increases in HCK cells. The fluorescence ratio f_{340}/f_{380} is plotted on the y-axis. The white bars demonstrate control measurements with and without RuR, whereas the filled bars show the experiment with moderate heat with and without RuR. The asterisks (****) indicate the statistically significant difference between the fluorescence ratios f_{340}/f_{380} in presence of the control solution at 100 seconds and in the presence of the moderate heated solution at 150 seconds (for measurements without RuR *n* = 79; $p < 0.0001$; tested with Wilcoxon matched-pairs signed rank test; for measurements in presence of RuR n = 192; $p < 0.0001$; also tested with Wilcoxon matched-pairs signed rank test). RuR partially reduced the heat-induced Ca^{2+} increase, but only just failed

to reach statistical significance (p = 0.5716, unpaired data tested with Mann-Whitney-U test). Error bars (SEM) are given in black in both directions. The numbers of experiments (n) are given in brackets. The measurements with control solution were repeated using 2 independent coverslips containing 41 cells. For the control vs. warm control experiments 12 different cell layers were used containing 79 cells. The measurements with RuR were repeated with 11 independent cell layers containing 192 cells.

3.4 Analyses of anion channel currents: the chloride conductivity of HCK

Since preliminary patch-clamp recordings showed outward whole-cell currents under control conditions, the next set of experiments was focused on anion (chloride) current analyses to test whether the HCK cells express a chloride conductance. To measure chloride conductivity, the experiments were performed using sodium gluconate (referred to as "NaGlu" in the following) instead of sodium chloride solution (henceforth referred to as "NaCl") in the bath solution, since outward currents may be carried either by Na^+ or by Cl^-. Conversely, inward currents are usually reflected the influx of Ca^{2+} with possible contributions of Na^+ because the internal solution was Ca^{2+} free. Since Gluconate is a large anion, any contribution of chloride outward currents should be at a lower level compared to the solution containing NaCl. Accordingly, an anion conductance should shift the membrane potential towards more negative values if gluconate is in the external solution. In patch-clamp recordings, the trace of the current voltage relationship crossed the x-axis at a certain voltage and then reversed sign, which demonstrated the reversal potential. This potential was shifted to more positive values in the presence of sodium gluconate, as shown in **Figure 27**. In the experiments, the concentration gradient of Ca^{2+} in the solutions was physiological. The concentrations of all other cations (including Na^+) were identical in the pipette and the bath, so that no concentration gradient could be established here. As shown in **Figure 27**, the reversal potential in NaCl was in the negative range. Since no other ion than chloride had a Nernst potential in the negative range, this is clear proof of a contribution of chloride to total conductance. In the next step, the NaCl solution was replaced by a bath solution containing gluconate as the primary anion ("NaGlu"; see Chapter 2.1 for compositions of the solutions in detail) (143). This resulted in a significant shift of the reversal potential, confirming an anion conductance, with subsequent recovery to negative values after a return to the original NaCl solution. Specifically, the mean reversal potential changed from -21.3 ± 5.4 mV to -4,6 ± 0.8 mV after the solution change from NaCl to NaGlu (n = 6; $p < 0.05$). After washout to NaCl, the reversal potential was -16.7 ± 4.3 mV (n = 6). The outward current was also reduced by replacement of chloride by gluconate, even though effects were not significant (**Figure 28**). Notably, the series

resistance (R_S in M) did not show a significant change (from 7.7 ± 1.3 over 8.2 ± 1.6 to 8.7 ± 2.1; n = 6; $p > 0.05$). This confirmed a stable patch-clamp recording quality. Furthermore, the capacitance values (C_S in pF) also remained stable (from 27 ± 5 over 26 ± 5 to 26 ± 6; $n = 6$). Taken together, these experiments show that the whole-cell currents not only contain TRPV4 channel currents but also chloride channel currents in HCK.

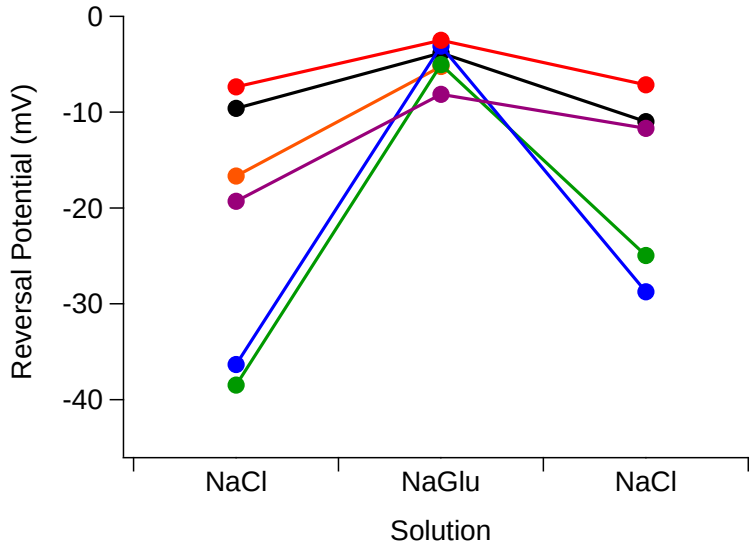

Figure 27: Proportion of chloride currents in the whole-cell recordings. The replacement of chloride by gluconate on six individual HCK cells (shown in different colors) led to a shift of the reversal potential (given in mV), which is plotted on the y-axis. The x-axis displays the different solutions: high chloride solution containing NaCl and a low chloride solution containing NaGlu with return to NaCl. The negative reversal potential at the beginning of the experiment in NaCl was caused by an influx of Cl^- and shifted to more positive potentials in the presence of NaGlu, with subsequent recovery to more negative values in NaCl.

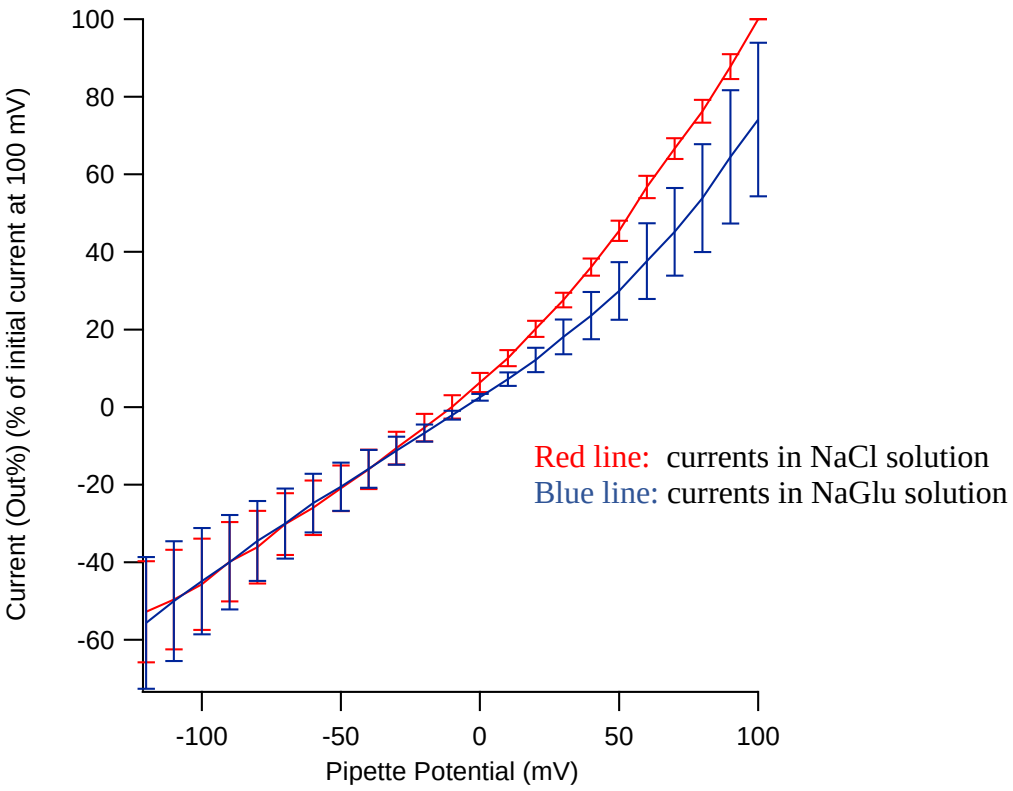

Figure 28: Effect of chloride on outward rectification shown in a current voltage relationship. The pipette potential (in mV) is plotted on the x-axis and the y-axis shows the current as a percentage of the initial current at 100 mV. The red line with error bars (SEM) indicates the currents in NaCl solution, and the blue line indicates them in NaGlu solution. While inward currents primarily reflecting the influx of Na^+ remain stable, outward currents are reduced by the removal of Chloride.

3.5 Morphological description of the HCK and their responses during calcium imaging measurements

As already shown in the chapters of the results section 3.1 – 3.3 (e.g. in Figure 23, 25 and 26), after activation of TRPV4 by an agonist or an activating stimulus (such as hypotonicity or moderate heat) the $[Ca^{2+}]_i$ increased during calcium imaging experiments. Notable, some of the cells underwent a morphological change during the measurements. This could be observed in the microscopic images. **Figure 29** shows the same group of cells during the "control vs. GSK1016790A" experiment before **(A)**, immediately after addition of the agonist **(B)** and afterwards in the end of the measurement **(C)**. In **Figure 29 B-C**, some cells changed their color indicating a changed (increased) fluorescence ratio due to the calcium influx. This color change was observed in several other cells during the experiments and indicated a strong response to the agonist.

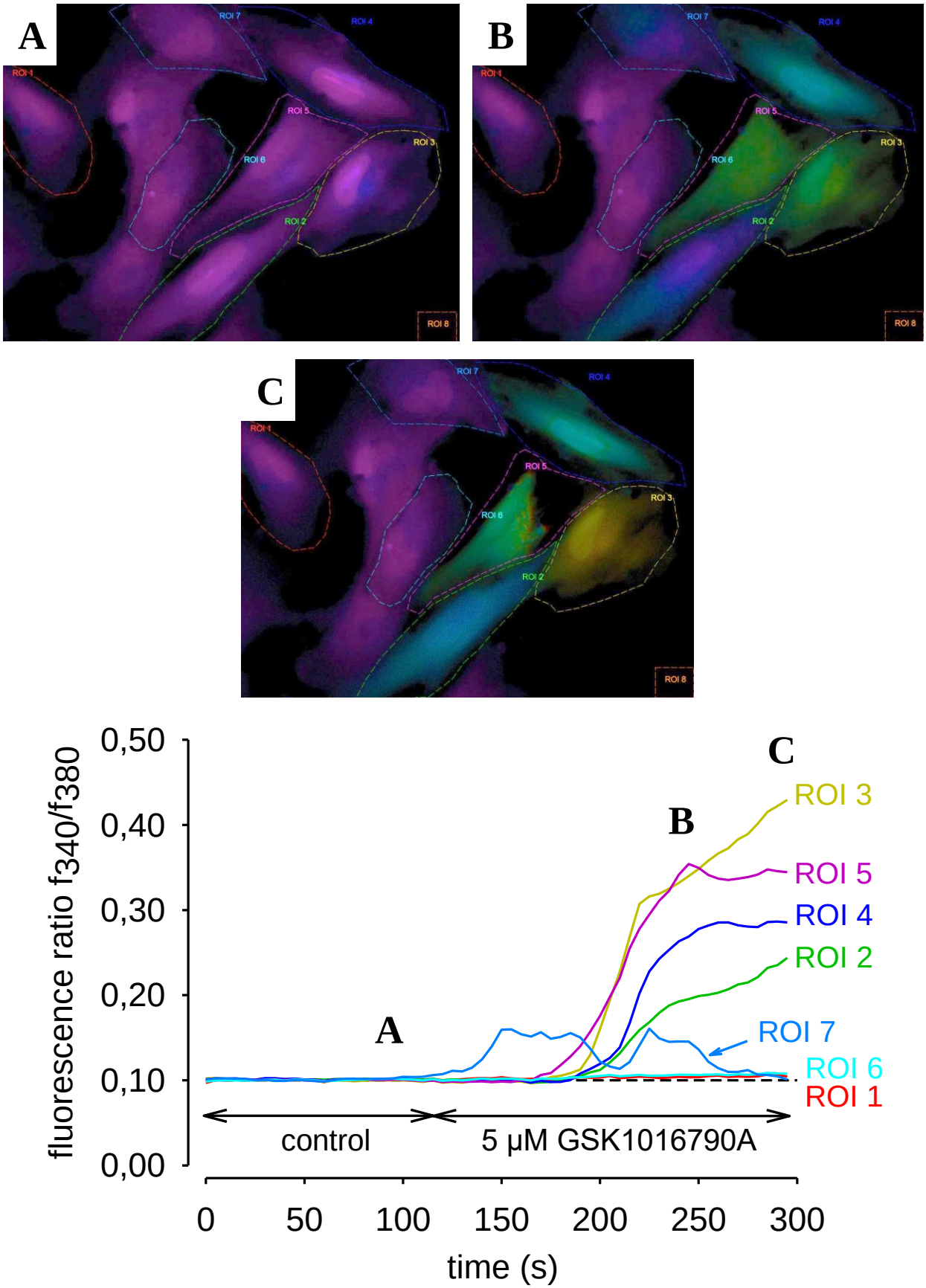

Figure 29: Microscopic fluorescence images (upper part of the figure) of a section of an HCK cell layer at different point of times before (A) and after extracellular application of 5 µmol/l GSK1016790A (B + C)

using the “cellSens” software and their corresponding single traces (colored) as fluorescence ratio f_{340}/f_{380} on y-axis against time in seconds on x-axis (lower part of the figure). There are 8 regions of interest (ROIs) selected, whereby the 8th ROI stands for the background. The both arrows above the x-axis means the start of adding the TRPV4 agonist GSK1016790A at 120 seconds. **(A)** marks a point of time during control measurements before adding the agonistic stimulus at 90 seconds. Each colored single trace of 7 selected cells (ROI 1 – 7) show the fluorescence ratio corresponding to the ROIs in the microscopic fluorescence. The traces show a zero line and the cells have almost the same coloration (upper part of the picture). **(B)** stands for a point of time after the extracellular application of GSK1016790A at 240 seconds. The fluorescence ratio of ROI 2, 3, 4, 5 and 7 raises and the cells undergo a color change with more green and blue shades. The graphs of ROI 1 and 6 remain stable and the cells don`t change their coloration. **(C)** marks the end of the experiment in the presence of the agonist at 300 seconds. The coloration change is progressing in some cells. ROI 5 now even undergoes a further morphological change and seems to slightly contract its cell body. The diagram was created with Sigmaplot and pictures were taken by Vivien Schmädicke.

Furthermore, the cells presented slightly different morphologies during the experiments. As already shown in the method section, some cell crowds were dense and some looser. In addition, some HCK contained fine granules as shown in **Figure 30** (arrow), whereas others appeared to have a homogeneous cytoplasm.

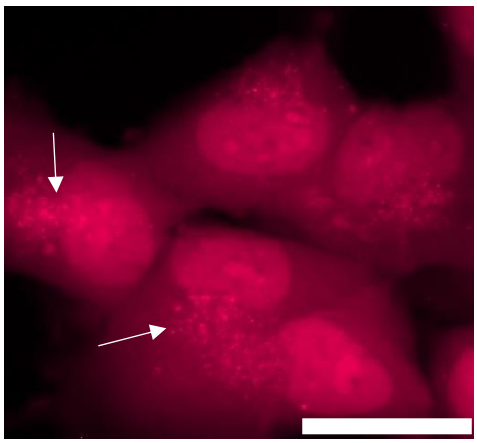

Figure 30: Fluorescence microscopic image (colored red by the software) showing some HCK cells with cell plasma granula (white arrows). The white scale bar is 50 µm. Screenshot taken by Vivien Schmädicke using cellSens software.

4. Discussion

4.1 Functional expression of TRPV4 in HCK

This thesis describes the pharmacological, osmo- and thermosensitive TRPV4 channel activity in HCK cells so as to validate its functional expression. To achieve this goal, highly sensitive functional assays like fluorometric calcium measurements as well as both classical and planar patch-clamp recordings were used. Based on the above-described results, there is convincing evidence for functional TRPV4 channel expression in HCK for the following reasons:

(1) The addition of the specific TRPV4 agonist GSK1016790A (126) to HCK cells led to the expected calcium transients **(Figure 21)**. The fluorescence ratio f_{340}/f_{380} during calcium imaging experiments rose, which is equivalent to the increase of $[Ca^{2+}]_i$. These calcium response patterns show similarities to those in human corneal endothelial cells, where the addition of 5 µmol/l GSK1016790A also led to a significant increase of fluorescence ratio f_{340}/f_{380} (73). In that study, it was also attributed to the presence of TRPV4 channels (73).

(2) The specific TRPV4 antagonist GSK2193874 (129) clearly suppressed these GSK1016790A-induced calcium transients in HCK in calcium imaging measurements. The same results could be applied to whole-cell currents. GSK1016790A increased the currents, whereas GSK2193874 suppressed these currents **(Figure 22)**. Notably, in these experiments specific GSK tools were used for detection of TRPV4, which was not the case in previous studies, e.g. concerning the epithelium of the cornea (72).

(3) Since the TRPV4 channel is an "osmosensor" (99, 100), HCK responded to the exposure to a hypotonic solution with increased $[Ca^{2+}]_i$ in calcium imaging measurements **(Figure 23 A)**. This effect was also observed in human corneal endothelial cells by Mergler et al. (73).

(4) Furthermore, GSK2193874 was also able to inhibit the hypotonicity-induced effect, even if this result did not reach statistical significance, due to not normally distributed values **(Figure 23 B)**.

(5) Moderate heat, another well-known stimulus for TRPV4 activation (115-117), also led to a rise in the fluorescence ratio f_{340}/f_{380} during the calcium imaging experiments **(Figure 24)**. Even if it is less specific compared to the pharmacological approach for TRPV4 identification, this is another indication for the functional expression of TRPV4 channels in HCK cells. The thermosensitivity of TRPV4 channels in human corneal and conjunctival epithelial cells was investigated by Mergler et al., 2011 (69, 166).

(6) Chloride channels are also present in HCK cells since an effect on the reverse potential of whole-cell currents between high- and low-chloride containing solution was detected (**Figure 25**). These currents were present in all patch-clamp recordings concerning TRPV4 identification.

Taken together, the results of this thesis concerning the GSK1016790A, hypotonicity and moderate heat response are in line with those of previous studies concerning other cell types in the human cornea.

4.2 Comparison of the results to other studies

For example, Mergler et al., who particularly studied the functional expression of different TRP channels in all layers of the human cornea, revealed similar behavior of TRPV4 channels in human corneal endothelial cells: GSK1016790A, moderate heat (< 40°C) as well as hypotonicity led to calcium transients and increased the $[Ca^{2+}]_i$ (69, 73).

Martinez-Rendon et al., 2017, also used the specific agonist GSK1016790A in calcium imaging experiments to confirm the functional activity of TRPV4 channels, in this case in rabbit corneal epithelial cells (RCEI cells, a corneal epithelial cell model established from rabbit cornea (168, 169)). They aimed to proof the effect of TRPV4 on tight junctions and cell differentiation in their cell model (169). They observed a calcium response pattern after extracellular application of GSK1016790A, which is in line with this thesis.

To point out another example of similar findings in other papers, Pan et al. noticed an increase of intracellular calcium as response to hypotonic medium as well in human corneal epithelial cells (HCEC) (72). It led - in conjunction with other observations (e.g. the agonistic effect of 4α-PDD) - to the conclusion of there being functional TRPV4 expression in HCEC (72). Furthermore, similar results concerning TRPV4 activation by moderate heat were also observed in human conjunctival epithelial cells by Mergler et al., 2012 (69). Specifically, this study demonstrated the different heat-induced Ca^{2+} increases by different heat-sensitive TRPs (69).

Very recently, Liebe et al. used GSK1016790A to prove the activation of TRPV4 channels in ruminal cells (HEK-293 overexpressing bTRPV4) (170). Whole-cell measurements were performed using the conventional patch-clamp method. After the addition of the agonist GSK1016790A, both inward and outward currents increased in these measurements (170). These current response patterns are consistent with the observations of the planar patch-clamp measurements from this thesis.

4.3 The effect of sodium gluconate in classical patch-clamp recordings

The results above provide evidence for chloride conductivity, since the negative reversal potentials at the beginning of the classical patch-clamp experiment in the presence of sodium chloride shifted to more positive values after solution exchange to sodium gluconate. In conclusion, anion channels such as chloride channels were also present in the whole-cell currents, which may overlay the effect of TRP4 channel modulators. Similar results concerning chloride conductivity were obtained in ruminal epithelial cells (171). Specifically, Stumpff et al. showed different values in their study for outward rectified currents after the solution exchange from NaCl to NaGlu, and they concluded that this is possible evidence for chloride influx (171).

4.4. Clinical relevance

TRPV4 in eye pathophysiology

The functional characterization of TRPV4 channels in HCK could be of great interest for developing therapies for certain diseases, such as dry eye disease (DED). According to Asbell et al., 2019, the three most common symptoms of DED are: “eye discomfort, eye sensitivity and eye pain” (quoted from Asbell et al., 2019 (172)), and especially burning eyes (172). Since TRPV4 are involved in pain sensation (173), this could be a potential target point for treating the symptoms by modulating TRPV4 channels. A similar approach was investigated using the TRPV1 blocker capsazepine to suppress TRPV1 activity, which in turn reduced corneal pain in severe DED (174). Like TRPV1, TRPV4 very likely has similar function in non-excitable cells. Notably, there is convincing evidence of TRPV4 expression in human corneal epithelial and endothelial cells ((72, 73) and reviewed by Mergler et al. (7)), which may be interesting in a clinical approach (reviewed in Grace et al., 2017, (175)). For example, Alessandri-Haber et al. revealed in 2003 that primary nociceptive afferent nerve fibers express TRPV4, and these channels perform as a transducer for osmotic changes and the resulting pain (125). Correspondingly, TRPV4 activation through hypotonic stimuli lead to inflammatory and even to neuropathic pain (125). They also found out that even hypertonic stress could induce pain via TRPV4 (173). This phenomenon was intensified by prostaglandin E_2 (PGE_2) (173). Furthermore, Suzuki et al. found out in the same year that TRPV4 knockout mice had a lowered pain response to pressure on their tail (176), which once again makes TRPV4 look like an important mechanosensor. Regarding the role of the trigeminal nerve, it was shown that the sensory nerve supports epithelial stem cell function in the healing of the corneal epithelium in mice (141). Taken together, the cornea has a large number of nerve endings, which are activated to varying degrees when injured, with the involvement of various

channels (including TRP channels) (reviewed by Belmonte et al., 2015, (177)). If TRPV4 modulation had an effect on the fine nerve endings in the cornea, this could also be an interesting starting point for the therapeutic use of TRPV4 channels in ophthalmologic diseases.

TRPV4 is also involved in mechanical hyperalgesia in tissues affected by inflammation (178). It has even been stated that the activation of the TRPV4 (e.g. by an agonist) is responsible for inflammation signs, and that there are more channels expressed in inflamed tissues (reviewed by Vergnolle, 2014, (179)). This has already been observed, amongst others, in the joints of rats (180). Furthermore, D'Aldebert et al. revealed in 2011 that TRPV4 activation in mouse intestines led to chemokine release and colitis (181). Ye et al. found out in 2012 that TRPV4 knockdown led to a decreased expression of inflammation-related genes like chemokines or cytokines (182). Since these are only a few selected examples showing the involvement of TRPV4 in inflammation processes in different tissues, the idea of TRPV4 playing a potential role in inflammation of the eye surface is obvious. This could make the channel a target for inflammation treatment, e.g. in connection with wound healing or in dry eye disease.

More research will be needed to reveal the specific role of TRPV4 in HCK in pain and inflammation.

Finding evidence for the functional expression of TRPV4 in HCK may also be of great importance for intervening in the complex process of corneal wound healing. Corneal opacities following infections, trauma and surgery are a major worldwide problem and cause many cases of blindness. This remains as an issue currently, since some cases of keratitis have been described in relation to an infection with the new SARS-CoV-2 virus (24, 183). As described in the introduction, in 2016 Okada et al. revealed the responsibility of TRPV4 for fibrosis and inflammation in wound repair (139). The outcome of the healing of a corneal wound was markedly better in TRPV4-null (KO) mice (139). The release of interleukin-6 (IL-6), an inflammatory mediator, from corneal macrophages decreased in TRPV4-null (KO) mice (139). Moreover, the expression of genes relevant for fibroses were downregulated (139). So, it would be an interesting approach to use TRPV4 antagonists like GSK2193874, for example as eye drops, as a therapeutic option for stromal wounds. The TRPV4 channels in HCK cells could be reached and blocked. In this way, stromal opacification caused by fibroses could be prevented, similarly to the knock-out of TRPV4 in the study by Okada et al. (139).

In conclusion, there is still the need for more research concerning the approach for utilizing the activation and blocking of the channel to an appropriate extent in the therapy of ophthalmological pathologies.

4.5 Limitations and strength of the studies

Cells and cell culture

As mentioned before, a SV40-induced immortalized permanent HCK cell-line was used for this thesis. Zorn-Kruppa et al. proved this well-established cell line to be a suitable cell model due to the comparability of responses in toxicology tests to primary human corneal keratocytes (145). Nonetheless, it is commonly known that the possibility to transfer the results of an *in vitro* experiment exactly to *in vivo* conditions, or to an organism like the human body, is limited (184). *In vivo*, more circumstances occur that have to be considered, e.g. the interaction between different types of cell and environmental conditions. Therefore, measurements at the fundamental level of cell biology can only give a well-founded suggestion about the functionality of specific cells and its channels.

Furthermore, it was not always possible to perform the calcium imaging experiments with coverslips populated with HCK cells in the same cell density. There were some fluctuations noted depending on the cell culture conditions. Because of these circumstances, there were sometimes loose cell associations with bigger and more branched cells as well as nearly dense cell lawns **(Figure 16)**.

Differences in HCK cell sizes also affected the cell membrane capacitance compensation (C-slow values) in the planar patch-clamp recordings. In some measurements, a high cell membrane capacity gave the impression of a huge cell, which is entirely possible amongst HCK. On the other hand, an explanation may be that in some patch-clamp recordings two cells were measured together.

Interfering factors during measurements

As explained in the methods section of this thesis, the fluorescent dye Fura-2/AM was used in the calcium imaging measurements. It is known that dye concentrations above 6 µmol/l or 10 µmol/l are able to have an influence on the calcium metabolism of a cell (150, 151). Therefore, these high concentrations were not used. Furthermore, overly long exposure to a light source can cause the dye to decompose (bleaching effect) (185). Therefore, the measurements were carried out in a darkened room to avoid any bleaching effect. Nonetheless, minor bleaching effects were fixed in some measurements using drift corrections with the help of the TIDA software mentioned in the methods section. Measurements with high bleaching effects were discarded from the evaluation.

Some cells underwent cell death prior to or during the measurement, which could be seen by their strong coloring. The data of possible non-vital cells as well as the ones that showed a clearly irregular baseline were excluded in the evaluation. A few cells presented some granula in their cell

plasma from time to time as already mentioned in the results section (see **Figure 30**), which could be an indication of imminent cell death, but this did not interfere with the outcome of the measurement. Furthermore, **Figure 29** shows a good example of cells that do not respond equally to a stimulus or do not respond at all (see ROI 1 and ROI 6 as possible avital cells and ROI 7 for an irregular increase after stimulus addition).

Despite working carefully during the calcium imaging experiments, pipetting artifacts could not always be prevented. The pipetting of a new solution as well as the suction of the pump to ensure a balanced liquid level caused liquid to move in the bath chamber. Sometimes, it led to spikes at the point of drug application in the analysis of the fluorescence ratio f_{340}/f_{380} **(Figure 31)**. Since these short-lasting spikes at the time point of application obviously did not represent the drug effect, they were calculated out.

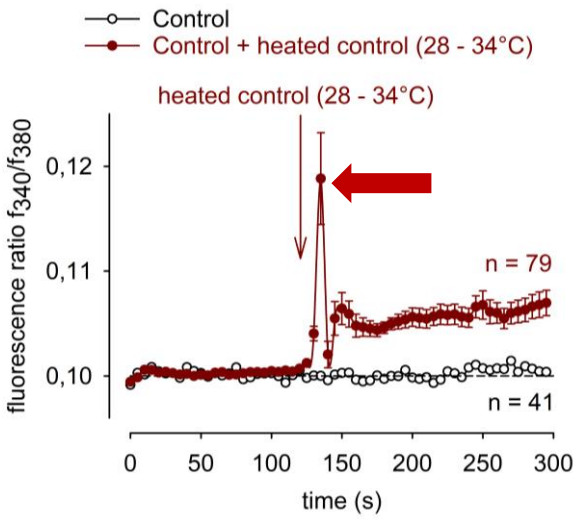

Figure 31: Example of a spike in the analysis of the fluorescence ratio f_{340}/f_{380} during calcium imaging measurements caused by pipetting artifacts. This is not a biological effect but rather an experimental issue. The spike in the calcium responses that the red arrow points at occurs at a time point of 135 s, and therefore shortly after the beginning of, as well as during, the application of the heated control solution. The artifact was easily cut out using the SigmaPlot software.

The calcium imaging experiments were carried out under non-physiological conditions. Therefore, an increased baseline in the measurements could not be excluded by a more or less high stress level for a cell. This was due to changed ambient conditions. To reduce the effect of temperature changes on intracellular Ca^{2+}, the cells were adapted to the room temperature for about 5 minutes when taken out of the incubator before the measurement **(Figure 15)**. Nonetheless, irregularities

in the baseline in the first minutes of a measurement were still observed, probably caused by temperature adaption. Additionally, the solution changes always provided a potential stress factor for the cells, since TRPV4 is also a mechanosensor. Interestingly, auto-store depletions of the cells were also observed under control conditions, possibly indicating secretion activity **(Figure 32)**. The secretion of biomarkers or other calcium dependent compounds of the HCK cells is probably involved. Unfortunately, the spontaneous release of Ca^{2+} from intracellular stores can overlay the drug effects on calcium regulation. Measurements with abnormal auto-store depletions were excluded from evaluation.

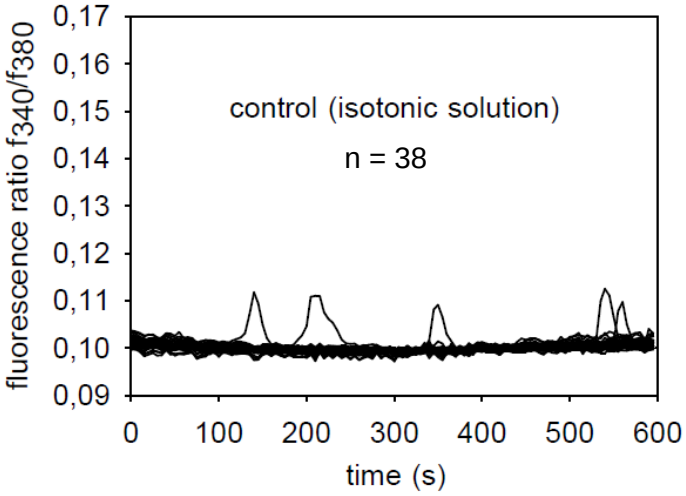

Figure 32: Calcium imaging experiment demonstrating auto-store depletions during baseline measurements with an isotonic solution. Notably, there was only one cell showing such Ca^{2+} transients. Specifically, at 5 different time points, one trace (one cell) showed Ca^{2+} transients. This effect was triggered due to spontaneous release of calcium from intracellular stores. The baselines of the different cells (n = 38) are mostly at the same level.

When working with highly sensitive measurements methods like calcium imaging and planar patch-clamp technique, the signal-noise ratio plays a role if there are low fluorescence signals or small cells have been used for whole-cell current measurements of the patch-clamp recordings. There was a high data scattering in several measurements due to a varying signal-to-noise ratio.
In some planar patch-clamp measurements, high control currents were noticeable even if the TRPV4-agonist GSK1016790A was not added. This might be due to high anion currents, since the extracellular solution contained more chloride than the intracellular solution. Therefore, the set of chloride conductivity tests of HCK cells was made, as described in the results section in Chapter 3.4. The fluoride hydrate-covering in the internal solution of the microchip may be able to inhibit

possible anion chloride channels. In contrast, Garreis et al. showed in 2016 that while performing measurements on pterygium cells, the chloride currents did not change, indicating that in this cell type chloride may only slightly contribute to the whole-cell currents (186). The chloride currents were only outward currents because there was more chloride in the external solution than in the internal solution. In addition, the external solution contained high Ca^{2+}, whereas the internal solution was Ca^{2+} free. Accordingly, the inward rectified currents were mainly charged by Ca^{2+} ions and the patterns were at a mirror interval equal to the Ca^{2+} response patterns of the calcium imaging experiment. The whole-cell inward currents increased after the addition of GSK1016790A, which is therefore attributable to a calcium intake into the cell due to the aforementioned high electrochemical Ca^{2+} concentration gradient. The TRP-typical outward rectification could not be clearly shown in every recording. An explanation may be that there is a high proportion of chloride currents overlapping with the TRPV4-like currents or possible leak currents involved. Therefore, the weak effect of the TRPV4 antagonist GSK2193874 on the outward currents may be overlapped by leak currents, which may occur when the seal is instable.
As mentioned in Chapter 2, the holding potential (HP) in the planar patch-clamp measurements was set to 0 mV. This is important for preventing any possible involvements of voltage-dependent calcium or sodium channel activity. Notably, voltage-operated calcium channels (VOCCs) cannot be activated at 0 mV. A small proportion of VOCCs cannot be excluded at -40 to -50 mV, which corresponds approximately to the resting membrane potential of HCK cells.

Limitations concerning TRPV4 stimuli and antagonists

During the measurements, the TRPV4 agonist GSK1016790A and the antagonist GSK2193874 were used at relative high concentrations to make sure that differences in fluorescence could be detected above the background noise. This might also be the reason for the irreversibility of the $[Ca^{2+}]_i$ increase – such a huge calcium influx cannot be compensated by the cell.
Furthermore, Ruthenium red (RuR) was used as an unspecific antagonist to inhibit the effect on the fluorescence ratio f_{340}/f_{380} caused by moderate heat, but it did not work out properly and did not reach statistical significance (**Figure 26 B**). The red dye in RuR may have an impact on the fluorescence and might have caused technical problems. Regarding that, RuR was regularly used for TRPV4 identification (115) before other more sensitive TRPV4 channel modulators were available (126).

Additionally, an interesting effect was observed during calcium imaging measurements with the TRPV4 agonist GSK1016790A. On each day that experiments with GSK1016790A were carried out, it was mostly the first measurement that showed the strongest effect on $[Ca^{2+}]_i$ (**Figure 33**). This did not, however, unsettle the conclusion of this set of experiments, and an explanation for this observation may be that GSK1016790A already has an effect in a nanomolar range. It may be possible that the glass cover slips on the microscope slide or the objective of the microscope, which dives into the bath chamber, had some negligible traces of GSK1016790A after the first measurement. This may be enough to activate the TRPV4 channels of a few cells prior to the start of the recording. Hence, only the remaining cells react to the solution change. Another reason might be the rising stress level of the cells, which may possibly induce apoptosis. 6 coverslips are stored together on one well plate, which is taken out of the incubator every time a coverslip must be preincubated with Fura-2/AM. These temperature changes may trigger changes in the control baseline Ca^{2+} levels.

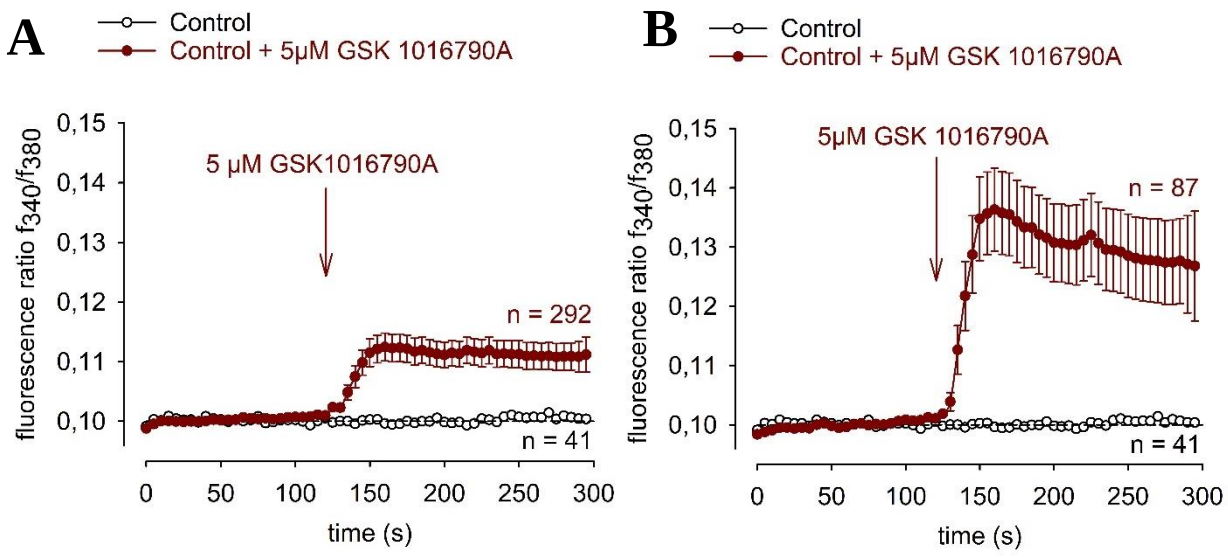

Figure 33: The effect of 5 µmol/l GSK1016790A on HCK cells. The fluorescence ratio f_{340}/f_{380} is plotted on the y-axis against the time on the x-axis. The arrow indicates the point of time when the TRPV4 agonist was added. **A:** All performed experiments with 5 µmol/l GSK1016790A taken together (*n* = 292; see results). **B:** The same experiment as shown in (A) but only the first measurements of the respective experiment days are outlined in this diagram (*n* = 87). The averaged GSK1016790A-induced effect on $[Ca^{2+}]_i$ was at higher levels since the fluorescence ratio showed higher values.

4.6 Conclusion

In conclusion, there is a functional TRPV4 expression in HCK and this was shown for the first time in this cell type. This was demonstrated by three different activation mechanisms and two different methods. The most convincing evidence was shown with the pharmacological approach using the very specific and potent TRPV4 agonist GSK1016790A (126, 187, 188). This result is in line with other TRPV4 channel activation mechanisms like moderate heating and hypotonic stress. These kinds of activations also induced an increase of $[Ca^{2+}]_i$. The functionality of TRPV4 was further validated by using GSK2196790A, which is a specific TRPV4 antagonist (130). This antagonist was able to clearly suppress the effects of GSK1016790A-induced increase of intracellular calcium level. This conclusion corresponds to similar observations of functional TRPV4 channel expression in human corneal epithelial cells (72), human conjunctival epithelial cells (69) and in human corneal endothelial cells (73). This study has closed the circle and confirms that functional TRPV4 is also expressed in the HCK within the corneal stroma – the main part of the cornea (16). Overall, TRPV4 is expressed in each non-excitable cell type of the cornea. Trigeminal nerve TRPV4 expression was also demonstrated in co-cultures with ganglion and corneal epithelial cells (141). With the knowledge of these different roles of TRPV4, it is suggested that TRPV4 in the cornea including the HCK may be a potential pharmacological target for the development of therapies against several diseases of the eye and the improvement of wound healing processes.

References

1. DelMonte DW, Kim T. Anatomy and physiology of the cornea. J Cataract Refract Surg. 2011;37(3):588-98.

2. Drenckhahn D, Rager G. Visuelles System. In: Drenckhahn D, editor. Anatomie: Makroskopische Anatomie, Histologie, Embryologie, Zellbiologie. 2. 16th ed. Würzburg: Elsevier; 2004. p. 650-705.

3. Rufer F, Schroder A, Erb C. White-to-white corneal diameter: normal values in healthy humans obtained with the Orbscan II topography system. Cornea. 2005;24(3):259-61.

4. Dua HS, Faraj LA, Said DG, Gray T, Lowe J. Human corneal anatomy redefined: a novel pre-Descemet's layer (Dua's layer). Ophthalmology. 2013;120(9):1778-85.

5. Schünke M, Schulte E, Schumacher U, Voll M, Wesker KH. 5.12 Brechende Medien des Auges: Linse (Lens cristallina) und Hornhaut (Cornea). In: Schünke M, Schulte E, Schumacher U, Voll M, Wesker KH, editors. Prometheus LernAtlas - Kopf, Hals und Neuroanatomie. 5. Auflage ed. Stuttgart: Georg Thieme Verlag; 2018.

6. Schuenke MS, Erik; Schumacher, Udo. Prometheus Kopf, Hals und Neuroanatomie. Stuttgart: Georg Thieme Verlag KG; 2018.

7. Mergler S, Valtink M, Takayoshi S, Okada Y, Miyajima M, Saika S, Reinach PS. Temperature-sensitive transient receptor potential channels in corneal tissue layers and cells. Ophthalmic Res. 2014;52(3):151-9.

8. Farjo A, McDermott M, Soong H. Corneal anatomy, physiology, and wound healing. In: Yanoff M, Duker J, editors. Ophthalmology. St. Louis: eds; 2008. p. 203-8.

9. Wiley L, SundarRaj N, Sun TT, Thoft RA. Regional heterogeneity in human corneal and limbal epithelia: an immunohistochemical evaluation. Invest Ophthalmol Vis Sci. 1991;32(3):594-602.

10. Hanna C, Bicknell DS, O'Brien JE. Cell turnover in the adult human eye. Arch Ophthalmol. 1961;65:695-8.

11. Thoft RA, Friend J. The X, Y, Z hypothesis of corneal epithelial maintenance. Invest Ophthalmol Vis Sci. 1983;24(10):1442-3.

12. Buck RC. Measurement of centripetal migration of normal corneal epithelial cells in the mouse. Invest Ophthalmol Vis Sci. 1985;26(9):1296-9.

13. Geroski DH, Matsuda M, Yee RW, Edelhauser HF. Pump function of the human corneal endothelium. Effects of age and cornea guttata. Ophthalmology. 1985;92(6):759-63.

14. Bourne WM, Nelson LR, Hodge DO. Central corneal endothelial cell changes over a ten-year period. Invest Ophthalmol Vis Sci. 1997;38(3):779-82.

15. Yee RW, Matsuda M, Schultz RO, Edelhauser HF. Changes in the normal corneal endothelial cellular pattern as a function of age. Curr Eye Res. 1985;4(6):671-8.

16. Beuerman RW, Pedroza L. Ultrastructure of the human cornea. Microsc Res Tech. 1996;33(4):320-35.

17. Patel S, McLaren J, Hodge D, Bourne W. Normal human keratocyte density and corneal thickness measurement by using confocal microscopy in vivo. Invest Ophthalmol Vis Sci. 2001;42(2):333-9.

18. Muller LJ, Pels L, Vrensen GF. Novel aspects of the ultrastructural organization of human corneal keratocytes. Invest Ophthalmol Vis Sci. 1995;36(13):2557-67.

19. Fini ME, Stramer BM. How the cornea heals: cornea-specific repair mechanisms affecting surgical outcomes. Cornea. 2005;24(8 Suppl):S2-S11.

20. Maurice DM. The transparency of the corneal stroma. Vision Res. 1970;10(1):107-8.

21. Boote C, Dennis S, Newton RH, Puri H, Meek KM. Collagen fibrils appear more closely packed in the prepupillary cornea: optical and biomechanical implications. Invest Ophthalmol Vis Sci. 2003;44(7):2941-8.

22. Maurice DM. The structure and transparency of the cornea. J Physiol. 1957;136(2):263-86.

23. Cheng X, Petsche SJ, Pinsky PM. A structural model for the in vivo human cornea including collagen-swelling interaction. J R Soc Interface. 2015;12(109):20150241.

24. Kuo IC, Mostafa HH. Detection of SARS-CoV-2 RNA in the corneal epithelium of a patient after recovery from COVID-19. Am J Ophthalmol Case Rep. 2021;22:101074.

25. Stepp MA, Zieske JD, Trinkaus-Randall V, Kyne BM, Pal-Ghosh S, Tadvalkar G, Pajoohesh-Ganji A. Wounding the cornea to learn how it heals. Exp Eye Res. 2014;121:178-93.

26. Ljubimov AV, Saghizadeh M. Progress in corneal wound healing. Prog Retin Eye Res. 2015;49:17-45.

27. Wilson SA, Last A. Management of corneal abrasions. Am Fam Physician. 2004;70(1):123-8.

28. Jester JV, Rodrigues MM, Herman IM. Characterization of avascular corneal wound healing fibroblasts. New insights into the myofibroblast. Am J Pathol. 1987;127(1):140-8.

29. Mohan RR, Hutcheon AE, Choi R, Hong J, Lee J, Mohan RR, Ambrosio R, Jr., Zieske JD, Wilson SE. Apoptosis, necrosis, proliferation, and myofibroblast generation in the stroma following LASIK and PRK. Exp Eye Res. 2003;76(1):71-87.

30. West-Mays JA, Dwivedi DJ. The keratocyte: corneal stromal cell with variable repair phenotypes. Int J Biochem Cell Biol. 2006;38(10):1625-31.

31. Zieske JD, Guimaraes SR, Hutcheon AE. Kinetics of keratocyte proliferation in response to epithelial debridement. Exp Eye Res. 2001;72(1):33-9.

32. Wilson SE, Mohan RR, Mohan RR, Ambrosio R, Jr., Hong J, Lee J. The corneal wound healing response: cytokine-mediated interaction of the epithelium, stroma, and inflammatory cells. Prog Retin Eye Res. 2001;20(5):625-37.

33. Jester JV, Huang J, Barry-Lane PA, Kao WW, Petroll WM, Cavanagh HD. Transforming growth factor(beta)-mediated corneal myofibroblast differentiation requires actin and fibronectin assembly. Invest Ophthalmol Vis Sci. 1999;40(9):1959-67.

34. Jester JV, Moller-Pedersen T, Huang J, Sax CM, Kays WT, Cavangh HD, Petroll WM, Piatigorsky J. The cellular basis of corneal transparency: evidence for 'corneal crystallins'. J Cell Sci. 1999;112 (Pt 5):613-22.

35. Jester JV, Petroll WM, Cavanagh HD. Corneal stromal wound healing in refractive surgery: the role of myofibroblasts. Prog Retin Eye Res. 1999;18(3):311-56.

36. Jester JV, Ho-Chang J. Modulation of cultured corneal keratocyte phenotype by growth factors/cytokines control in vitro contractility and extracellular matrix contraction. Exp Eye Res. 2003;77(5):581-92.

37. Netto MV, Mohan RR, Sinha S, Sharma A, Dupps W, Wilson SE. Stromal haze, myofibroblasts, and surface irregularity after PRK. Exp Eye Res. 2006;82(5):788-97.

38. Torricelli AA, Singh V, Agrawal V, Santhiago MR, Wilson SE. Transmission electron microscopy analysis of epithelial basement membrane repair in rabbit corneas with haze. Invest Ophthalmol Vis Sci. 2013;54(6):4026-33.

39. Sandvig KU, Haaskjold E, Bjerknes R, Refsum SB, Kravik K. Cell kinetics of conjunctival and corneal epithelium during regeneration of different-sized corneal epithelial defects. Acta Ophthalmol (Copenh). 1994;72(1):43-8.

40. Cox EA, Huttenlocher A. Regulation of integrin-mediated adhesion during cell migration. Microsc Res Tech. 1998;43(5):412-9.

41. Sammak PJ, Hinman LE, Tran PO, Sjaastad MD, Machen TE. How do injured cells communicate with the surviving cell monolayer? J Cell Sci. 1997;110 (Pt 4):465-75.

42. Tran PO, Hinman LE, Unger GM, Sammak PJ. A wound-induced [Ca2+]i increase and its transcriptional activation of immediate early genes is important in the regulation of motility. Exp Cell Res. 1999;246(2):319-26.

43. Bian X, Hughes FM, Jr., Huang Y, Cidlowski JA, Putney JW, Jr. Roles of cytoplasmic Ca2+ and intracellular Ca2+ stores in induction and suppression of apoptosis in S49 cells. Am J Physiol. 1997;272(4 Pt 1):C1241-9.

44. Zhu WH, Loh TT. Roles of calcium in the regulation of apoptosis in HL-60 promyelocytic leukemia cells. Life Sci. 1995;57(23):2091-9.

45. Saris NE, Carafoli E. A historical review of cellular calcium handling, with emphasis on mitochondria. Biochemistry (Mosc). 2005;70(2):187-94.

46. Clapham DE. TRP channels as cellular sensors. Nature. 2003;426(6966):517-24.

47. Köhling Rd, Hescheler Jr, Speckmann E-J. Physiologie. Munich: Urban & Fischer; 2013. 771 p.

48. Clapham DE, Runnels LW, Strubing C. The TRP ion channel family. Nat Rev Neurosci. 2001;2(6):387-96.

49. Lytton J. Na+/Ca2+ exchangers: three mammalian gene families control Ca2+ transport. Biochem J. 2007;406(3):365-82.

50. Ottolini M, Hong K, Sonkusare SK. Calcium signals that determine vascular resistance. Wiley Interdiscip Rev Syst Biol Med. 2019;11(5):e1448.

51. Streb H, Irvine RF, Berridge MJ, Schulz I. Release of Ca2+ from a nonmitochondrial intracellular store in pancreatic acinar cells by inositol-1,4,5-trisphosphate. Nature. 1983;306(5938):67-9.

52. Ramsey IS, Delling M, Clapham DE. An introduction to TRP channels. Annu Rev Physiol. 2006;68:619-47.

53. Montell C. The TRP superfamily of cation channels. Sci STKE. 2005;2005(272):re3.

54. Nilius B, Owsianik G. The transient receptor potential family of ion channels. Genome Biol. 2011;12(3):218.

55. Cosens DJ, Manning A. Abnormal electroretinogram from a Drosophila mutant. Nature. 1969;224(5216):285-7.

56. Montell C. Molecular genetics of Drosophila vision. Bioessays. 1989;11(2-3):43-8.

57. Minke B. Light-induced reduction in excitation efficiency in the trp mutant of Drosophila. J Gen Physiol. 1982;79(3):361-85.

58. Montell C, Rubin GM. Molecular characterization of the Drosophila trp locus: a putative integral membrane protein required for phototransduction. Neuron. 1989;2(4):1313-23.

59. Venkatachalam K, Montell C. TRP channels. Annu Rev Biochem. 2007;76:387-417.

60. Cordeiro S, Seyler S, Stindl J, Milenkovic VM, Strauss O. Heat-Sensitive TRPV Channels in Retinal Pigment Epithelial Cells: Regulation of VEGF-A Secretion. Invest Ophth Vis Sci. 2010;51(11):6001-8.

61. Mergler S, Boehm A, Derckx R, Schmelzer L, Garreis F, Riechardt A, Electropyhsiology V. Calcium regulation by transient receptor potential channels in human uveal melanoma cells. Invest Ophth Vis Sci. 2013;54(15).

62. Klooster J, Blokker J, ten Brink JB, Unmehopa U, Fluiter K, Bergen AAB, Kamermans M. Ultrastructural Localization and Expression of TRPM1 in the Human Retina. Invest Ophth Vis Sci. 2011;52(11):8356-62.

63. Bennett TM, Mackay DS, Siegfried CJ, Shiels A. Mutation of the melastatin-related cation channel, TRPM3, underlies inherited cataract and glaucoma. PLoS One. 2014;9(8):e104000.

64. Yang H, Mergler S, Sun X, Wang Z, Lu L, Bonanno JA, Pleyer U, Reinach PS. TRPC4 knockdown suppresses epidermal growth factor-induced store-operated channel activation and growth in human corneal epithelial cells. J Biol Chem. 2005;280(37):32230-7.

65. Parra A, Gonzalez-Gonzalez O, Gallar J, Belmonte C. Tear fluid hyperosmolality increases nerve impulse activity of cold thermoreceptor endings of the cornea. Pain. 2014;155(8):1481-91.

66. Zhang F, Yang H, Wang Z, Mergler S, Liu H, Kawakita T, Tachado SD, Pan Z, Capo-Aponte JE, Pleyer U, Koziel H, Kao WW, Reinach PS. Transient receptor potential vanilloid 1 activation induces inflammatory cytokine release in corneal epithelium through MAPK signaling. J Cell Physiol. 2007;213(3):730-9.

67. Turker E, Garreis F, Khajavi N, Reinach PS, Joshi P, Brockmann T, Lucius A, Ljubojevic N, Turan E, Cooper D, Schick F, Reinholz R, Pleyer U, Kohrle J, Mergler S. Vascular Endothelial Growth Factor (VEGF) Induced Downstream Responses to Transient Receptor Potential Vanilloid 1 (TRPV1) and 3-Iodothyronamine (3-T1AM) in Human Corneal Keratocytes. Front Endocrinol (Lausanne). 2018;9:670.

68. Mergler S, Valtink M, Coulson-Thomas VJ, Lindemann D, Reinach PS, Engelmann K, Pleyer U. TRPV channels mediate temperature-sensing in human corneal endothelial cells. Exp Eye Res. 2010;90(6):758-70.

69. Mergler S, Garreis F, Sahlmuller M, Lyras EM, Reinach PS, Dwarakanath A, Paulsen F, Pleyer U. Calcium regulation by thermo- and osmosensing transient receptor potential vanilloid channels (TRPVs) in human conjunctival epithelial cells. Histochem Cell Biol. 2012;137(6):743-61.

70. Yang Y, Yang H, Wang Z, Mergler S, Wolosin JM, Reinach PS. Functional TRPV1 expression in human corneal fibroblasts. Exp Eye Res. 2013;107:121-9.

71. Yamada T, Ueda T, Ugawa S, Ishida Y, Imayasu M, Koyama S, Shimada S. Functional expression of transient receptor potential vanilloid 3 (TRPV3) in corneal epithelial cells: involvement in thermosensation and wound healing. Exp Eye Res. 2010;90(1):121-9.

72. Pan Z, Yang H, Mergler S, Liu H, Tachado SD, Zhang F, Kao WW, Koziel H, Pleyer U, Reinach PS. Dependence of regulatory volume decrease on transient receptor potential vanilloid 4 (TRPV4) expression in human corneal epithelial cells. Cell Calcium. 2008;44(4):374-85.

73. Mergler S, Valtink M, Taetz K, Sahlmuller M, Fels G, Reinach PS, Engelmann K, Pleyer U. Characterization of transient receptor potential vanilloid channel 4 (TRPV4) in human corneal endothelial cells. Exp Eye Res. 2011;93(5):710-9.

74. Mergler S, Pleyer U, Reinach P, Bednarz J, Dannowski H, Engelmann K, Hartmann C, Yousif T. EGF suppresses hydrogen peroxide induced Ca2+ influx by inhibiting L-type channel activity in cultured human corneal endothelial cells. Exp Eye Res. 2005;80(2):285-93.

75. Parra A, Madrid R, Echevarria D, del Olmo S, Morenilla-Palao C, Acosta MC, Gallar J, Dhaka A, Viana F, Belmonte C. Ocular surface wetness is regulated by TRPM8-dependent cold thermoreceptors of the cornea. Nat Med. 2010;16(12):1396-9.

76. Lucius A, Khajavi N, Reinach PS, Kohrle J, Dhandapani P, Huimann P, Ljubojevic N, Grotzinger C, Mergler S. 3-Iodothyronamine increases transient receptor potential melastatin channel 8 (TRPM8) activity in immortalized human corneal epithelial cells. Cell Signal. 2016;28(3):136-47.

77. Mergler S, Mertens C, Valtink M, Reinach PS, Szekely VC, Slavi N, Garreis F, Abdelmessih S, Turker E, Fels G, Pleyer U. Functional significance of thermosensitive transient receptor potential melastatin channel 8 (TRPM8) expression in immortalized human corneal endothelial cells. Exp Eye Res. 2013;116:337-49.

78. Canner JP, Linsenmayer TF, Kubilus JK. Developmental regulation of trigeminal TRPA1 by the cornea. Invest Ophthalmol Vis Sci. 2014;56(1):29-36.

79. Steven P, Cursiefen C. [Anti-inflammatory treatment in dry eye disease]. Klin Monbl Augenheilkd. 2012;229(5):500-5.

80. Mergler S, Pleyer U. [Importance of Transient Receptor Potential Channels of the Ocular Surface: Insights and Outlook - from Laboratory Research to Clinical Practice]. Klin Monbl Augenheilkd. 2020;237(5):637-43.

81. Mergler S, Dietrich-Ntoukas T, Pleyer U. [Neurotrophic keratopathy : Principles, diagnostics and treatment]. Ophthalmologe. 2019;116(8):797-810.

82. Reinach PS, Chen W, Mergler S. Polymodal roles of transient receptor potential channels in the control of ocular function. Eye Vis (Lond). 2015;2:5.

83. Reinach PS, Mergler S, Okada Y, Saika S. Ocular transient receptor potential channel function in health and disease. BMC Ophthalmol. 2015;15 Suppl 1:153.

84. Launay P, Fleig A, Perraud AL, Scharenberg AM, Penner R, Kinet JP. TRPM4 is a Ca2+-activated nonselective cation channel mediating cell membrane depolarization. Cell. 2002;109(3):397-407.

85. Hofmann T, Chubanov V, Gudermann T, Montell C. TRPM5 is a voltage-modulated and Ca(2+)-activated monovalent selective cation channel. Curr Biol. 2003;13(13):1153-8.

86. Liu D, Liman ER. Intracellular Ca2+ and the phospholipid PIP2 regulate the taste transduction ion channel TRPM5. Proc Natl Acad Sci U S A. 2003;100(25):15160-5.

87. Prawitt D, Monteilh-Zoller MK, Brixel L, Spangenberg C, Zabel B, Fleig A, Penner R. TRPM5 is a transient Ca2+-activated cation channel responding to rapid changes in [Ca2+]i. Proc Natl Acad Sci U S A. 2003;100(25):15166-71.

88. Nilius B, Owsianik G, Voets T, Peters JA. Transient receptor potential cation channels in disease. Physiol Rev. 2007;87(1):165-217.

89. Damann N, Voets T, Nilius B. TRPs in our senses. Curr Biol. 2008;18(18):R880-9.

90. Nilius B, Prenen J, Droogmans G, Voets T, Vennekens R, Freichel M, Wissenbach U, Flockerzi V. Voltage dependence of the Ca2+-activated cation channel TRPM4. J Biol Chem. 2003;278(33):30813-20.

91. Nilius B, Talavera K, Owsianik G, Prenen J, Droogmans G, Voets T. Gating of TRP channels: a voltage connection? J Physiol. 2005;567(Pt 1):35-44.

92. Karashima Y, Prenen J, Meseguer V, Owsianik G, Voets T, Nilius B. Modulation of the transient receptor potential channel TRPA1 by phosphatidylinositol 4,5-biphosphate manipulators. Pflugers Arch. 2008;457(1):77-89.

93. Caterina MJ, Schumacher MA, Tominaga M, Rosen TA, Levine JD, Julius D. The capsaicin receptor: a heat-activated ion channel in the pain pathway. Nature. 1997;389(6653):816-24.

94. McKemy DD, Neuhausser WM, Julius D. Identification of a cold receptor reveals a general role for TRP channels in thermosensation. Nature. 2002;416(6876):52-8.

95. Peier AM, Moqrich A, Hergarden AC, Reeve AJ, Andersson DA, Story GM, Earley TJ, Dragoni I, McIntyre P, Bevan S, Patapoutian A. A TRP channel that senses cold stimuli and menthol. Cell. 2002;108(5):705-15.

96. Nilius B, Owsianik G. Transient receptor potential channelopathies. Pflugers Arch. 2010;460(2):437-50.

97. Rock MJ, Prenen J, Funari VA, Funari TL, Merriman B, Nelson SF, Lachman RS, Wilcox WR, Reyno S, Quadrelli R, Vaglio A, Owsianik G, Janssens A, Voets T, Ikegawa S, Nagai T, Rimoin DL, Nilius B, Cohn DH. Gain-of-function mutations in TRPV4 cause autosomal dominant brachyolmia. Nat Genet. 2008;40(8):999-1003.

98. Tsavaler L, Shapero MH, Morkowski S, Laus R. Trp-p8, a novel prostate-specific gene, is up-regulated in prostate cancer and other malignancies and shares high homology with transient receptor potential calcium channel proteins. Cancer Res. 2001;61(9):3760-9.

99. Liedtke W, Choe Y, Marti-Renom MA, Bell AM, Denis CS, Sali A, Hudspeth AJ, Friedman JM, Heller S. Vanilloid receptor-related osmotically activated channel (VR-OAC), a candidate vertebrate osmoreceptor. Cell. 2000;103(3):525-35.

100. Strotmann R, Harteneck C, Nunnenmacher K, Schultz G, Plant TD. OTRPC4, a nonselective cation channel that confers sensitivity to extracellular osmolarity. Nat Cell Biol. 2000;2(10):695-702.

101. Wissenbach U, Bodding M, Freichel M, Flockerzi V. Trp12, a novel Trp related protein from kidney. FEBS Lett. 2000;485(2-3):127-34.

102. Delany NS, Hurle M, Facer P, Alnadaf T, Plumpton C, Kinghorn I, See CG, Costigan M, Anand P, Woolf CJ, Crowther D, Sanseau P, Tate SN. Identification and characterization of a novel human vanilloid receptor-like protein, VRL-2. Physiol Genomics. 2001;4(3):165-74.

103. Deng Z, Paknejad N, Maksaev G, Sala-Rabanal M, Nichols CG, Hite RK, Yuan P. Cryo-EM and X-ray structures of TRPV4 reveal insight into ion permeation and gating mechanisms. Nat Struct Mol Biol. 2018;25(3):252-60.

104. Hellwig N, Albrecht N, Harteneck C, Schultz G, Schaefer M. Homo- and heteromeric assembly of TRPV channel subunits. J Cell Sci. 2005;118(Pt 5):917-28.

105. Ma X, Cheng KT, Wong CO, O'Neil RG, Birnbaumer L, Ambudkar IS, Yao X. Heteromeric TRPV4-C1 channels contribute to store-operated Ca(2+) entry in vascular endothelial cells. Cell Calcium. 2011;50(6):502-9.

106. Stewart AP, Smith GD, Sandford RN, Edwardson JM. Atomic force microscopy reveals the alternating subunit arrangement of the TRPP2-TRPV4 heterotetramer. Biophys J. 2010;99(3):790-7.

107. Lawhorn BG, Brnardic EJ, Behm DJ. Recent advances in TRPV4 agonists and antagonists. Bioorg Med Chem Lett. 2020;30(8):127022.

108. Voets T, Prenen J, Vriens J, Watanabe H, Janssens A, Wissenbach U, Bodding M, Droogmans G, Nilius B. Molecular determinants of permeation through the cation channel TRPV4. J Biol Chem. 2002;277(37):33704-10.

109. Watanabe H, Davis JB, Smart D, Jerman JC, Smith GD, Hayes P, Vriens J, Cairns W, Wissenbach U, Prenen J, Flockerzi V, Droogmans G, Benham CD, Nilius B. Activation of TRPV4 channels (hVRL-2/mTRP12) by phorbol derivatives. J Biol Chem. 2002;277(16):13569-77.

110. Nilius B, Vriens J, Prenen J, Droogmans G, Voets T. TRPV4 calcium entry channel: a paradigm for gating diversity. Am J Physiol Cell Physiol. 2004;286(2):C195-205.

111. Nilius B, Watanabe H, Vriens J. The TRPV4 channel: structure-function relationship and promiscuous gating behaviour. Pflugers Arch. 2003;446(3):298-303.

112. Nilius B, Prenen J, Wissenbach U, Bodding M, Droogmans G. Differential activation of the volume-sensitive cation channel TRP12 (OTRPC4) and volume-regulated anion currents in HEK-293 cells. Pflugers Arch. 2001;443(2):227-33.

113. Becker D, Blase C, Bereiter-Hahn J, Jendrach M. TRPV4 exhibits a functional role in cell-volume regulation. J Cell Sci. 2005;118(Pt 11):2435-40.

114. Argyropoulos C, Rondon-Berrios H, Raj DS, Malhotra D, Agaba EI, Rohrscheib M, Khitan Z, Murata GH, Shapiro JI, Tzamaloukas AH. Hypertonicity: Pathophysiologic Concept and Experimental Studies. Cureus. 2016;8(5):e596.

115. Guler AD, Lee H, Iida T, Shimizu I, Tominaga M, Caterina M. Heat-evoked activation of the ion channel, TRPV4. J Neurosci. 2002;22(15):6408-14.

116. Watanabe H, Vriens J, Suh SH, Benham CD, Droogmans G, Nilius B. Heat-evoked activation of TRPV4 channels in a HEK293 cell expression system and in native mouse aorta endothelial cells. J Biol Chem. 2002;277(49):47044-51.

117. Tominaga M, Caterina MJ. Thermosensation and pain. J Neurobiol. 2004;61(1):3-12.

118. Shibasaki K, Suzuki M, Mizuno A, Tominaga M. Effects of body temperature on neural activity in the hippocampus: regulation of resting membrane potentials by transient receptor potential vanilloid 4. J Neurosci. 2007;27(7):1566-75.

119. Kocak I, Orgul S, Flammer J. Variability in the measurement of corneal temperature using a noncontact infrared thermometer. Ophthalmologica. 1999;213(6):345-9.

120. White JP, Cibelli M, Urban L, Nilius B, McGeown JG, Nagy I. TRPV4: Molecular Conductor of a Diverse Orchestra. Physiol Rev. 2016;96(3):911-73.

121. Kohler R, Heyken WT, Heinau P, Schubert R, Si H, Kacik M, Busch C, Grgic I, Maier T, Hoyer J. Evidence for a functional role of endothelial transient receptor potential V4 in shear stress-induced vasodilatation. Arterioscler Thromb Vasc Biol. 2006;26(7):1495-502.

122. Watanabe H, Vriens J, Prenen J, Droogmans G, Voets T, Nilius B. Anandamide and arachidonic acid use epoxyeicosatrienoic acids to activate TRPV4 channels. Nature. 2003;424(6947):434-8.

123. Sonkusare SK, Bonev AD, Ledoux J, Liedtke W, Kotlikoff MI, Heppner TJ, Hill-Eubanks DC, Nelson MT. Elementary Ca2+ signals through endothelial TRPV4 channels regulate vascular function. Science. 2012;336(6081):597-601.

124. Masuyama R, Vriens J, Voets T, Karashima Y, Owsianik G, Vennekens R, Lieben L, Torrekens S, Moermans K, Vanden Bosch A, Bouillon R, Nilius B, Carmeliet G. TRPV4-mediated calcium influx regulates terminal differentiation of osteoclasts. Cell Metab. 2008;8(3):257-65.

125. Alessandri-Haber N, Yeh JJ, Boyd AE, Parada CA, Chen X, Reichling DB, Levine JD. Hypotonicity induces TRPV4-mediated nociception in rat. Neuron. 2003;39(3):497-511.

126. Thorneloe KS, Sulpizio AC, Lin Z, Figueroa DJ, Clouse AK, McCafferty GP, Chendrimada TP, Lashinger ES, Gordon E, Evans L, Misajet BA, Demarini DJ, Nation JH, Casillas LN, Marquis RW, Votta BJ, Sheardown SA, Xu X, Brooks DP, Laping NJ, Westfall TD. N-((1S)-1-{[4-((2S)-2-{[(2,4-dichlorophenyl)sulfonyl]amino}-3-hydroxypropanoyl)-1 -piperazinyl]carbonyl}-3-methylbutyl)-1-benzothiophene-2-carboxamide (GSK1016790A), a novel and potent transient receptor potential vanilloid 4 channel agonist induces urinary bladder contraction and hyperactivity: Part I. J Pharmacol Exp Ther. 2008;326(2):432-42.

127. Vincent F, Acevedo A, Nguyen MT, Dourado M, DeFalco J, Gustafson A, Spiro P, Emerling DE, Kelly MG, Duncton MA. Identification and characterization of novel TRPV4 modulators. Biochem Biophys Res Commun. 2009;389(3):490-4.

128. Everaerts W, Zhen X, Ghosh D, Vriens J, Gevaert T, Gilbert JP, Hayward NJ, McNamara CR, Xue F, Moran MM, Strassmaier T, Uykal E, Owsianik G, Vennekens R, De Ridder D,

Nilius B, Fanger CM, Voets T. Inhibition of the cation channel TRPV4 improves bladder function in mice and rats with cyclophosphamide-induced cystitis. Proc Natl Acad Sci U S A. 2010;107(44):19084-9.

129. Cheung M, Bao W, Behm DJ, Brooks CA, Bury MJ, Dowdell SE, Eidam HS, Fox RM, Goodman KB, Holt DA, Lee D, Roethke TJ, Willette RN, Xu X, Ye G, Thorneloe KS. Discovery of GSK2193874: An Orally Active, Potent, and Selective Blocker of Transient Receptor Potential Vanilloid 4. ACS Med Chem Lett. 2017;8(5):549-54.

130. Thorneloe KS, Cheung M, Bao W, Alsaid H, Lenhard S, Jian MY, Costell M, Maniscalco-Hauk K, Krawiec JA, Olzinski A, Gordon E, Lozinskaya I, Elefante L, Qin P, Matasic DS, James C, Tunstead J, Donovan B, Kallal L, Waszkiewicz A, Vaidya K, Davenport EA, Larkin J, Burgert M, Casillas LN, Marquis RW, Ye G, Eidam HS, Goodman KB, Toomey JR, Roethke TJ, Jucker BM, Schnackenberg CG, Townsley MI, Lepore JJ, Willette RN. An orally active TRPV4 channel blocker prevents and resolves pulmonary edema induced by heart failure. Sci Transl Med. 2012;4(159):159ra48.

131. Kuebler W, Jordt SE, Liedtke W. COVID-19: Urgent Reconsideration of Lung Edema as a Preventable Outcome: Inhibition of TRPV4 As a Promising and Feasible Approach. SSRN. 2020:3558887.

132. Kuebler WM, Jordt SE, Liedtke WB. Urgent reconsideration of lung edema as a preventable outcome in COVID-19: inhibition of TRPV4 represents a promising and feasible approach. Am J Physiol Lung Cell Mol Physiol. 2020;318(6):L1239-L43.

133. Shahidullah M, Mandal A, Delamere NA. TRPV4 in porcine lens epithelium regulates hemichannel-mediated ATP release and Na-K-ATPase activity. Am J Physiol Cell Physiol. 2012;302(12):C1751-61.

134. Mergler S, Pleyer U. The human corneal endothelium: new insights into electrophysiology and ion channels. Prog Retin Eye Res. 2007;26(4):359-78.

135. Ryskamp DA, Frye AM, Phuong TT, Yarishkin O, Jo AO, Xu Y, Lakk M, Iuso A, Redmon SN, Ambati B, Hageman G, Prestwich GD, Torrejon KY, Krizaj D. TRPV4 regulates calcium homeostasis, cytoskeletal remodeling, conventional outflow and intraocular pressure in the mammalian eye. Sci Rep. 2016;6:30583.

136. Torricelli AA, Santhanam A, Wu J, Singh V, Wilson SE. The corneal fibrosis response to epithelial-stromal injury. Exp Eye Res. 2016;142:110-8.

137. Okada Y, Reinach PS, Shirai K, Kitano A, Kao WW, Flanders KC, Miyajima M, Liu H, Zhang J, Saika S. TRPV1 involvement in inflammatory tissue fibrosis in mice. Am J Pathol. 2011;178(6):2654-64.

138. Turan E, Valtink M, Reinach PS, Skupin A, Luo H, Brockmann T, Ba Salem MHO, Pleyer U, Mergler S. L-carnitine suppresses transient receptor potential vanilloid type 1 activity and myofibroblast transdifferentiation in human corneal keratocytes. Lab Invest. 2021;101(6):680-9.

139. Okada Y, Shirai K, Miyajima M, Reinach PS, Yamanaka O, Sumioka T, Kokado M, Tomoyose K, Saika S. Loss of TRPV4 Function Suppresses Inflammatory Fibrosis Induced by Alkali-Burning Mouse Corneas. PLoS One. 2016;11(12):e0167200.

140. Rahaman SO, Grove LM, Paruchuri S, Southern BD, Abraham S, Niese KA, Scheraga RG, Ghosh S, Thodeti CK, Zhang DX, Moran MM, Schilling WP, Tschumperlin DJ, Olman MA. TRPV4 mediates myofibroblast differentiation and pulmonary fibrosis in mice. J Clin Invest. 2014;124(12):5225-38.

141. Okada Y, Sumioka T, Ichikawa K, Sano H, Nambu A, Kobayashi K, Uchida K, Suzuki Y, Tominaga M, Reinach PS, Hirai SI, Jester JV, Miyajima M, Shirai K, Iwanishi H, Kao WW, Liu CY, Saika S. Sensory nerve supports epithelial stem cell function in healing of corneal epithelium in mice: the role of trigeminal nerve transient receptor potential vanilloid 4. Lab Invest. 2019;99(2):210-30.

142. Voets T, Droogmans G, Wissenbach U, Janssens A, Flockerzi V, Nilius B. The principle of temperature-dependent gating in cold- and heat-sensitive TRP channels. Nature. 2004;430(7001):748-54.

143. Spahn V, Stein C, Zollner C. Modulation of transient receptor vanilloid 1 activity by transient receptor potential ankyrin 1. Mol Pharmacol. 2014;85(2):335-44.

144. Zorn-Kruppa M, Tykhonova S, Belge G, Bednarz J, Diehl HA, Engelke M. A human corneal equivalent constructed from SV40-immortalised corneal cell lines. Altern Lab Anim. 2005;33(1):37-45.

145. Zorn-Kruppa M, Tykhonova S, Belge G, Diehl HA, Engelke M. Comparison of human corneal cell cultures in cytotoxicity testing. ALTEX. 2004;21(3):129-34.

146. Grynkiewicz G, Poenie M, Tsien RY. A new generation of Ca2+ indicators with greatly improved fluorescence properties. J Biol Chem. 1985;260(6):3440-50.

147. Barreto-Chang OL, Dolmetsch RE. Calcium imaging of cortical neurons using Fura-2 AM. J Vis Exp. 2009(23).

148. technologies MPId. Fluo Calcium Indicators [Product Information]. Molecular Probes, Inc.; 2011 [Available from: http://tools.thermofisher.com/content/sfs/manuals/mp01240.pdf.

149. Kakkassery M. [Characterization of the transient-receptor-potential cation channel TRPV4 in insuline producing INS-1-cells] [doctoral thesis]. Berlin: Medizinische Fakultät Charité-Universitätsmedizin Berlin; 2013.

150. Timmerman MP, Ashley CC. Fura-2 diffusion and its use as an indicator of transient free calcium changes in single striated muscle cells. FEBS Lett. 1986;209(1):1-8.

151. Noble D, Powell T. The slowing of Ca2+ signals by Ca2+ indicators in cardiac muscle. Proc Biol Sci. 1991;246(1316):167-72.

152. Neher E, Sakmann B. Single-channel currents recorded from membrane of denervated frog muscle fibres. Nature. 1976;260(5554):799-802.

153. Hamill OP, Marty A, Neher E, Sakmann B, Sigworth FJ. Improved patch-clamp techniques for high-resolution current recording from cells and cell-free membrane patches. Pflugers Arch. 1981;391(2):85-100.

154. Bruggemann A, Farre C, Haarmann C, Haythornthwaite A, Kreir M, Stoelzle S, George M, Fertig N. Planar patch clamp: advances in electrophysiology. Methods Mol Biol. 2008;491:165-76.

155. Stumpff F, Georgi MI, Mundhenk L, Rabbani I, Fromm M, Martens H, Gunzel D. Sheep rumen and omasum primary cultures and source epithelia: barrier function aligns with expression of tight junction proteins. J Exp Biol. 2011;214(Pt 17):2871-82.

156. Georgi MI, Rosendahl J, Ernst F, Gunzel D, Aschenbach JR, Martens H, Stumpff F. Epithelia of the ovine and bovine forestomach express basolateral maxi-anion channels permeable to the anions of short-chain fatty acids. Pflugers Arch. 2014;466(9):1689-712.

157. Schrapers KT, Sponder G, Liebe F, Liebe H, Stumpff F. The bovine TRPV3 as a pathway for the uptake of Na(+), Ca(2+), and NH4(+). PLoS One. 2018;13(3):e0193519.

158. Bruggemann A, Stoelzle S, George M, Behrends JC, Fertig N. Microchip technology for automated and parallel patch-clamp recording. Small. 2006;2(7):840-6.

159. Milligan CJ, Li J, Sukumar P, Majeed Y, Dallas ML, English A, Emery P, Porter KE, Smith AM, McFadzean I, Beccano-Kelly D, Bahnasi Y, Cheong A, Naylor J, Zeng F, Liu X, Gamper N, Jiang LH, Pearson HA, Peers C, Robertson B, Beech DJ. Robotic multiwell planar patch-clamp for native and primary mammalian cells. Nat Protoc. 2009;4(2):244-55.

160. Mergler S, Derckx R, Reinach PS, Garreis F, Bohm A, Schmelzer L, Skosyrski S, Ramesh N, Abdelmessih S, Polat OK, Khajavi N, Riechardt AI. Calcium regulation by temperature-sensitive transient receptor potential channels in human uveal melanoma cells. Cell Signal. 2014;26(1):56-69.

161. Barry PH. JPCalc, a software package for calculating liquid junction potential corrections in patch-clamp, intracellular, epithelial and bilayer measurements and for correcting junction potential measurements. J Neurosci Methods. 1994;51(1):107-16.

162. Berlin C-U. Neufassung der Satzung der Charité – Universitätsmedizin Berlin zur Sicherung Guter Wissenschaftlicher Praxis vom 20.06.2012 (AMB Charité Nr. 092, S. 658). 2018.

163. Shaffer JP. Controlling the false discovery rate with constraints: the Newman-Keuls test revisited. Biom J. 2007;49(1):136-43.

164. Vriens J, Appendino G, Nilius B. Pharmacology of vanilloid transient receptor potential cation channels. Mol Pharmacol. 2009;75(6):1262-79.

165. Vincent F, Duncton MA. TRPV4 agonists and antagonists. Curr Top Med Chem. 2011;11(17):2216-26.

166. Mergler S, Garreis F, Sahlmuller M, Reinach PS, Paulsen F, Pleyer U. Thermosensitive transient receptor potential channels in human corneal epithelial cells. J Cell Physiol. 2011;226(7):1828-42.

167. Chung MK, Lee H, Caterina MJ. Warm temperatures activate TRPV4 in mouse 308 keratinocytes. J Biol Chem. 2003;278(34):32037-46.

168. Castro-Munozledo F. Development of a spontaneous permanent cell line of rabbit corneal epithelial cells that undergoes sequential stages of differentiation in cell culture. J Cell Sci. 1994;107 (Pt 8):2343-51.

169. Martinez-Rendon J, Sanchez-Guzman E, Rueda A, Gonzalez J, Gulias-Canizo R, Aquino-Jarquin G, Castro-Munozledo F, Garcia-Villegas R. TRPV4 Regulates Tight Junctions and Affects Differentiation in a Cell Culture Model of the Corneal Epithelium. J Cell Physiol. 2017;232(7):1794-807.

170. Liebe F, Liebe H, Sponder G, Mergler S, Stumpff F. Effects of butyrate(-) on ruminal Ca(2+) transport: evidence for the involvement of apically expressed TRPV3 and TRPV4 channels. Pflugers Arch. 2022;474(3):315-42.

171. Stumpff F, Bondzio A, Einspanier R, Martens H. Effects of the Bacillus thuringiensis toxin Cry1Ab on membrane currents of isolated cells of the ruminal epithelium. J Membr Biol. 2007;219(1-3):37-47.

172. Asbell P, Messmer E, Chan C, Johnson G, Sloesen B, Cook N. Defining the needs and preferences of patients with dry eye disease. BMJ Open Ophthalmol. 2019;4(1):e000315.

173. Alessandri-Haber N, Joseph E, Dina OA, Liedtke W, Levine JD. TRPV4 mediates pain-related behavior induced by mild hypertonic stimuli in the presence of inflammatory mediator. Pain. 2005;118(1-2):70-9.

174. Fakih D, Guerrero-Moreno A, Baudouin C, Goazigo AR, Parsadaniantz SM. Capsazepine decreases corneal pain syndrome in severe dry eye disease. J Neuroinflammation. 2021;18(1):111.

175. Grace MS, Bonvini SJ, Belvisi MG, McIntyre P. Modulation of the TRPV4 ion channel as a therapeutic target for disease. Pharmacol Ther. 2017;177:9-22.

176. Suzuki M, Mizuno A, Kodaira K, Imai M. Impaired pressure sensation in mice lacking TRPV4. J Biol Chem. 2003;278(25):22664-8.

177. Belmonte C, Acosta MC, Merayo-Lloves J, Gallar J. What Causes Eye Pain? Curr Ophthalmol Rep. 2015;3(2):111-21.

178. Alessandri-Haber N, Dina OA, Joseph EK, Reichling D, Levine JD. A transient receptor potential vanilloid 4-dependent mechanism of hyperalgesia is engaged by concerted action of inflammatory mediators. J Neurosci. 2006;26(14):3864-74.

179. Vergnolle N. TRPV4: new therapeutic target for inflammatory bowel diseases. Biochem Pharmacol. 2014;89(2):157-61.

180. Denadai-Souza A, Martin L, de Paula MA, de Avellar MC, Muscara MN, Vergnolle N, Cenac N. Role of transient receptor potential vanilloid 4 in rat joint inflammation. Arthritis Rheum. 2012;64(6):1848-58.

181. D'Aldebert E, Cenac N, Rousset P, Martin L, Rolland C, Chapman K, Selves J, Alric L, Vinel JP, Vergnolle N. Transient receptor potential vanilloid 4 activated inflammatory signals by intestinal epithelial cells and colitis in mice. Gastroenterology. 2011;140(1):275-85.

182. Ye L, Kleiner S, Wu J, Sah R, Gupta RK, Banks AS, Cohen P, Khandekar MJ, Bostrom P, Mepani RJ, Laznik D, Kamenecka TM, Song X, Liedtke W, Mootha VK, Puigserver P, Griffin PR, Clapham DE, Spiegelman BM. TRPV4 is a regulator of adipose oxidative metabolism, inflammation, and energy homeostasis. Cell. 2012;151(1):96-110.

183. Majtanova N, Kriskova P, Keri P, Fellner Z, Majtan J, Kolar P. Herpes Simplex Keratitis in Patients with SARS-CoV-2 Infection: A Series of Five Cases. Medicina (Kaunas). 2021;57(5).

184. Mergler S. Functional expression of temperature-sensitive transient receptor potential channels (TRPs) in cultured human corneal and conjunctival cells: Relevance in the pathophysiology of ocular surgace diseases. 2015.

185. Almers W, Neher E. The Ca signal from fura-2 loaded mast cells depends strongly on the method of dye-loading. FEBS Lett. 1985;192(1):13-8.

186. Garreis F, Schroder A, Reinach PS, Zoll S, Khajavi N, Dhandapani P, Lucius A, Pleyer U, Paulsen F, Mergler S. Upregulation of Transient Receptor Potential Vanilloid Type-1 Channel

Activity and Ca2+ Influx Dysfunction in Human Pterygial Cells. Invest Ophthalmol Vis Sci. 2016;57(6):2564-77.

187. Willette RN, Bao W, Nerurkar S, Yue TL, Doe CP, Stankus G, Turner GH, Ju H, Thomas H, Fishman CE, Sulpizio A, Behm DJ, Hoffman S, Lin Z, Lozinskaya I, Casillas LN, Lin M, Trout RE, Votta BJ, Thorneloe K, Lashinger ES, Figueroa DJ, Marquis R, Xu X. Systemic activation of the transient receptor potential vanilloid subtype 4 channel causes endothelial failure and circulatory collapse: Part 2. J Pharmacol Exp Ther. 2008;326(2):443-52.

188. Thorneloe KS, Cheung M, Holt DA, Willette RN. PROPERTIES OF THE TRPV4 AGONIST GSK1016790A AND the TRPV4 ANTAGONIST GSK2193874. Physiol Rev. 2017;97(4):1231-2.

Statutory Declaration

"I, Vivien Schmädicke, by personally signing this document in lieu of an oath, hereby affirm that I prepared the submitted dissertation on the topic "Characterization of transient receptor potential vanilloid 4 (TRPV4) channels in human corneal keratocytes" resp. "Die Charakterisierung von "transient receptor potential vanilloid" 4 (TRPV4)-Kanälen in humanen Hornhautkeratozyten", independently and without the support of third parties, and that I used no other sources and aids than those stated.

All parts which are based on the publications or presentations of other authors, either in letter or in spirit, are specified as such in accordance with the citing guidelines. The sections on methodology (in particular regarding practical work, laboratory regulations, statistical processing) and results (in particular regarding figures, charts and tables) are exclusively my responsibility.

Furthermore, I declare that I have correctly marked all of the data, the analyses, and the conclusions generated from data obtained in collaboration with other persons, and that I have correctly marked my own contribution and the contributions of other persons (cf. declaration of contribution). I have correctly marked all texts or parts of texts that were generated in collaboration with other persons.

My contributions to any publications to this dissertation correspond to those stated in the below joint declaration made together with the supervisor. All publications created within the scope of the dissertation comply with the guidelines of the ICMJE (International Committee of Medical Journal Editors; www.icmje.org) on authorship. In addition, I declare that I shall comply with the regulations of Charité – Universitätsmedizin Berlin on ensuring good scientific practice.

I declare that I have not yet submitted this dissertation in identical or similar form to another Faculty.

The significance of this statutory declaration and the consequences of a false statutory declaration under criminal law (Sections 156, 161 of the German Criminal Code) are known to me."

Date Signature

Curriculum Vitae

Mein Lebenslauf wird aus datenschutzrechtlichen Gründen in der elektronischen Version meiner Arbeit nicht veröffentlicht.

Acknowledgements

First of all, I would like to thank my supervisor PD Dr. phil. nat. Stefan Mergler (Department of Experimental Ophthalmology at Charité Virchow Clinic in Berlin) for giving me the best support while working on this thesis – including the assignment of the topic, the patiently teaching of the experimental methods and good scientific practice and the fast answers to my questions in interesting discussions and via email. I never felt alone with problems that arose during this thesis. He always gave my good advices and his motivation to bring students closer to experimental basic research was always noticeable. It was easy to get carried away with his enthusiasm for ophthalmic research around TRP channels.

Furthermore, I would like to appreciate the support of PD Dr. med. Friederike Stumpff (Institute of Veterinary Physiology, Faculty of Veterinary Medicine, Freie Universität Berlin). She gave me good advices throughout my research and the opportunity to work on a classic patch-clamp setup in her laboratory. At this point a special thank goes to Mrs. Manz for patiently showing me how to work with the setup.

Moreover, I would like to thank the members of the research department, the other doctoral students like Elizabeth Turan and the interns for the great work atmosphere.

I would especially like to express my gratitude to my dear family and friends for their love and unlimited support.

Mom and dad, this is for you!